HOLTEC INTERNATIONAL

Holtec Center, 555 Lincoln Drive West, Marlton, NJ 08053
Telephone (856) 797-0900
Fax (856) 797-0909

Kimberly Hardin
C/O U.S. Nuclear Regulatory Commission
ATTN: Document Control Desk
Washington, DC 20555-0001

February 27, 2009

Reference:
1. USNRC Docket No. 71-9261 (HI-STAR 100), TAC L24029
2. Holtec Project 5014
3. Conversation Record for Phone Call held on January 14, 2009 (ML
4. Holtec Letter 5014666 dated September 39, 2008

Subject: Supplemental Information to Support Response to 2nd Request for Additional Information (RAI) on License Amendment Request (LAR) 9261-5 to HI-STAR 100 Certificate of Compliance (CoC) No. 9261

Dear Ms. Hardin:

On January 14, 2009 the NRC and Holtec held a teleconference (Reference 3) to discuss some clarifying questions on the second response to RAI (Reference 4). This letter and the attachments provide the reconciliation of those clarifying questions.

Attachment 1 to this letter contains the specific responses to the questions; and Attachment 2 contains the updated SAR sections. As stated in the conversation record, Staff will be adding the necessary clarifications to the CoC and SER as presented in question 5 and 6; therefore no response is provided.

Document ID: 5014678

NMSS01
NMSS

HOLTEC INTERNATIONAL

Holtec Center, 555 Lincoln Drive West, Marlton, NJ 08053
Telephone (856) 797-0900
Fax (856) 797-0909

The following attachments are provided with this letter:

Attachment 1: Response to Clarifying Questions.

Attachment 2: Proposed Revised SAR Sections 2.7, 2.A, 2.I, 7.1, and 8.1. All changed sections are provided and are labeled as "Proposed Rev. 13c".

Sincerely,

Tammy Morin
Acting Licensing Manager,
Project Manager, LAR 9261-5
Holtec International

cc: USNRC Document Control Desk, hardcopy only
Ms. Kimberly Hardin, Sr. Project Manager, NRC/NMSS/SFST
Mr. Eric Benner, Licensing Branch Chief, NRC/NMSS/SFST, Letter only
Mr. Larry Pulley, PSE&G, Letter only via email
Group 1, Holtec, Letter only via email

Question 1:

On Drawing 4082, Sheet 6, Mid-Plane, for HI-STAR HB and drawing 3913 for HI-STAR 100, Staff questioned to removal of radial gussets, exterior shell holding Holtite-A, neutron shielding material. Was this evaluated for structural effects. There needs to be some recognition as a design changem in Supplement 2.I and provide an evaluation summary.

Holtec Response to Question 1:

The radial gussets were removed from the space between the inner and outer shells. The heat load of the HI-STAR HB casks are so low they are not needed to conduct the heat radially. The description of the design difference has been added to 2.I.0. An evaluation summary was added to 2.I.6.

Question 2:

Regarding question 2-4, Section 2.I.7.I needs to be revised to include the RAI response, which justifies the use of the Holtec differential equation method for HI-STAR HB implementation. Specifically,

- Clarify the use of the wording in the SAR – the Hexel manufacturer's catalogue states that dynamic crush strengths are a function of "initial" velocity. There is no information suggesting that the "Z" factors in the differential equation method are a function of crush material density – (maybe crush strength).
- Use of identical dynamic multiplier (or dynamic correlation function), represented by a linear function of concomitant crush velocity, should be captured in the SAR as the basis for using the predictive simulation without impact limiter drop testing.
- Holtec proprietary report results need to be summarized (RAI response and key technical basis) in Section 2.I.7.1.
- Per page 23 of 26, Holtec Calculation Package HI-208417, Rev. 0, 9/29/08, do not give the explicit for of the Dynamic Correlation Function in the SAR.

Holtec Response to Question 2:

Additional discussion and summary with appropriate clarification was added to 2.I.7.1 consistent with the response that was provided in the second RAI, question 2-4.

Question 3:

Clarify wording in Chapter 7 about pocket trunnions possible use as tie-down devices.

Holtec Response to Question 3:

Pocket trunnions will not be used as tie-down devices therefore the wording in 7.1.5, Step 3, was modified as requested.

Question 4:

Clarify the neutron shield tests.

Holtec Response to Question 4:

Wording in 8.1.5.4 was modified as requested.

Question 7:

Page 2.7-3P: Reference 2.I.7.4 – not found in supplement 2.I.11 reference.

Holtec Response to Question 7:

The incorrect reference was eliminated in four places (two in Section 2.7 and two in section 2.A). The ¼ scale model drawings of the impact limiters tested were never a part of the application and therefore the sentences that indicated this were also removed.

Question 8:

Page 2.A-23: Revision 2 for Reference 2.A.7, "Impact Limiter Test Report – Second Series, 1998. Referenece 10 of the calculation package, HI-208417 is Revision 3-undated.

Holtec Response to Question 8:

The correct Revision number and date are provided in Reference 2.A.7.

Attachment 2 to Holtec Letter 5014678
(110 pages)

2.7 HYPOTHETICAL ACCIDENT CONDITIONS

It was shown in the preceding section that the load combinations for normal conditions of transport do not induce stresses or stress intensities in excess of allowables. Therefore, it is concluded that the effectiveness of the HI-STAR 100 System is not reduced under normal conditions of transport.

The hypothetical accident conditions, as defined in 10CFR71.73 and Regulatory Guide 7.9, are applied to the HI-STAR 100 System in the required sequence. The system is first subjected to a 9 meter (30 foot) drop in the most damaging orientation, then subject to a 1 meter (40 inch) drop onto a 6 inch diameter mild steel pin (of length sufficient to cause damage to the steel structure), followed by a 1475°F temperature fire environment for 30 minutes, and finally to a water immersion test.

The overpack containment boundary is also subjected to deep immersion in accordance with 10CFR71.61.

It is shown in the following subsections that the HI-STAR 100 System meets the standards set forth in 10CFR71, when it is subjected to the hypothetical accident conditions specified in 10CFR71.73. In particular, sufficient analytical and experimental evidence is presented herein to support the conclusion that HI-STAR 100 packaging, when subjected to hypothetical accident conditions, has adequate structural integrity to satisfy the subcriticality, containment, shielding, and temperature requirements of 10CFR71.

2.7.1 Free Drop

In this section the performance and structural integrity of the HI-STAR 100 System is evaluated for the most severe drop events. The drop events that are potentially most damaging are the end drops (top or bottom), the side drop, the orientation for which the center of gravity is directly over the point of impact, an oblique drop where the angle of impact is somewhere between center of gravity over corner and a near side drop, and an orientation where package rotation after an impact at one end induces a larger impact deceleration when the other end impacts the target (e.g., slapdown).

The structural assessment of the package is performed in two parts. In the first part, a numerical model to simulate the drop events is prepared and benchmarked against 1/8 scale static tests of the HI-STAR 100 impact limiters, and ¼-scale dynamic drop tests of the HI-STAR 100 Package. This numerical/experimental effort is carried out to confirm that the maximum rigid body decelerations experienced by the package are less than the design basis values set forth in Table 2.1.10. In the second part, the structural integrity of components under the inertia loads due to design basis deceleration levels is evaluated. The deceleration sustained by the internals, such as the fuel basket, are further amplified in recognition of the elasticity of the internal structures. The dynamic amplifier is considered as an added multiplier on the rigid body deceleration in the structural assessments. Dynamic amplifiers applicable to components of the package have been developed from evaluating the behavior of simplified models.

Part One: Maximum Rigid Body Deceleration Under 10CFR71.73 Free Drop Event

The determination of the AL-STAR impact limiter performance under postulated 10CFR71.73 free drop events was carried out in six phases as summarized below and further elaborated in Appendix 2.A.

i. Characterize honeycomb material crush behavior: Coupons of both unidirectional and cross-core honeycomb materials at different nominal crush strength values were prepared and tested. A typical pressure vs. deflection curve is shown in Figure 2.A.2.1 in Appendix 2.A. The pressure in the flat portion of the curve denotes the crush pressure.

   Mathematical correlation of the data from the population of coupons tested showed that the pressure/crush curve for a honeycomb stock can be represented by one equation wherein the crush pressure, p_c, is the sole variable. This commonality in the deformation characteristic of the AL-STAR honeycomb materials of different crush strength is extremely helpful in simplifying the dynamic model for the impact limiter.

ii. AL-STAR Force-Crush Relationship: The AL-STAR impact limiter is a radially symmetric structure whose external and internal diameters are fixed: the I.D. is set by the overpack diameter at its extremities and the O.D. is limited by rail transport considerations to 128". Within this annular space, the arrangement of the aluminum honeycomb material is specified so that the impact limiter can absorb the kinetic energy from a 30' drop event in *any* orientation. The axial dimension of the impact limiter is also limited by considerations of the overall weight of the packaging. To design the impact limiter within the above-mentioned constraints called for a method to predict the force required to crush the impact limiter by a given amount in any given orientation. The mathematical model to define the force-crush (F-d) curve is described in Appendix 2.A. The F-d model was used to establish the nominal crush strengths of the honeycomb sectors used in the various locations of the AL-STAR honeycomb volume to obtain the desired energy absorption characteristics in the equipment.

iii. Static Scale Model Tests: The static 1/8 scale model tests consisted of preparing 1/8 scale models of the AL-STAR impact limiter and subjecting them to static crush tests in various orientations under normal and abnormal temperature conditions. One object of these tests was to confirm the validity of the theoretical F-d model. Confirming the structural adequacy of the AL-STAR backing structure (which is a thick carbon steel weldment) and the external skin were also objectives of the scale model test. The 1/8 scale static tests, as described in Appendix 2.A, met all project goals: a weakness in the AL-STAR backing structure was identified and corrected in a redesign of the backing structure. The test data also showed that Holtec's F-d model provided a reasonably accurate analytical tool to predict the static crushing behavior of AL-STAR in the various potential crushing orientations. The adequacy of the F-d model to predict static crush behavior was an essential prerequisite for the dynamic test correlation effort that followed.

iv. Dynamic Scale Model Tests: A 1/4 scale model of the HI-STAR 100 Package, including AL-STAR impact limiters, was used for drop testing. Appendix 2.A herein provides a complete synopsis of the AL-STAR impact limiter design development program, including the 1/4 scale model drop tests which demonstrated the performance of the package. The objectives of the drop tests may be stated as follows:

i. Select a sufficient number of drop orientations to ensure that under the worst-case orientations, the structural adequacy of the package is demonstrated by testing.

ii. Prove that the peak rigid body decelerations experienced by the package in any of the tests is below the Table 2.1.10 design basis value.

iii. Demonstrate that the impact limiters prevent the cask from direct contact with the unyielding surface and remain attached through the end of the drop event.

Four drop configurations, namely, vertical (top end), horizontal (side), center-of-gravity-over-corner (CGOC), and slap-down (fully described in Appendix 2.A) were identified as a complete set capable of realizing the aforementioned objectives. The tests were performed in two distinct series as described below.

The first test series, conducted in August 1997, indicated the need to modify the honeycomb material crush strength utilized. The first dynamic test series also helped quantify the dynamic multiplier applicable to the statically determined honeycomb crush strength under impact conditions.

The second test series showed that the peak deceleration in all four drop orientations tested met the Table 2.1.10 limits. Despite meeting deceleration limits, the attachment bolts between the bottom impact limiter and the overpack failed in the side drop test. This required an additional design improvement to the bottom impact limiter-to-overpack attachment design, and re-performance of the side drop test. For the final four tests used for evaluation in Appendix 2.A, no attachment bolts sustained a failure.

v. AL-STAR Dynamic Response Model: The 1/4 scale tests provided valuable information on the package response which was used to confirm the veracity of Holtec's dynamic simulation model developed for predicting the package response under the other drop conditions. Like all orthotropic materials, the crushing of the honeycomb requires greater force under an impact load than the load necessary to achieve the same extent of crush under static conditions. The conversion of the static "force (F) - crush (d)" model to dynamic conditions simply means applying a dynamic factor to the formula. In other words, under dynamic conditions, the relation between crush force "F" and crush "d" is given as:

$$F = Z\, f(d)$$

where f(d) is the crush force corresponding to the compression "d" under static conditions

and Z is the dynamic multiplier function. The value of Z was quantified by the first series of 1/4 scale dynamic scale model test, such that a dynamic response simulation model could be developed that satisfied all equilibrium expectations.

In addition to comparing the predicted peak decelerations with the measured value, the duration of crushing and crush depth predicted by the dynamic model were also compared with the measured test data. The comparisons, presented in Appendix 2.A, confirm the ability of the dynamic model to simulate the behavior of the package under a drop event.

vi. Sensitivity Studies: A significant result from the 1/4 scale model dynamic tests was a complete validation of the dynamic model. For every test performed, the AL-STAR dynamic model was able to simulate the peak accelerations, total crush, *and* crush duration with reasonable agreement. The experimentally benchmarked mathematical model could now be used to simulate drop events for a variety of HI-STAR 100 package weights and honeycomb crush strengths. Results of the simulations to determine the effects of variations in aluminum honeycomb crush strengths and package weights are presented in Appendix 2.A.

The results summarized in Table 2.A.5 of Appendix 2.A demonstrates that the maximum rigid body deceleration experienced by the HI-STAR 100 package equipped with the AL-STAR impact limiter will be less than 60g's regardless of the orientation of impact. Therefore, in the balance of analyses performed to evaluate the consequences of "free drop" under the provisions of 10CFR71.73, the package will be assumed to be subject to a rigid body deceleration equal to 60 g's. It is clear from inspection of the geometry of the package that the most vulnerable direction of inertia loading for the HI-STAR fuel basket is the transverse direction wherein the flat panels of the basket are subjected to lateral inertia loading from the contained SNF. As mentioned earlier, the flexibility of basket panel acts to further amplify the package deceleration, which must be considered in the evaluation of results from the stress analysis model. In summary, the net result of the work effort described in the foregoing and further elaborated in Appendix 2.A was to confirm the validity of 60g as the *design basis* rigid body deceleration for the 10CFR71.73 drop event.

In Appendix 2.A, additional supporting technical information requested in Paragraph 2.7 of Reg. Guide 7.9 is provided. Information provided includes free-body diagrams, sketches, governing equations, test method for model testing, scaling factors, discussion of the law of similitude, measurements of crush, impact duration, deceleration histograms, effect of tolerances on package response, and demonstration that the model test will give conservative results for peak g-force and maximum deformation.

Additionally, Reg. Guide 7.9 calls for evaluation of the response of the package in terms of stress and strain to components and structural members, including investigation of structural stability as well as the consequences of the combined effects of temperature gradients, pressure, and other loads. Part Two of the work effort, described in the following, fulfills the above Reg. Guide 7.9 stipulations.

Part Two: Stress Analysis

The second part of the analysis is performed using the ANSYS finite element software [2.6.4]. The MPC and overpack models used here are identical to those presented in Section 2.6. The loads are applied to the models in accordance with the load combinations defined in Table 2.1.6 (Load Cases F3), Table 2.1.7 (Load Cases E3), and Table 2.1.9 (Load Cases 1-16) for hypothetical accident conditions of transport. The detailed application of each load case is described in the subsections that follow. The presentation and content follows the formatting requirements of Regulatory Guide 7.9. The results from conditions of "Heat" and "Cold" are considered together in the following presentation.

The analysis of the different hypothetical accident conditions of transport are carried out using general finite element models of the MPC and the overpack as well as calculations based on simplified models amenable to strength of materials solutions. The analyses using strength of materials solutions focus on specific loading conditions applied to component parts of the MPC and/or the overpack. The finite element analysis of the overpack involves a complex 3-D model of the overpack to which a series of loads are applied. The results from the solutions are then combined in a post-processing phase to make up the different accident load combination. Given the complexity of the overpack finite element analysis model, some discussion of the stress report is presented to facilitate an understanding of the conclusions. For each of the load combinations, the following components are identified for reporting purposes:

1. Seal
2. Bolts
3. Lid
4. Inner Shell (including the top flange)
5. Intermediate Shells
6. Baseplate
7. Enclosure

The postprocessor collects the nodal stresses from the finite element solution, for each of the components in turn, and reports the principal stresses and the stress intensity at selected locations where physical reasoning suggests that high stresses may occur under the different postulated load combinations. In order to identify the minimum safety factor for each of the above components after the load cases are combined, the collection of nodes is sorted by stress intensity magnitude in descending order. Therefore, since the hypothetical accident condition load combinations involve a comparison of primary stress intensities, a minimum safety factor for each of the defined components in the model may be identified as occurring at the node point with the largest calculated stress intensity. Safety factors are computed using the allowable stress intensities for the material at the reference temperature identified for the component and reported under one of the seven groups identified above. The post-processor collects, sorts, and reports the necessary information to enable documentation of the satisfaction of the applicable requirements. The following items are collected and evaluated for each load combination:

Seals: The normal force in each of the springs representing the seal is reported and shown to remain in compression under the load. Maintaining a compressive load in the seal springs assures that there is no separation at the component interfaces.

Bolts: The bolts are initially preloaded by applying an initial strain sufficient to result in the desired pre-stress. Subsequent to the application of the different loads to form a specified load combination, the bolts are shown not to unload.

Lid: For each load combination, the lid primary membrane plus primary bending stress intensities are compared to the allowable values at the designated reference temperature.

Inner Shell: Primary membrane and primary membrane plus bending stress intensity distributions are examined and compared to allowable stress intensity values

Intermediate Shells: The five intermediate shells are examined at stress location points and compared to allowable stress intensities at the appropriate reference temperature. Since accident conditions of transport represent a Level D condition (where the comparison of calculated value vs. allowable value is always based on stress intensity), there is no differentiation between intermediate shells considered as Class 1 or Class 3 components.

Baseplate: Primary membrane plus bending stress intensities are compared to allowable values at the component reference temperature.

Enclosure: The plate and shell elements making up the enclosure for the Holtite-A material are compared to primary membrane stress intensity allowable values.

In the finite element analysis of all load combinations associated with hypothetical accident events, the initial preload case of the bolts and the internal pressure case are included in the final combination. Since no secondary stresses need be evaluated per the ASME Code requirements for an accident level event, the thermal stress load case for the "Heat" condition is not included as a specific load case. However, the allowable stress intensities used for the safety factor evaluation are obtained at the appropriate "Heat" condition reference temperature. In the reporting of safety factors, the variation in allowable stress intensity with temperature is ignored; this introduces an additional measure of conservatism in the reported safety factors since the reference temperatures (Table 2.1.21) are higher than the actual calculated temperatures. For the "Cold" condition, there are no temperature gradients developed. The interaction stresses developed to maintain compatibility under the uniform ambient temperature change are included in the analysis and are treated as primary stresses in the evaluation of the safety factor.

2.7.1.1 End Drop

- Overpack Stress (Load Cases 1,2,9, and 10 in Table 2.1.9)

The overpack is evaluated under both a top end drop and a bottom end drop. In both cases, the impact limiter reaction is assumed to act over the entire area that is backed by structural metal. Given that the total dropped weight is W and that the maximum acceleration is A, the impact

$$|R| = \frac{WA}{g}$$

limiter total reaction load follows from force equilibrium.
This reaction load R is imposed on the appropriate region of the overpack (either lid outer surface or bottom plate outer surface as a uniform pressure load to maximize the bending of the lid or bottom plate.

Since the same finite element model described and used in Section 2.6 for evaluation of loading associated with normal conditions of transport is used here with different applied loads, no further discussion of the model or the analysis methodology is required. Figures 2.1.7 and 2.1.8 show the loading on the overpack in the bottom down and the top down configurations, respectively. The results of the analyses for the top end and bottom end drops are collected and safety factors from the limiting locations in the model are reported in Tables 2.7.5 and 2.7.6 for both heat and cold environments. Table 2.7.5 presents the minimum safety factors for each of the components identified above for the "Heat" condition and Table 2.7.6 presents the safety factors for the "Cold" condition. Within each table, the component is identified, and the minimum safety factor reported.

- Overpack Stability

Structural stability of the overpack containment inner shell under the end drop is assessed. The case of the accident end drop is evaluated for elastic and plastic stability in accordance with the methodology of ASME Code Case N-284 [2.1.8]. All required interaction equation requirements set by [2.1.8] are met. For this event, yield strength limits rather than instability limits govern the minimum safety factor. The minimum safety factor for this case is summarized below:

Code Case N-284 Minimum Safety Factors - (Load Case 1 and 2 in Table 2.1.9)			
Item	Calculated Interaction Value	Allowable Interaction Value†	Safety Factor against Yield†
Load Case 1 and 2 in Table 2.1.9	0.62*	1.34	2.16*

* Applicable to inner shell fabricated from SA203-E material. Safety factor must be multiplied by 0.93 if inner shell is fabricated from optional SA350-LF3 material.

† Note that in computing the safety factor against yield for this table, the safety factor implicit in the Code Case N-284 allowable interaction equation is included. Note also that the safety factors given above from the Code Case analysis are all safety factors against the circumferential or longitudinal

stresses reaching the material yield stress. The actual safety factors against instability are larger than the factors reported in the table. In other words, yield strength rather than stability is the limiting condition. Finally, note that fabrication stresses have been included in the stability calculations even though these stresses are self-limiting. Therefore, all results corresponding to the calculated stability interaction equations are very conservative.

The result for the heat environment bound the similar result for the cold environment since yield strengths and elastic modulus are higher. Therefore, no analysis is performed for stability under cold conditions.

- Closure Bolt Analysis

Stresses are developed in the closure bolts due to pre-load, pressure loads, temperature loads, and accident loads. Closure bolts are explored in detail in Reference [2.6.3], which deals with the analysis of shipping casks. The analysis of the overpack closure bolts under normal conditions of transport has been reported in Section 2.6. This subsection presents the results for the analysis for the hypothetical accident end drop. The analysis follows the procedures defined in Reference [2.6.3]. The allowable stresses used for the closure bolts follows that reference. Note that the analyses provide alternative confirmation of the results from the finite element analysis; namely, under any of the identified load combinations, the bolts do not unload.

The following combined load case is for the hypothetical top end drop accident condition of transport. This drop conservatively assumes a nearly vertical orientation with the impact limiter reaction load applied at the outermost location of the lid. This results in the closure bolts resisting the inertial load from the MPC plus contents in addition to the inertia load from the closure lid itself. In reality, the load from the MPC would not load the bolts.

Top End Drop: Pressure, temperature, and pre-load loads are included.

Reference [2.6.3] reports safety factors defined as the calculated stress divided by the allowable stress for the load combination. This definition of safety factor is the inverse of the definition consistently used in this SAR. In summarizing the closure bolt analyses, results are reported using the safety factor definition of allowable stress divided by calculated stress. The following result for closure lid bolting for the top end drop hypothetical accident condition of transport is obtained.

Overpack Closure Bolt - Safety Factor (Load Case 2 in Table 2.1.9)	
Combined Load Case	Safety Factor on Bolt Tension
Average Tensile Stress	1.30

It is seen from the above table that the safety factor is greater than 1.0 as required. Note that the average tensile stress reflects the preload stress required for successful performance of the bolts as well as the applied load from the hypothetical accident drop event.

- MPC Fuel Basket Stability and Stress (Load Case F3.a in Table 2.1.6)

Under top or bottom end drop in a hypothetical accident condition of transport, the MPC is subject to its own amplified self-weight, causing compressive longitudinal stress in the fuel basket cell walls. The following analysis demonstrates that stability or yield is not a credible safety concern in the fuel basket walls under a hypothetical end drop accident condition of transport.

- MPC Fuel Basket Stability

Stability of the basket panels, under longitudinal deceleration loading (Load Cases F3.a in Table 2.1.6), is demonstrated in the following manner. Table 2.2.1 provides the weight of each fuel basket (including sheathing and neutron absorber panels). The corresponding metal areas of the basket bearing on the MPC baseplate or top lid can be computed for each MPC basket by direct calculation from the appropriate drawings. Dividing weight by bearing area and multiplying by the design basis deceleration for the hypothetical accident from Table 2.1.10 gives the axial stress in the load bearing walls. The results for each basket are compared and the bounding result (maximum weight/area) reported below:

Fuel Basket Compressive Stress For End Drop (Load Case F3.a)			
Item	Weight (lb.)	Bearing Area (sq. inch)	Stress (psi)
Bounding Basket (at 60g's deceleration)	23,535	346.61	4,074

To demonstrate that elastic instability in the basket panels is not credible, the flat panel buckling stress, σ_{cr}, (critical stress level at which elastic buckling may occur) is computed using the formula in reference [2.6.1].

For conservatism, the MPC fuel basket is modeled as a rectangular plate simply supported along two sides and uniformly compressed in the parallel direction. The width of the plate is equal to the maximum unsupported width of a panel from all fuel basket types. Reference [2.6.1] provides the critical stress formula for these conditions as

$$\sigma_{cr} = \frac{2.3\,\pi^2 E}{12\,(1-\nu^2)}\left(\frac{T}{W}\right)^2$$

where T is the panel thickness and W is the width of the panel, E is the Young's Modulus at the metal temperature and ν is the metal Poisson's Ratio. The following table summarizes the calculation for the critical buckling stress using the formula given above:

Elastic Stability Result for a Flat Panel	
Reference Temperature	725 degrees F
T (bounding thickness)	9/32 inch
W (bounding width)	11.0 inch
E	24,600,000 psi
Critical Axial Stress	33,430 psi

It is noted that the critical axial stress is an order of magnitude greater than the computed basket axial stress reported in the foregoing. Therefore, it is demonstrated that elastic stability under hypothetical accident condition of transport longitudinal deceleration inertia load is not a concern.

- MPC Fuel Basket Stress

The safety factor against yielding of the basket under longitudinal compressive stress from a design basis inertial loading is given by

$$SF = 17{,}100/4{,}074 = 4.198$$

where the yield stress of Alloy X has been taken from Table 2.3.1 at 725 degrees F.

Therefore, plastic deformation of the fuel basket under design basis deceleration is not credible.

Analyses of the Damaged Fuel canisters to be transported in the HI-STAR 100 Package are performed to demonstrate structural integrity under an end drop condition. A summary of the methodology and the results for all canisters is provided in Appendix 2.B.

- MPC Enclosure Shell Stability

Structural stability of the MPC enclosure shell under the end drop is evaluated for elastic and plastic/stability in accordance with the ASME Code Case N-284 [2.1.8]. All required interaction equation requirements set by [2.1.8] are met. It is shown that yield strength limits rather than instability limits govern the minimum safety factor. The minimum safety factor for this case is summarized below:

MPC Shell Elastic/Plastic Stability (Load Case E3.a Table 2.1.7)			
Item	Value	Allowable*	Safety Factor
Yield	0.698	1.34	1.92

* For Load Case E3.a, the yield strength criteria in the Code Case N-284 method govern. In this event, the safety factor 1.34, built into the Code Case, is included in the tabular result in order to obtain the actual safety factor with respect to the yield strength of the material.

- MPC Closure Lid Stress (Load Case E3.a)

The closure lid, the closure lid peripheral weld, and the closure ring are examined for maximum stresses developed during the hypothetical end drop accident event.

The closure lid is modeled as a single simply supported plate and is subject to deceleration from an end drop plus appropriate design pressures. Results are presented for both the single and dual lid configurations (in parentheses) for top end and bottom end drops. For the dual lid configuration, the two plates each support their own amplified weight as simply supported plates under a bottom end drop. The inner lid transfers the total load to the outer plate through the peripheral weld between the two lids. Under a top end drop scenario, the inner lid is partially supported by the outer lid and the amplified load is transmitted by a combination of peripheral support and interface contact pressure. The results for minimum safety factor are reported in the table below:

MPC Top Closure Lid - Minimum Safety Factors - Load Case E3.a in Table 2.1.7			
Item	Stress(ksi) or Load(lb.)	Allowable Stress (ksi) or Load Capacity (lb.)	Safety Factor
Lid Bending Stress - Load Case E3.a (bottom end drop)	3.35/(7.94)	60.7	18.1/(7.65)
Lid Bending Stress* - Load Case E3.a (top end drop)	21.9/(43.8)	60.7	2.77/(1.39)
Lid-to-Shell Peripheral Weld Load - Load Case E3.a	624,000	1,477,000**	2.37
Lid-to-Lid Peripheral Weld Load - Load Case E3.a (bottom end drop)	312,000	443,200***	1.42

* Stress computation is conservatively based on peripheral support at the outer diameter of the MPC lid. For a top end drop, the actual support diameter is .77 of the outer diameter. Therefore, an analysis based on an overhung plate would provide stresses reduced by a multiplier of 0.59. Consequently, the safety factors would be amplified by the factor 1.69.

** Based on a 0.625" single groove weld and conservatively includes a quality factor of 0.45.

*** This is a non-Code weld; limit is based on a 0.1875 groove weld and includes a quality factor of 0.45 for additional conservatism

Safety factors are greater than 1.0 as required. The limiting condition for the lid bending evaluation is a top end hypothetical accident end drop because the lid supports the amplified fuel weight as well as the lid amplified self-weight.

- MPC Baseplate and Canister Stress (Load Case E3.a)

Load Case E3.a provides the limiting accident loading on the baseplate wherein the combined effect of a 60g deceleration plus external pressure is considered. The top end hypothetical accident condition is limiting in transport, and here it is conservatively assumed that accident external pressure acts simultaneously, which exceeds the requirements of Table 2.1.7. The results are summarized below:

MPC Baseplate Minimum Safety Factors – Load Cases E3, Table 2.1.7			
Item	Value (ksi)	Allowable (ksi)	Safety Factor
Center of Baseplate - Primary Bending (Load Case E3)	22.12	67.32	3.04
Shell Bending Stress at Connection to Baseplate	31.47	67.32	2.14

Note that all safety factors are greater than 1.0. Also, note that the calculated stress conservatively includes both primary and secondary self-limiting stress components. For the hypothetical transport drop accident, the safety factor computed for the shell bending stress intensity need only consider the effect of primary membrane plus bending stresses that are to be compared against the ultimate stress at temperature for this ASME Code Service Level D event. Since secondary stresses have been included in the evaluation, the reported result for safety factor is conservatively low.

- Trojan MPC Spacer

The Trojan MPC-24E/EF enclosure vessel is 9 inches shorter in length than the generic MPC-24E/EF enclosure vessel. Thus, when the Trojan MPC-24E/EF is transported inside the HI-STAR 100, the axial clearance between the MPC lid and the HI-STAR 100 closure plate is greater than 10 inches. In order to prevent the Trojan MPC from thrusting forward and impacting the closure plate during a top-end drop or a tip-over event (i.e., slapdown), a spacer device is positioned on top of the MPC lid. The Trojan MPC spacer, depicted in Figure 1.1.5, is fabricated from SA240-304 stainless steel in the shape of a circular I-beam. The web of the spacer measures 1-inch thick and has a mean diameter of 60 inches. The total height of the MPC spacer is 9 inches.

During a top end drop, the MPC spacer must support the amplified weight of a fully loaded Trojan MPC-24E/EF. Based on a bounding MPC weight of 90,000 lb (Table 2.2.4) and a bounding deceleration of 60g (Table 2.1.10), the maximum compressive stress in the web is computed as follows.

Cross-sectional area of web (A) = $\pi \times D \times t = \pi\ (60)\ (1) = 188.5\ in^2$

Amplified weight of MPC (P) = $G \times W = (60)\ (90{,}000) = 5.4 \times 10^6$ lb

Compressive stress in web = $P/A = (5.4 \times 10^6) / 188.5 = 28{,}647$ psi

From Table 2.1.18, the primary membrane stress intensity limit for Alloy X (of which SA240-304 is a member) under Level D conditions is 44.9 ksi at 400°F. Therefore, the safety factor against compressive failure of the Trojan MPC spacer, per ASME Code Subsection NB stress limits, is

SF = 44,900 / 28,647 = 1.56

2.7.1.2 Side Drop (Load Cases F3 in Table 2.1.6, E3 in Table 2.1.7, and 3 and 11 in Table 2.1.9)

- MPC Fuel Basket and Canister Finite Element Analysis (Load Cases E3.b, E3.c in Table 2.1.7 and Load Cases F3.b, F3.c in Table 2.1.6)

The MPC configurations are assessed for a hypothetical accident condition of transport side drop. All fuel cells are loaded with design basis spent nuclear fuel (SNF). Evaluations are performed for the 0 degree and the 45 degree circumferential orientations of the fuel basket as defined in Figures 2.1.3 and 2.1.4 and are obtained using the finite element model described in Section 2.6.

The results for each MPC configuration for the two different drop orientations are evaluated for each appropriate load case listed in Tables 2.1.6 and 2.1.7. Analyses are performed only for the hot ambient temperature condition since this is the bounding case for the MPC; as noted in Section 2.6, allowable stresses are lower for the "heat" environmental condition.

- Elastic/Plastic Stability of the MPC Fuel Basket

Following the provisions of Appendix F of the ASME Code [2.1.12] for stability analysis of Subsection NG structures, (F1331.5(a)(1)), a comprehensive buckling analysis is performed using ANSYS. For this analysis, ANSYS's large deformation capabilities are used. This feature allows ANSYS to account for large nodal rotations in the fuel basket, which are characteristic of column buckling. The large deflection option is "turned on" so that equilibrium equations for each load increment are computed based on the current deformed shape. The interaction between compressive and lateral loading, caused by the deformation, is included in a rigorous manner. Subsequent to the large deformation analysis, the basket panel that is most susceptible to buckling failure is identified by a review of the results. The lateral displacement of a node located at the mid-span of the panel is measured for the range of impact decelerations. The buckling or collapse load is defined as the impact deceleration for which a slight increase in its magnitude results in a disproportionate increase in the lateral displacement.

The stability requirement for the MPC fuel basket under lateral loading is satisfied if two-thirds of the collapse deceleration load is greater than the design basis horizontal acceleration (Table 2.1.10). Figures 2.7.1, through 2.7.6 are plots of lateral displacement versus impact deceleration for representative fuel baskets. It should be noted that the displacements in Figures 2.7.1, 2.7.2, 2.73, 2.74, and 2.7.5 are expressed in 1×10^{-1} inch and Figure 2.7.6 is expressed in 1×10^{-2} inch. The plots clearly show that the large deflection collapse load of the MPC fuel basket is greater than 1.5 times the inertia load corresponding to the design basis deceleration for all baskets in all orientations. Thus, the requirements of Appendix F are met for lateral deceleration loading under Subsection NG stress limits for faulted conditions. Therefore, it is concluded that stability of the spent fuel basket cell walls is assured under the hypothetical accident side drop (from 30') condition of transport.

An alternative solution for the stability of the fuel basket panel is obtained using the methodology espoused in NUREG/CR-6322 [2.7.3]. In particular, the fuel basket panels are considered as wide plates in accordance with Section 5 of NUREG/CR-6322. Eq.(19) in that section is utilized with the "K" factor set to the value appropriate to a clamped panel. Material properties are selected corresponding to a metal temperature of 500 degrees F which bounds computed metal temperatures at the periphery of the basket. The critical buckling stress is:

$$\sigma_{cr} = \left(\frac{\pi}{K}\right)^2 \frac{E}{12\left(1-\nu^2\right)}\left(h/a\right)^2$$

where h is the panel thickness, a is the unsupported panel length, E is the Young's Modulus of Alloy X at 500 degrees F (Table 2.3.1), ν is Poisson's Ratio, and K=0.65 (per Figure 6 of NUREG/CR-6322).

Parameters appropriate to a MPC-24E basket are used; the following table shows the results from the finite element stress analysis and from the stability calculation.

Panel Buckling Results From NUREG/CR-6322			
Item	Finite Element Stress (ksi)	Critical Buckling Stress (ksi)	Factor of Safety
Stress	13.339	49.826	3.74

For a stainless steel member under an accident condition load, the recommended safety factor is 2.12. It is seen that the calculated safety factor exceeds this value; therefore, an independent confirmation of the stability predictions of the large deflection analysis is obtained based on classical plate stability analysis.

- <u>Overpack Stress Analysis (Load Cases 3 and 11 in Table 2.1.9)</u>

The overpack is assumed to be subject to a 60g side drop in the manner of the load combinations of Table 2.1.9 for both heat and cold environmental conditions as prescribed by Regulatory Guide 7.9. Reaction loads provided by the impact limiters are imposed as vertical pressures at each end of the overpack on areas of the structure that serve as backing. The applied mechanical loading is internal pressure, inertia load from the MPC and inertia load from the overpack self-weight. Figure 2.1.9 shows the assumed loading for this simulation. Figures 2.7.7, and Figures 2.7.11-2.7.13 are useful to aid in understanding the methodology used to apply the MPC loads and the balancing impact limiter reactions. Figure 2.7.7 shows a view of the overpack looking along the longitudinal axis for the general case of an oblique drop. While the intent of the figure is to describe the reaction loads from the impact limiter under a general oblique drop orientation, only the features necessary to elaborate on the side drop reaction load are discussed here. A region defined by the angle θ supports the applied loading in a side drop.

This angle is 18 degrees for the side drop and is chosen based on two considerations. First, the predictions from the theoretical model at the time of maximum "g" loading are examined and a projected loaded area on the top forging and bottom plate estimated. Second, the post-drop evaluation of the tested impact limiters from the one-eighth scale static test and the one-quarter scale dynamic test were visually examined and provided insight into the extent of the loaded region of the overpack at the impact limiter-hard surface interface. From these two evaluations, a conservatively low angle estimate is made for the finite element analysis. Figure 2.7.12 shows the extent around the periphery of the loading imposed by the MPC. From Section 2.6, the angle over which the MPC load is applied to the inner shell of the overpack is 72 degrees from the vertical on each half of the overpack. This angle is determined from the detailed analysis of the MPC enclosure shell and the fuel basket under 60g loading. The inertia load from overpack self-weight is applied by imposing an amplified value for the gravitational constant. Details of the finite element model have been discussed in Section 2.6. The results of the finite element analyses for load cases 3 and 11 in Table 2.1.9, for the overpack, are post-processed as previously discussed; Tables 2.7.5 and 2.7.6 summarize the results for each overpack component and identify the minimum safety factors.

2.7.1.3 Corner Drop

Figures 2.1.10 and 2.1.11 show the assumed loading for the bottom center of gravity over corner (CGOC) drop and the top CGOC drop, respectively. The impact limiter reaction load is applied as a pressure loading acting on two surfaces. From the geometry of the cask, with impact limiters in place, the angle of impact is 67.5 degrees from the horizontal plane. Although the theoretical and tested deceleration levels are below 60g's, the design basis 60g-deceleration load is used as the input loading and applied vertically. Therefore, a 55g load is applied along the longitudinal axis of the cask, and a 23g load is applied perpendicular to the cask longitudinal axis.

The lateral inertia load from the MPC, amplified by the appropriate multiplier corresponding to 23g's, is applied in the manner shown in Figures 2.7.11 and 2.7.12. The longitudinal component of the load from the MPC, amplified by 55g, is applied as a pressure over the inside surface of the lid as shown in Figure 2.7.8. In reality, the load would be applied over a narrow annulus near the outside radius of the lid because of the raised "landing region". To maximize lid and bolt stress, however, the load is applied as a uniform pressure in the finite element model. The corresponding lateral and longitudinal loads from the overpack self-weight are applied by imposing amplified gravitational accelerations in the appropriate directions.

The loading from the impact limiter at the other end of the overpack, not involved in the impact, is applied as a uniform pressure over the surface of the backed area at the other impact limiter. Figure 2.7.10 shows the loading on the outside surface of the bottom plate that arises from the bottom end impact limiter during simulation of a top end drop. The total bottom impact limiter weight is amplified by 55g's and applied as a pressure load. At the top end, where the impact limiter provides the distributed crush force to balance the inertia forces, the balancing reaction loads from the impact limiter are applied as a distributed side pressure loading and a distributed end surface pressure. The extent of the loaded region for this drop orientation is defined by the angle θ in Figure 2.7.7. For this case, the angle is approximately 68 degrees since a large "backed" area of the impact limiter is involved in resisting the crush. The angle is consistent with the predictions from the intersection geometry analysis used to develop the force-deformation data used in Appendix 2.A. That force-

crush model has been successfully used to predict maximum decelerations and extent of crush. Static finite element models require setting a fixed origin to insure satisfaction of all equilibrium equations. The center of gravity-over-corner orientation, in theory, provides automatic satisfaction of moment equilibrium so that all forces and moments at such a fixed origin location should be zero.

In this analysis and in the general oblique drop analysis, the fixed point is assumed at a location at the end of the overpack not impacted. The results from the finite element simulation confirm that the computed reactions are negligibly small compared to the applied loads. The loads from internal pressure are self -balancing and do not alter the calculation of equilibrium reactions. Tables 2.7.5 and 2.7.6 summarize the results from these analyses.

Results for the MPC and its internals have been discussed in Subsections 2.7.1.1 and 2.7.1.2 for the end and side drops, respectively, under the action of 60g deceleration and appropriate pressure loading. Under an oblique drop at an angle θ with respect to the target plane ($\theta = 0$ degrees equals the side drop), the MPC and its internals experience deceleration loads parallel and perpendicular to the MPC longitudinal axis. Each of these deceleration components, however, is less than the 60g design basis deceleration used in the end and side drop analyses. For the pure end drop, all stresses in the fuel basket and in the MPC canister (enclosure vessel) are axial. For the pure side drop, the conservative analysis of a 2-D section of the fuel basket and enclosure vessel gives rise to stresses in a plane perpendicular to the longitudinal axis of the MPC/fuel basket.

The results for any oblique drop can be obtained by a linear combination of the results for pure end drop and pure side drop. That is, the combined stress intensity is formed from the results of the two individual cases, after adjustment for the actual lateral and longitudinal "g" levels experienced by the components.

The MPC lid and baseplate are thick plate components; as such, the stress intensities experienced in the end drop orientation (which loads the lid and/or the baseplate in flexure) bound all other cases. Therefore, in what follows; only the enclosure vessel and the fuel basket need be considered. For each of these structures, the result "R_θ", at a general oblique drop angle θ, is expressed in terms of the result for an end drop "R_{90}" and the result obtained for a pure side drop "R_0" as:

$$R_\Theta = R_{90}\left(\frac{g_E}{60}\right) + R_0\left(\frac{g_S}{60}\right)$$

where g_E and g_S are the axial and lateral decelerations imposed on the MPC canister and fuel basket during the oblique drop at angle θ.

Since $g_E = 60 \sin\theta$, and $g_S = 60 \cos\theta$,

for a design basis oblique drop where the <u>vertical</u> deceleration is 60 g's, the result for the oblique drop is always expressed in the form,

$$R_\theta = R_{90} \sin\theta + R_0 \cos\theta$$

The following results are obtained for the end drop and side drop analyses:

End Drop:

Fuel Basket – maximum longitudinal membrane stress = 4,074 psi

Enclosure Vessel – maximum longitudinal compressive stress = 11,260 psi

The enclosure vessel result is obtained from the Code Case N-284 evaluation for a bottom end drop and conservatively bounds the result for a top end drop. The longitudinal compressive stress in the enclosure vessel includes the effect of external pressure.

Side Drop:

Stress intensity results for the fuel basket and enclosure vessel are summarized in Table 2.7.4. From Table 2.7.4, for the pure side drop, the minimum safety factor for the fuel basket is 1.17 (primary membrane plus primary bending). The corresponding minimum safety factor for the enclosure vessel is 2.64 (again, for primary membrane plus primary bending). The preceding results are obtained by surveying the summary of minimum safety factors in Table 2.7.4 for all MPC's and both fuel basket orientations within the MPC.

For the pure side drop orientation, the stress intensities (SI) associated with the minimum safety factors are:

Fuel Basket SI = 47,060 psi
Enclosure Vessel SI = 24,650 psi

The stress intensities at the most limiting location for the general oblique drop orientation are then computed as:

Fuel Basket SI = 4,074 sin θ + 47,060 cos θ

Enclosure Vessel SI = 11,260 sin θ + 24,650 cos θ

For the corner drop, θ = 67.5° leading to the following final results:

C.G. OVER CORNER DROP MPC SAFETY FACTORS			
Item	Calculated S.I.	Allowable S.I.	Safety Factor
Fuel Basket	21,773 psi	55,450 psi†	2.55
Enclosure Vessel	19,836 psi	65,200 psi ††	3.29

† at 725°F
†† at 450°F

As expected, the safety factors obtained for the corner drop are larger than the corresponding values obtained for the side drop.

Results for general oblique drop angles are now considered for the overpack. In particular, a 30-degree oblique drop is deemed to be most representative of a scenario where only a primary impact is involved. The general formula utilized in the preceding for the specific case of center-of-gravity-over-corner can also be used for a 30-degree drop angle. The following results are reported for the fuel basket and enclosure vessel.

30 DEGREE OBLIQUE DROP MPC SAFETY FACTORS			
Item	Calculated S.I. (psi)	Allowable S.I. (psi)	Safety Factor
Fuel Basket	42,792	55,450†	1.30
Enclosure Vessel	26,978	65,200††	2.42

† at 725°F
†† at 450°F

2.7.1.3.1 MPC "F Class" Enclosure Vessel Lid-to-Shell Weld

The Holtec MPCs labeled with the suffix "F" (designated as "F Class" in this subsection) are intended to store non-intact fuel (defined as damaged fuel in the latest revision of ISG-1 and "failed fuel and fuel debris" in this SAR).

To be certified to store loose fuel debris, the MPC must fulfill the function of the "secondary containment" required by 10CFR71.63(b). To qualify as a "secondary containment", the MPC Enclosure Vessel must be able to withstand the accident condition loading without releasing its contents. The accident condition mechanical loading for the secondary containment is identical to those for the primary containment, namely the inertia forces produced by a 60g deceleration. From Table 2.1.7, the pressure loads applicable to the MPC Enclosure Vessel during a hypothetical vertical end drop (Load Case E3.a) are the normal condition pressures. Therefore, per Table 2.1.1, the maximum pressure differential that exists across the MPC shell when a drop occurs is 60 psig. For conservatism, however, the accident condition internal pressure of 200 psig is used to qualify the MPC Enclosure Vessel as a secondary containment. All candidate vulnerable locations in the MPC Enclosure Vessel must be analyzed to ensure that a thru-wall breach in the pressure-retaining boundary does not occur under the loading combination defined above. In the case of the primary containment (the HI-STAR 100 overpack), the location of containment vulnerability is the cask lid-to-body forging bolted joint; the evaluation of the lid-to-body closure bolt has been analyzed to demonstrate containment integrity and the results of the evaluation summarized in Subsection 2.7.1.1 of the SAR. For the MPC "F Class", considered as secondary containment, the corresponding locations of vulnerability are the two extremities of the Enclosure Vessel where the vessel shell is joined to flat (plate-like) members.

The top lid-to-shell joint, a J-groove (partial penetration) joint made at the plant after fuel loading, is one candidate location, as this weld cannot be volumetrically examined even though the top lid is relatively thick. The MPC baseplate to the shell weld, on the other hand, is a shop-fabricated and volumetrically examined junction. However, because the baseplate is thinner than

the top lid, it may experience greater flexural action under the accident condition mechanical loading, resulting in somewhat greater junction region stresses. Therefore, the weld joints at both extremities of the MPC Enclosure Vessel are denoted as candidate locations whose structural integrity under the load combination appropriate to the MPC's secondary containment function must be demonstrated.

a. Top lid-to-shell joint

For MPCs with the "F" designation, this joint has been buttressed with a thick tapered shell and deeper J-groove weld than that utilized in the standard MPC Enclosure Vessel. A Holtec proprietary position paper, DS-213, "Acceptable Flaw Size in MPC Lid-to-Shell Welds", submitted to the NRC in support of the original certification of HI-STAR 100 in 1999 demonstrates that the largest postulated flaw in the most adverse orientation in the lid-to-shell joint in the "F" canister will not propagate under the impulsive inertia loading arising from a 60g axial deceleration of the MPC's contents.

An elastic stress analysis in the spirit of the ASME Code documented below likewise shows a large margin of safety against joint failure. For conservatism, the following assumptions are made.

i. The closure ring (the structural member present to provide a second welded barrier against leakage of the contents) is assumed to be absent.

ii. Even though a thru-wall failure of the joint is the appropriate failure criterion for the joint, non-exceedance of the ASME Code Section III Subsection NB stress intensity limits appropriate to Level D limits, which will occur at a much lower loading level, is set down as the acceptance limit. However, no weld efficiency factor is applied to the lid-to-shell weld since it is not required by Subsection NB.

iii. The MPC model with the heaviest contents (MPC-32) is used in the analysis to bound the results for all "Type F" MPC models.

The MPC top lid may be fabricated as a single thick circular plate, or may by fabricated as a dual lid with the outer lid attached to the shell with the "J" groove weld, and the inner lid attached to the outer lid around the common periphery. The dual lid configuration has been analyzed for both Normal Conditions of Transport and Hypothetical Accident Conditions of Transport for MPC's carrying intact fuel; the results are documented in Subsection 2.6.1.3.1.2, and 2.7.1.1, respectively. The evaluation for the "F Class" MPC to provide secondary containment capability utilizes the same analytical model but introduces additional assumptions into the analysis to direct load to the lid-to-shell weld. In particular, a top end drop is postulated with the dual lids subjected to a 60g deceleration loading from the fuel, fuel basket, and lid weight, together with the accident internal pressure of the MPC. During a top end drop, the MPC cannot rotate relative to the HI-STAR overpack because of close clearances between the vessel shell and the inner surface of the overpack cavity. Therefore, regardless of the angle of impact, the reaction load from the HI-STAR to equilibrate the applied loads on the lid is uniformly distributed around the circumference. A bounding condition for this analysis for secondary containment is presumed to

be a top end drop where the Enclosure Vessel shell is assumed to contact the support (the HI-STAR lid) before the Enclosure Vessel lid; with this conservative assumption, the peripheral weld is subject to the entire applied load. The key results from the analyses (the case of dual lids bounds the analysis assuming a single thick lid) to support qualification of the MPC "F Class" as secondary containment are summarized in the table below:

KEY RESULTS FOR SECONDARY CONTAINMENT QUALIFICATION OF F CLASS MPC's – Load Case E3.a in Table 2.1.7 (Top End Drop)			
Item	Stress Intensity (ksi) or Load (lb)	Allowable Stress Intensity @ 550 Degrees F (ksi) or Load Capacity (lb)	Safety Factor
Structural Lid Bending Stress Intensity	46.05	60.7	1.32
Shield Plug Bending Stress Intensity	46.65	60.7	1.30
Lid-to-Shell Weld Load	5,268,000	6,627,000	1.26
Primary Local Axial Membrane Stress Intensity at Shell Contact Interface	24.53	40.45	1.65

b. Baseplate-to-Shell Joint

Because the baseplate-to-shell connection is a volumetrically examined, full penetration joint, flaw propagation under the accident condition inertia loads is not a concern for this location. As in the case of the top lid-to-shell junction, the baseplate-to-shell joint is established to be sufficiently robust if the stress intensity limits under the above load combination (appropriate for §71.63(b)) are below their corresponding limits for level D condition for Section III Class 1 (NB) components. Since the baseplate-to-shell joint in the MPC "F Class" units is identical to the joint in the MPC's used for intact fuel, no new analyses are required. The results of evaluation of this joint are reported in Subsection 2.7.1.1 and demonstrate substantial safety factors.

The above analyses demonstrate that the Enclosure Vessel for "Type F" MPCs is capable of serving as a "secondary containment" as required by §71.63(b).

2.7.1.4 Oblique Drops

Appendix 2.A contains results of analytical simulations for various orientations of the cask at impact. In Appendix 2.A, it is shown that lateral decelerations are large for the near side drop (slapdown) and decrease as the angle of orientation, with respect to the horizontal plane, increases. Therefore, it is likely that results presented in Subsections 2.7.1.1 through 2.7.1.3 are bounding for all orientations other than the near side drop (slapdown) in that at any other angle, the resulting g-loads in each direction (longitudinal and lateral) are smaller than the bounding deceleration loads applied in the end, side, and corner drops. Nevertheless, based on the results obtained in Appendix 2.A, the case of an oblique drop with primary impact at 30 degrees from the horizontal is analyzed in detail. This case covers all orientations where the maximum deceleration load occurs and is reacted by the primary impact limiter. For this case, moment equilibrium includes inertia loads from overpack rotation as well as linear deceleration. For the 30-degree drop orientation at the primary impact location, the design basis deceleration load is applied with 52g lateral component and 30g longitudinal component. The loads are applied in the same manner as discussed in Subsection 2.7.1.3 with one additional complication. In contrast to the center of gravity over corner orientation where moment equilibrium is automatically satisfied when the loads are correctly applied, the applied loads and the reaction loads from the impact limiter are not initially in moment equilibrium. No inertial loading due to overpack rotational motion at the instant being considered is included. Without an additional inertial moment loading component, a large reaction force would develop at the far-removed arbitrary fixed reference point because the impact limiter reaction loads are offset from the overpack and MPC inertia loads from the linear decelerations. Figure 2.7.14 shows the overpack in a general oblique orientation. Appropriate arrows show the impact limiter reaction forces and the components of the applied linear decelerations. The loads from the MPC are not shown on the figure but they are applied as previously described for the corner drop. It is clear that moment equilibrium is not satisfied unless reaction loads develop at the arbitrarily chosen fixed support location far removed from the impact point. In the real drop scenario, since there is only a primary impact reaction, the cask must have angular accelerations imposed to insure moment equilibrium since the fixed point is an artifact to meet the requirements of the finite element analysis. To zero this reaction load at the point far-removed from the impact location, an additional load case with a unit angular velocity imposed at the mass center of the system and no other loads is developed. An angular acceleration is internally generated by ANSYS for this load case. The solution to this load case provides a reaction at the hypothetical fixed point assumed at the end of the overpack far removed from the impact location to balance the imposed inertial moment. The addition of this load case, with proper magnitude and sign ascribed to the input angular velocity, serves to eliminate all reactions at the far-removed fixed point. By adding this inertia moment load case, both force and moment equilibrium equations are satisfied for the oblique drop case where there is only a single impact limiter providing external forces to react the cask motion. With reference to Figure 2.7.7, the extent of the impact limiter loaded region on the overpack for this case is $\theta = 63$ degrees. This angle is estimated from the projected geometry from the theoretical analysis in Appendix 2.A. Figure 2.7.9 shows a side view of the top forging with the end loading from the impact limiter applied as a pressure over the loaded region.

The finite element solution provides stress intensity results for the hot and cold conditions. The safety factors are summarized in Tables 2.7.5 and 2.7.6 (identified as Load Cases 20 and 21 corresponding to the "heat" and "cold" environmental conditions).

The near side drop with impact at the secondary impact limiter (slapdown) is a special case that also merits detailed analysis. For this case, the angle of the cask with the target is near zero degrees, similar to that used for the side drop analysis. The nature of the equilibrium equations is quite different, however. For the side drop, Figure 2.7.17 shows that equilibrium is satisfied by impact limiter reaction pressures at both impact locations. The reaction lateral pressure distribution at each impact limiter is distributed in the manner described by Figure 2.7.7. For the side drop evaluation, no introduction of a rotational component to the overpack is required to insure moment equilibrium. For the analysis of the near side drop secondary impact case, all of the reaction force required to insure that force equilibrium is maintained under the inertia induced loads, is imposed at the location of the secondary impact limiter. Figure 2.7.18 shows a side view of the overpack with the reaction load applied over a specified arc in the same manner as described by Figure 2.7.7. At the time of peak secondary impact deceleration, the theoretical analysis predicted minimal axial deceleration. Therefore, to perform the stress analysis using the finite element model, no axial deceleration is imposed. Referring to Figure 2.7.7, the angle θ for this evaluation is chosen on the basis of observed experimental results and theoretical prediction. The angle is related to the angle associated with the observed crush depth of the impact limiter itself. For a near side drop, the outer diameter of the impact limiter is known, and if the crush depth is observed, calculated, or measured, the angular extent of impact limiter crushed material is easily determined. The outer radius, "Ri" of the impact limiter, and the observed and calculated crush depth (see results in Appendix 2.A for a full scale impact limiter), "d", are:

$Ri = 64"; \quad d = 15"$

Therefore, the angle "φ" (on either side of a vertical diameter through the impact limiter) that is associated with the extent of loaded crushed surface of the impact limiter is obtained from simple geometry as:

$\mathrm{Cos}(\varphi) = 1\text{-}d/Ri$

The angle over which the load is applied at the crushed surface of the impact limiter is calculated to be:

$\varphi = 40$ degrees (measured from the vertical, on both sides of the vertical centerline).

The angle of significant reaction loads on the interface surface of the top forging, is greater than this angle. However, it is conservative to perform the finite element analysis of the "slapdown" secondary impact event, using the load angle

$\theta = \varphi = 40$ degrees.

Note that this angle used for the "slapdown" evaluation is larger than the conservative value used to evaluate the side drop. This reflects the increased crush imparted to the impact limiter since the entire amplified load is reacted at the top end. The load from the MPC is imposed on the appropriate inside surface of the inner shell as a uniform load in the same manner as for the side drop analysis. Moment equilibrium is provided by imposing the additional pure rotation on the overpack sufficient to generate opposite reaction forces that zero out the combined reactions at the "balance point" from

the applied inertia decelerations plus the pure rotation case. Because the MPC is constrained within the overpack, no departure from a uniform load transfer to the overpack is anticipated. Therefore, the enforcement of moment equilibrium for this condition is ensured solely by the determination of a proper balancing moment by determining an appropriate angular acceleration for the overpack. This assumption has little effect on the computation of the primary stress intensity distribution that results from the impact.

The results of the analysis are tabulated and combined with other load conditions, and the combined load case is designated as "Load Case 22". Bolt preload, internal pressure, and the inertia loads are combined to form this "slapdown" simulation. The top-end secondary impact analysis reported herein bounds a similar analysis of the bottom end secondary impact case. Summary results for minimum safety factors are reported in Table 2.7.5 only for the "Heat" environmental condition as previous results have demonstrated that this case produces the minimum safety factors. Only primary stress intensities are surveyed and reported in accordance with ASME requirements. Also evaluated is the bolt stress, the net friction force, and the state of the seals and lands. From the post-processed results, it is concluded that no bolts are overstressed, no portion of the seals suffer unloading, and that there is sufficient frictional force to insure that the lid is maintained in position.

The preceding discussion focussed on the transport overpack analyses. The minimum safety factors for the MPC fuel basket and enclosure vessel, for arbitrary drop orientation, are obtained from the general formulation in the preceding subsection 2.7.1.3. The angle that provides the maximum combined stress intensity (S.I.) can be determined by classical means, and the minimum safety factor established. The results are summarized in the table below:

GENERAL OBLIQUE DROP ORIENTATION MPC – SAFETY FACTORS				
Item	Drop Orientation Angle (Degrees)	Calculated S.I. (psi)	Allowable S.I. (psi)	Safety Factor
Fuel Basket	4.54	47,208	55,450	1.17
Enclosure Vessel	24.55	27,100	65,200	2.41

2.7.1.5 Comparison with Allowable Stresses

Tables 2.7.4 through 2.7.8 summarize the limiting safety factor obtained for each hypothetical free drop accident condition of transport defined by the requirements of Regulatory Guide 7.9. In particular, Table 2.7.4 is a summary of safety factors from the analyses of the MPC fuel basket and enclosure vessel, and Tables 2.7.5 and 2.7.6 report safety factors from the overpack analyses. Finally, Tables 2.7.7 and 2.7.8 contain safety factor summary results from miscellaneous evaluations reported within the text. From these results, tables are constructed that summarize limiting safety factors for all of the hypothetical accident conditions of transport that are associated with drop events. Tables 2.7.1 through Tables 2.7.3 present the overall summary of the most limiting safety factor for each of the components of interest for all hypothetical accident conditions of transport. It is concluded from these tables that large factors of safety exist in the fuel basket, in the MPC shell, and in the various components of the overpack under all hypothetical accident conditions of

transport associated with free drop events.

It is noted that the overpack finite element results are developed using a 3-D model of the overpack. Even though symmetry conditions reduce the size of the model, there are over 8000 elements and 11000 nodes.

The postulated accident conditions all tend to load localized regions of the overpack. As an illustration, consider Load Case 20, the 30-degree oblique top-end impact with the target. The limiting results for safety factors are reported in Table 2.7.5. Figures 2.7.15 and 2.7.16 show stress intensity distributions for the inner shell and for the assemblage of intermediate shells, respectively. As expected, the regions of highest stress intensity are naturally concentrated near the impacted region.

2.7.2 Puncture

- Overpack Structural Components

10CFR71 mandates that a puncture event be considered as a hypothetical accident condition. For this event, it is postulated that the package falls freely through a distance of 1 meter and impacts a 6 inch diameter mild steel bar. The effects of the puncture drop are most severe when the steel bar is perpendicular to the impact surface. Therefore, all puncture analyses assume that the bar is perpendicular to the impact surface. It is assumed that the steel bar has a flow stress equal to 48,000 psi, which is representative of mild steel. The maximum resisting force can then be calculated as

$$F_R = \frac{\pi D^2}{4} \, x \, 48{,}000 \; psi = 1.357 \, x \, 10^6 \; lb$$

where D equals the diameter of the steel bar.

$$|A_p| = \frac{F_R \, g}{W}$$

Since the maximum force applied to the cask is limited to the above value, the average deceleration of the cask can be computed assuming it to be rigid. The average deceleration of the cask (plus contents) (weight = W) is determined as:

For a bounding (low) weight of 230,000 lb. (Table 2.2.1), for example, the rigid body average deceleration over the time duration of impact, is 5.9g.

Candidate locations for impact that have the potential to cause the most severe damage are near the center of the closure plate (top-end puncture), the center of the bottom plate (bottom puncture), and the center height of the overpack shells (side puncture). In accordance with Regulatory Guide 7.9, local damage near the point of impact and the overall effect on the package must be assessed.

An estimate of local puncture resistance is obtained by using Nelms' equation [2.7.1] that is

generally applicable only for lead backed shells. Nevertheless, it is useful to obtain an indication as to whether a potential problem exists in the HI-STAR 100 System. The equation is applied using an ultimate strength of 70,000 psi that is appropriate for the selected impact regions. Nelms' equation predicts a minimum thickness of material necessary to preclude significant puncture damage. For the HI-STAR 100 System,

$$t_m = \left(W / S_u \right)^{0.71} = 2.65 \quad inch$$

Inasmuch as the HI-STAR 100 overpack has substantially more material thickness in the baseplate, the closure plate, the top flange and the inner plus the initial intermediate shell, the overpack meets local puncture requirements as required by Nelms' equation.

The global effects of puncture are calculated using the overpack model described in Section 2.6, which is the same model that is used for the drop assessments. Figures 2.1.12 through 2.1.14 show free body diagrams of the overpack for the side, top, and bottom puncture events, respectively. In each case, the nodes on the surface of the overpack that directly impact the steel bar are fixed in all degrees of freedom. By then applying acceleration, A_p, a reaction force develops at those nodes equal in magnitude with F_R. Tables 2.7.5 and 2.7.6 summarize the safety factors for the overpack components obtained for the puncture acceleration computed above for both heat and cold environmental conditions. Note that for the stress intensities in the lid and baseplate, the highest stresses are exactly under the impact point. The results include the effect of the interface contact stress between the puncture pin and the plate surface. This local effect is not required to be included in the stress intensity comparison with allowable values for the hypothetical accident. Therefore, in the reporting of safety factors, the effect of local surface pressure is not included; rather, the radial and tangential stresses at the load point are used to form the stress intensity and set the lateral surface stress to zero. Tables 2.7.5 and 2.7.6 specifically identify this item by a note. Figure 2.7.17 shows the stress intensity distribution in the lid resulting from a top-end puncture analysis. The localized nature of the stress intensity distribution is clearly evident. The reported safety factors in the summary tables are adjusted to eliminate the effect of non-primary stress components.

- <u>Closure Bolts</u>

The methodology to analyze closure bolts is provided in reference [2.6.3] prepared for analysis of shipping casks. The analysis of the overpack closure bolts under normal conditions of transport, in accordance with the provisions of [2.6.3], has been reported in Section 2.6. In this subsection, the similar analysis for the hypothetical puncture accident is summarized. The analysis follows the procedures defined in Reference [2.6.3] and uses the allowable stresses for the closure bolts in that reference.

The following combined load case is analyzed for the hypothetical pin puncture accident condition of transport.

Puncture: Pressure, temperature, and pre-load loads are included.

Reference [2.6.3] reports safety factors defined as the calculated stress combination divided by the allowable stress for the load combination. This definition of safety factor is the inverse of the definition consistently used in this SAR. In summarizing the closure bolt analysis, results are reported using the SAR safety factor definition of allowable stress divided by calculated stress. The following result for closure lid bolting for the top end drop hypothetical accident condition of transport is obtained.

Overpack Closure Bolt - Safety Factor (Load Case 7 in Table 2.1.9)	
Item	Safety Factor on Bolt Tension
Average Tensile Stress in Bolt	1.86

2.7.3 Thermal

In this subsection, the structural consequences of the thirty-minute fire event are evaluated using the metal temperature data from Section 3.5 where a detailed analysis of the fire and post-fire condition is presented. Specifically, it desired to establish that:

1. The metal temperature, averaged across any section of the containment boundary, remains below the maximum permissible temperature for the Level A condition in the ASME Code for NB components. Strictly speaking, the fire event is a Level D condition for which Subsection NB of the ASME Code, Section III does not prescribe a specific metal temperature limit. The Level A limit is imposed herein for convenience because it obviates the need for creep considerations to ascertain post-fire containment integrity.

2. The external skin of the overpack, directly exposed to the fire will not slump (i.e., suffer rapid primary creep). This condition is readily ruled out for steel components if the metal temperature remains below 50% of the metal melting point.

3. Internal interferences among the constituents of the HI-STAR 100 System do not develop due to their differential thermal expansion during and after the fire transient.

4. Overpack closure bolts will not unload during a transport fire.

5. The helium retention boundary and the containment boundary both continue to perform their function as ASME "NB" pressure vessels.

2.7.3.1 Summary of Pressures and Temperatures

The following peak temperatures (per Tables 3.5.4 and 3.4.11) and pressures are used in Subsections 2.7.3.2, 2.7.3.3, and 2.7.3.4.

Overpack closure plate/bolts	514 degrees F (post-fire)
Overpack bottom plate	662 degrees F (post-fire)

Overpack outer closure	226 degrees F (initial pre-fire cold temperature); 1348 degrees F (maximum)
Overpack containment shell	395 degrees F (MPC –Shell post-fire temp. - increment of 24 degrees F (from data in Table 3.4.11))
MPC-Shell	419 degrees F (post-fire)
Basket (center)	751 degrees F (post-fire)
Basket (periphery)	478 degrees F (MPC-Shell post fire + 59 degrees F - (from data in Table 3.4.11))

It should be noted that the overpack containment shell, closure plate, and bottom plate temperatures are not specifically reported in Table 3.5.4. The temperatures listed above are based on the closest temperature report location. The overpack containment shell temperature is the lowest temperature that occurs prior to the fire accident and is used for the differential thermal expansion analysis. The overpack containment shell temperature falls (post-fire) below the outside basket temperature and subsequently lags the basket temperature by 24 degrees F. The 24 degree F lag is the same lag that occurs in the normal heat condition listed in Table 3.4.11 (i.e., 306 degrees F for the MPC outer shell surface - 282 degrees F for the overpack inner surface). This will maximize the potential for interference between the overpack and the MPC. Similarly, the temperature difference between the MPC shell and the fuel basket periphery will be essentially the same exists in the normal heat conditions of transport. Therefore, from Table 3.4.11, the basket peripheral temperature for the fire event analyses is set as the MPC shell temperature plus the maximum difference (365-306) degrees F from the table.

Subsection 3.5.3 contains a discussion of the peak bulk temperatures occurring during and after the fire transient. It is concluded in that section that:

1. The containment boundary protected by the intermediate shells remains below 500 degrees F (SA-203-E material).
2. The containment boundary that is within the confines of the impact limiters remains below 700 degrees F (SA-350 LF3 material).
3. The portion of the containment boundary directly exposed to the fire may have local outer surface temperatures in excess of 700 degrees F, but the bulk metal temperature of the material volume remains under 700 degrees F (SA-350 LF3 material).

The conclusions in Subsection 3.5.3 enable the statement that the containment boundary metal bulk temperatures remain at or below the upper limits permitted by the ASME Code. Therefore, stress evaluations that make comparisons to allowable stresses to demonstrate that the containment boundary continues to perform as a viable pressure vessel use allowable stresses that are given in the ASME Code (i.e., there is no extrapolation of allowable stresses beyond the recognized code limits). For the helium retention boundary stress calculations, however, allowable stresses for a conservatively high temperature (see Table 2.1.2 and 2.1.21) are used when pressure vessel code compliance is demonstrated.

From Table 3.5.4 in Subsection 3.5.4 of Chapter 3, it is concluded that:

The maximum temperature of the ferritic steel material in the body of the HI-STAR 100 overpack (the outer enclosure and the intermediate shells outside of the containment boundary is well below 50% of the material melting point. (The melting point of carbon and low alloy steels is approximately 2750 degrees F, per Mark's Standard Handbook, Ninth Edition, pp 6-11.)

The shielding experiences temperatures above its stated limit for effectiveness. This means that a limited loss of shielding effectiveness may occur. The shielding analysis in Chapter 5 (Subsection 5.1.2) recognizes this and conservatively assumes that all shielding is lost in post-fire shielding analyses.

Pressures during the fire transient are bounded by the internal and the external design pressures for accident conditions for the MPC shell as stated in Section 2.1. For internal pressure, Table 3.5.3 supports this conclusion. The following calculation is presented to support the conclusion for MPC external pressure.

The overpack annulus initial fill pressure is 14 psig (max.) per the specification in Chapter 7. The overpack annulus lower bound fill temperature is 70 degrees F. The fire condition MPC shell peak temperature is 419 degrees F per Table 3.5.4 and the use of this as the average gas temperature in the annulus is conservative.

Using the above data, the fire condition peak pressure in the annulus between the overpack and the MPC shell is calculated by using the ideal gas law with constant volume assumed in the gap as:

p_{fire}= (14+14.7) x (419 + 460)/(70 + 460) = 47.6 psia = 32.9 psig.

2.7.3.2 Differential Thermal Expansion

The methodology for establishing that there will be no restraint of free thermal expansion has been presented in Subsection 2.6.1.2 for normal conditions of transport. The same methodology is applied in this subsection to evaluate the potential for component interference during and after the postulated hypothetical fire. For conservatism, use the temperatures in the overpack and the MPC temperatures that will maximize the potential for interference between the overpack and the MPC regardless of at what point in time the temperatures occurred. It is shown that there is no structural restraint of free-end expansion in the axial or radial directions under the most limiting temperature difference between the hot basket and the colder overpack/enclosure vessel. Thus, the ability to remove fuel by normal means is not inhibited by structural constraint of free-end expansion. The table below summarizes the results obtained for the limiting MPC temperature distributions assumed.

THERMOELASTIC DISPLACEMENTS IN THE MPC AND OVERPACK UNDER FIRE CONDITION				
CANISTER - FUEL BASKET				
	Radial Direction(in.)		Axial Direction (in.)	
Worst Case Unit	Initial Clearance	Final Gap	Initial Clearance	Final Gap
Bounding MPC	0.1875	0.117	2.0	1.672

CANISTER – OVERPACK				
	Radial Direction (in.)		Axial Direction (in.)	
Worst Case Unit	Initial Clearance	Final Gap	Initial Clearance	Final Gap
Bounding MPC	0.09375	0.004	0.625	0.291

Using the most conservative assumptions (i.e., do not consider a real "snapshot" in time during and after the fire, but rather assume the most detrimental temperature distribution occurs at the same instant in time) that maximize the potential for interference, it is demonstrated that no restraint of free thermal expansion in either the radial or axial directions occurs.

2.7.3.3 Stress Calculations

Under the fire accident, pressures in the MPC and overpack increase simultaneously, while the allowable strengths of the material may decrease from their values under normal conditions of transport. The MPC and overpack stresses are shown below (allowables are taken from Tables 2.1.21). It is required that both the helium retention boundary and the containment boundary meet Level D Service Limits of the ASME Code and continue to function as pressure vessels.

2.7.3.3.1 MPC

- Top Closure

The MPC Top Closure analysis for the fire condition is Load Case E5 in Table 2.1.7. The top closure is conservatively modeled as a simply supported plate considered to be loaded by the accident internal pressure plus self-weight acting in the same direction. For determination of the safety factor, the value of allowable stress from Table 2.1.20 appropriate to the fire temperature is used. The table below summarizes the result (where a multiplier of 2.0 has been incorporated to reflect the bounding dual lid design):

MPC Top Closure Safety Factor for Load Case E5 in Table 2.1.7			
Item	Value (ksi)	Allowable (ksi)	Safety Factor
Bending Stress	3.158 x 2	54.23	8.59

- Baseplate

Under the fire accident condition, the baseplate is subject to accident internal pressure (200 psi). If the HI-STAR 100 is assumed to be in the vertical position, then the baseplate also may support the weight of the fuel basket and the fuel loading. If the HI-STAR 100 is assumed to be oriented in the horizontal position, then the baseplate supports only internal pressure. For a conservative analysis, it is assumed that the internal pressure stress and the stress from basket weight and from fuel weight add. This Load Case E5 is summarized below. The second row is the result that is obtained if the basket and fuel weight is neglected.

MPC Baseplate Safety Factor under Hypothetical Fire Accident			
Item	Value (ksi)	Allowable (ksi)	Safety Factor
Baseplate Bending Stress (Including Basket and Fuel Weight)	46.32	54.23	1.17
Baseplate Bending Stress (Neglecting Basket, Fuel, and Self Weight)	42.28	54.23	1.28

- Shell

The MPC shell is examined for elastic/plastic stability under the fire accident external pressure using the ASME Code Case N-284 analysis method. The result from the stability analysis for Load Case E5 in Table 2.1.7 is summarized below:

MPC Canister Safety Factor - Stability under External Accident Pressure			
Item	Calculated Interaction Factor	Allowable Interaction Factor	Safety Factor
Elastic Stability	0.845	1.00	1.18

The shell is also analyzed for stress under the accident internal pressure by using the Lame' solution previously used in Section 2.6. The stress due to the internal accident pressure of 200 psi is (P = pressure, r = MPC radius, t = shell thickness):

$$\sigma_1 = \frac{Pr}{t} = \frac{(200\text{ psi})(68.375\text{ in}/2)}{0.5\text{ in}} = 13{,}675\text{ psi}$$

$$\sigma_2 = \frac{Pr}{2t} = 6{,}838\text{ psi}$$

$$\sigma_3 = -P = -200\text{ psi}$$

The maximum stress intensity is $\sigma_1 - \sigma_3 = 13{,}875$ psi

The safety factor is,

$$SF = \frac{36.15\text{ ksi}}{13.875\text{ ksi}} = 2.61$$

2.7.3.3.2 Overpack

The overpack stresses for normal heat conditions of transport are reported in Section 2.6. Since these stress solutions are based on linear elasticity, the stresses reported can be scaled up to account for the accident internal pressure and the safety factor computed based on the allowable stress for the fire temperature.

Generally, in the fire accident case, only primary stresses are of interest to demonstrate continued containment. Secondary stresses may be included in the evaluation, but they merely demonstrate additional levels of conservatism. Table 2.6.4 gives the minimum safety factor for the primary stress case of $T_h + P_i + F + W_s$.

The highest stress occurs in the inner shell, and has the value 2,832 psi.

The ratio of the accident pressure to normal pressure is (see Table 2.1.1) $\frac{200}{100} = 2.00$.

Using this factor, the safety factor is computed as follows:

For the inner shell at 500 degree F fire temperature per Table 2.1.14, the allowable membrane stress intensity under the fire condition is compared to the amplified mean stress and the safety factor computed as

$$SF = \frac{42.5\text{ ksi}}{(5.664 + 0.200)\text{ ksi}} = 7.25$$

2.7.3.3.3 Closure Bolts

Under the fire transient, it is required to demonstrate that the stresses in the closure bolts do not exceed allowable limits and the bolted joint does not unload to the extent that the pressure boundary is breached. To that end, an analysis of the fire condition is carried out with the purpose of determining the bolt stresses under the applied loading. The methodology employed for this analysis is that presented in the report, "Stress Analysis for Closure Bolts for Shipping Casks" [2.6.3]. The loadings applied are fire temperature, bolt preload, and accident internal pressure. The following result for closure lid bolting for the hypothetical fire accident is obtained.

Overpack Closure Bolt - Safety Factor (Load Case 19 in Table 2.1.9)	
Combined Load Case	Safety Factor on Bolt Tension
Average Tensile Stress	1.69

The average bolt tensile stress under the conditions of pressure, preload, and thermal effects appropriate to the hypothetical fire accident condition of transport is 8.5% greater than the average bolt tensile stress computed under the normal heat condition of transport. Therefore, it is concluded that there will be only minor unloading of the bolted joint and no breach of containment.

2.7.3.3.4 Bounding Thermal Stresses During the Fire Transient

Regulatory Guide 7.6, Section C.7 states that the extreme total stress intensity range between the initial state and accident conditions should be less than twice the adjusted value of the alternating stress intensity at 10 cycles given by the appropriate fatigue curves. It is demonstrated here that under very conservative assumptions on the calculation of thermal stresses, this regulatory requirement is met by the HI-STAR 100 System.

Under the fire transient, thermal gradients can lead to secondary or peak stresses due to local constraint by adjacent material that is at a lower temperature. The ASME Code does not require that secondary stresses be held to any limit for Level D Service Conditions. Nevertheless, bounding calculations are performed here to estimate the magnitude of the thermal stress. The most limiting secondary stress intensity state arises by conservatively assuming complete restraint of material by surrounding cooler material and has the solution:

$$|\sigma| = E\,\alpha\,\Delta T$$

where

E =	Young's Modulus at temperature
α =	coefficient of linear thermal expansion
ΔT =	temperature change from 70 degrees F, the assumed assembly temperature

For the fuel basket, ΔT = 775 - 70 = 705 degrees F. The use of 775 degrees F is justified as follows:

The peak temperature of the fuel basket is 950 degrees F during the fire per Table 2.1.2. For a conservative estimate of the temperature between *two adjacent points* on the fuel basket, use the bounding hypothetical accident temperature limit for the enclosure vessel lid or baseplate from Table 2.1.2 as representative of the change between *two adjacent points* on the fuel basket. Therefore, no extrapolation of data is required for the calculations to follow.

From the material property table for Alloy X,

$$E = 24.282 \times 10^{6} \text{ psi}$$
$$\alpha = 9.853 \times 10^{-6} \text{ inch/inch- degree F}$$

Therefore,

$$\sigma = 24.282 \times 9.853 \times 705 = 168{,}672 \text{ psi}$$

The conservative assumption is made that the maximum peak stress intensity due to mechanical loading plus thermal constraint occur at the same point at the same instant in time and reaches the value of S_u at room temperature. Thus, the total stress intensity range from assembly to this hypothetical conservative state is

$$S_R = 168{,}672 + 75{,}000 = 243{,}672 \text{ psi}$$

The alternating stress intensity range, after accounting for temperature effects of Young's Modulus, is

$$S_a = \frac{S_R}{2} x \frac{\text{Young's Modulus (70° F)}}{\text{Young's Modulus (775° F)}}$$
$$= 121{,}836 \text{ psi } x \frac{28.14}{24.282} = 141{,}194 \text{ psi}$$

For the overpack, the most severely constrained material is at the bottom plate. Material properties for this calculation are the values available at 700 degrees F and the peak temperature is conservatively set at 700 degrees F.

Young's Modulus = E = 24.9×10^{6} psi (at 700 degrees F)

Coefficient of linear thermal expansion = $\alpha = 7.52 \times 10^{-6}$ inch/inch-degrees F (Estimated)

Therefore, the secondary stress intensity due to fully constrained thermal growth is

$$\sigma = 24.9 \times 7.52 \times (700\text{-}70) = 117{,}966 \text{ psi}$$

Conservatively, assuming that the membrane plus primary bending stress intensity achieves the ultimate strength at room temperature, at the same location in space and at the same instant in time, gives the total stress intensity range at this hypothetical location as

$$S_R = 117{,}966 + 75{,}000 = 192{,}966 \text{ psi}$$

The alternating stress intensity range, after accounting for temperature effects of Young's Modulus, is

$$S_a = \frac{192{,}966}{2} x \frac{28.14}{24.9} = 109{,}037 \text{ psi}$$

These computed values for bounding alternating stress intensities are used in the next subsection for comparisons with allowable values.

2.7.3.4 Comparison of Fire Accident Results with Allowable Stresses

Stress

The safety factors for the MPC and overpack during a fire are addressed in Section 2.7.3.3. The lowest safety factors are 1.18 and 7.74 for the MPC and overpack, respectively.

Bounding Fire Transient

In accordance with Regulatory Position C.7 of the Regulatory Guide 7.6, Figure I-9.2.1 of ASME, Section III, Appendix I, gives the 10-cycle alternating stress intensity range as

S_{ALT} (Alloy X) = 700,000 psi

Using the calculated stress intensity range from Subsection 2.7.3.3, the safety factor for the MPC basket is

$$SF = \frac{700{,}000}{141{,}194} = 4.96$$

Figure I-9.1 of ASME Section III, Appendix I is used for the overpack even though the temperature is limited to below 700 degrees F. It is conservative to use this curve for this short time event since increased temperatures will improve the material ductility. From that table, the 10-cycle alternating stress intensity range is given as 400,000 psi. Therefore using the aforementioned calculated results for stress intensity range from Subsection 2.7.3.3, the safety factor is computed as:

$$SF = \frac{400{,}000}{109{,}037} = 3.67$$

An analysis of the threaded holes in the top closure has been performed to assess the length of

engagement and stress requirements imposed on the connection by the transport loads. The methodology used to evaluate the connection is that set forth in Machinery's Handbook and uses the specific characteristics of the threaded joint. As part of the calculation, it is demonstrated that the bolt force required to maintain the seal (seal seating load plus pressure force) is only 27% of the total bolt preload force that must be applied to ensure bolt performance under the various drop scenarios. That is, there is 73% excess capacity. Therefore, the momentary joint decompression due to the hypothetical fire accident is not sufficient to unload the seal.

The above calculations demonstrate that the requirements of Paragraph C.7 of Regulatory Guide 7.6 are satisfied.

2.7.4 Immersion - Fissile Material

In order for the spent nuclear fuel in the HI-STAR 100 System to become flooded with water, a leak must develop in both the overpack containment structure and the MPC enclosure vessel. The analysis provided demonstrates that both the overpack containment boundary and the MPC enclosure vessel meet the applicable stress and stress intensity allowables for normal conditions of transport and hypothetical accident conditions. Therefore, no leak will develop.

10CFR71.73(c)(5) specifies that fissile material packages, in those cases where water inleakage has not been assumed for criticality analysis, must be evaluated for immersion under a head of water of at least 0.9 m (3 ft.) in the attitude for which maximum leakage is expected. The criticality analyses presented in Chapter 6 conservatively assumes flooding with water at optimum moderation. Therefore, this paragraph is not applicable. However, analysis is presented to demonstrate that there is no water inleakage and verify that the flooded assumption made in the criticality analysis is conservative.

A head of water at a depth of 0.9 m (3 ft.) is equal to 1.3 psi. This pressure is bounded by the MPC enclosure vessel normal condition of transport and hypothetical accident condition external pressures listed in Table 2.1.1. The head of water (1.3 psi) is also bounded by the hypothetical accident condition external pressure for the overpack. Analysis provided in this chapter demonstrates that both the overpack containment boundary and the MPC enclosure vessel meet the applicable stress and stress intensity allowables for normal conditions of transport and hypothetical accident conditions. Therefore, there is no in-leakage of water into the overpack or MPC under a head of water at a depth of 0.9 m (3 ft.).

2.7.5 Immersion - All Packages

Deep submergence of the HI-STAR 100 System in 200 meters (656 ft.) of water creates an external pressure load equal to 284 psi, which is less than the external design pressure of 300 psi. This condition is established as Load Case 18 in Table 2.1.9. Since the containment boundary is not punctured, stability of the package can be evaluated considering an undamaged package. The results for an external pressure of 300 psi bound the results for 21.7 psi gauge pressure that is established in 10CFR71.73(c)(6) as the applicable external pressure for this evaluation. The elastic/plastic stability of the overpack has been examined using the methodology of ASME Code Case N-284. In the analysis, all structural resistance to the external pressure is conservatively concentrated in the inner

containment shell. No credit is given to any structural support by the intermediate shells. The external pressure is assumed to act directly on the outer surface of the inner containment shell and the secondary fabrication stress is assumed to add to the stress due to the deep submergence pressure. The results for this case are summarized below:

Overpack Stability using ASME Code Case N-284 - Load Case 18 in Table 2.1.9			
Item	Value from Interaction Curve	Allowable Interaction Curve Value	Safety Factor
Yield Stress Limit	0.577*	1.34	2.32*
Elastic Stability	0.253	1.0	3.95

* Applicable to inner shell fabricated from SA203-E material. Safety factor must be multiplied by 0.93 if inner shell is fabricated from optional SA350-LF3 material.

It is noted that Code Case N-284 imposes limits on both stress and stability and includes a built-in safety factor of 1.34 for the Level D Service Limit. Therefore, the first row in the table above reports the true safety factor existing against exceeding the yield stress in the inner containment shell; the second row in the table provides the safety factor against elastic instability of the inner shell. The large values for the safety factors that are obtained, even with the conservative assumptions, attests to the ruggedness of the inner containment shell.

The analysis performed above for a 300 psi external pressure also confirms that the package meets the requirements of 10CFR71.61 that a 290 psi external pressure can be supported without any instability.

2.7.6 Summary of Damage

The results presented in Subsections 2.7.1 through 2.7.5 show that the HI-STAR 100 System meets the requirements of 10CFR71.61 and 10CFR71.73. All safety factors are greater than 1.0 for the hypothetical accident conditions of transport. Therefore, the HI-STAR 100 package, under the hypothetical accident conditions of transport, has adequate structural integrity to satisfy the subcriticality, containment, shielding, and temperature requirements of 10CFR71.

Table 2.7.1

MINIMUM SAFETY FACTORS FOR THE MPC FUEL BASKET UNDER HYPOTHETICAL ACCIDENT CONDITIONS OF TRANSPORT

Load Case Number	Load Combination†	Safety Factor	Location in SAR where Calculations or Results are Presented
F3			
F3.a	D + H', end drop	4.19	Subsection 2.7.1.1; Table 2.7.7
F3.b	D + H', 0° side drop	1.16	Table 2.7.4
F3.c	D + H', 45° side drop	1.28	Table 2.7.4

† The symbols used for loads are defined in Subsection 2.1.2.1.

Table 2.7.2

MINIMUM SAFETY FACTORS FOR THE MPC ENCLOSURE VESSEL
FOR HYPOTHETICAL CONDITIONS OF TRANSPORT

Load Case Number	Load Combination†	Safety Factor	Location in SAR where Calculations or Results are Presented	
E3				
E3.a	$D + H' + P_o$, end drop	1.4 3.04 1.92	Lid Baseplate Shell	Table 2.7.7 Table 2.7.7 Table 2.7.7
E3.b	$D + H' + P_i$, 0 deg. side drop	2.14 1.16	Shell Supports	Table 2.7.4 Table 2.7.4
E3.c	$D + H' + P_i$, 45 deg. side drop	2.74 1.51	Shell Supports	Table 2.7.4 Table 2.7.4
E5	P_i^* or P_o^*	8.59 1.17 1.18 (buckling) 4.16 (mean stress)	Lid Baseplate Shell	Table 2.7.7 Table 2.7.7 Table 2.7.7 Subsection 2.7.3.3.1

† The symbols used for loads are defined in Subsection 2.1.2.1.

Table 2.7.3

MINIMUM SAFETY FACTORS FOR THE OVERPACK
FOR HYPOTHETICAL ACCIDENT CONDITIONS OF TRANSPORT

Load Case Number	Load Combination†	Safety Factor	Location in SAR where Calculations or Results are Presented
1	$T_h + D_{ba} + P_i + F + W_s$	2.16	Table 2.7.8
2	$T_h + D_{ta} + P_i + F + W_s$	1.75	Table 2.7.5
3	$T_h + D_{sa} + P_i + F + W_s$	2.19 (see note 2)	Table 2.7.5
4	$T_h + D_{ea} + P_i + F + W_s$	1.49	Table 2.7.5
5	$T_h + D_{ga} + P_i + F + W_s$	2.60 (see note 2)	Table 2.7.5
6	$T_h + P_s + P_i + F + W_s$	2.80 (see note 2)	Table 2.7.5
7	$T_h + P_t + P_i + F + W_s$	2.03 (see note 1)	Table 2.7.5
8	$T_h + P_b + P_i + F + W_s$	1.46	Table 2.7.5
9	$T_c + D_{ba} + P_o + F + W_s$	4.17	Table 2.7.6
10	$T_c + D_{ta} + P_o + F + W_s$	1.87	Table 2.7.6
11	$T_c + D_{sa} + P_o + F + W_s$	2.19	Table 2.7.6
12	$T_c + D_{ea} + P_o + F + W_s$	1.73	Table 2.7.6
13	$T_c + D_{ga} + P_o + F + W_s$	2.65	Table 2.7.6
14	$T_c + P_s + P_o + F + W_s$	3.05	Table 2.7.6
15	$T_c + P_t + P_o + F + W_s$	2.09 (see note 1)	Table 2.7.6
16	$T_c + P_b + P_o + F + W_s$	1.46	Table 2.7.6
17	$T_f + P_i + F + W_s$	pre-load maintained	Subsection 2.7.3.4
18	P_o*	2.32	Table 2.7.8
19	$P_i^* + T_f + F + W_s$	7.25	Subsection 2.7.3.3.2
20	$T_h + D_{ga} + P_i + F + W_s$	1.77	Table 2.7.5
21	$T_c + D_{ga} + P_i + F + W_s$	1.84	Table 2.7.6
22	$T_c + D_{ga} + P_i + F + W_s$	2.14 (see note 2)	Table 2.7.5

Note: 1. This reported stress is directly under the point of impact. Therefore, the calculated value does not represent a primary stress; however, primary stress levels are met by this peak stress intensity.

2. Applicable to inner shell fabricated from SA203-E material. Safety factor must be multiplied by 0.93 if inner shell is fabricated from optional SA350-LF3 material.

† The symbols used here are defined in Subsection 2.1.2.1.

Table 2.7.4 - FINITE ELEMENT ANALYSIS RESULTS
MINIMUM SAFETY FACTORS FOR MPC COMPONENTS UNDER ACCIDENT CONDITIONS

Component - Stress Result	MPC-24		MPC-32		MPC-68	
	30 Ft. Side Drop, 0° Orientation Load Case F3.b or E3.b	30 Ft. Side Drop, 45° Orientation Load Case F3.c or E3.c	30 Ft. Side Drop, 0° Orientation Load Case F3.b or E3.b	30 Ft. Side Drop, 45° Orientation Load Case F3.c or E3.c	30 Ft. Side Drop, 0° Orientation Load Case F3.b or E3.b	30 Ft. Side Drop, 45° Orientation Load Case F3.c or E3.c
Fuel Basket – Primary Membrane (P_m)	2.80	3.85	2.78	3.90	3.07	4.30
Fuel Basket - Local Membrane Plus Primary Bending ($P_L + P_b$)	1.19	1.29	1.19	1.28	2.64	1.56
Enclosure Vessel - Primary Membrane (P_m)	6.43	6.88	5.77	6.95	5.65	7.13
Enclosure Vessel - Local Membrane Plus Primary Bending ($P_L + P_b$)	4.24	4.28	2.14	3.56	3.07	2.74
Basket Supports - Primary Membrane (P_m)	N/A	N/A	2.72	3.83	6.68	8.68
Basket Supports - Local Membrane Plus Primary Bending ($P_L + P_b$)	N/A	N/A	3.89	4.75	1.16	1.51

Table 2.7.4 (Continued) - FINITE ELEMENT ANALYSIS RESULTS
MINIMUM SAFETY FACTORS FOR MPC COMPONENTS UNDER ACCIDENT CONDITIONS

Component - Stress Result	MPC-24E/EF	
	30 Ft. Side Drop, 0 deg Orientation Load Case F3.b or E3.b	30 Ft. Side Drop, 45 deg Orientation Load Case F3.c or E3.c
Fuel Basket – Primary Membrane (P_m)	2.75	3.80
Fuel Basket - Local Membrane Plus Primary Bending ($P_L + P_b$)	1.16	1.28
Enclosure Vessel - Primary Membrane (P_m)	6.41	6.88
Enclosure Vessel - Local Membrane Plus Primary Bending ($P_L + P_b$)	3.15	4.14

Table 2.7.5 - FINITE ELEMENT ANALYSIS RESULTS
MINIMUM SAFETY FACTORS FOR OVERPACK COMPONENTS UNDER ACCIDENT CONDITIONS (Hot Environment)

Component – Stress Result	30 Ft. Bottom End Drop Load Case 1	30 Ft. Top End Drop Load Case 2	30 Ft. Side Drop Load Case 3	30 Ft. C.G. Over-the-Bottom-Corner Drop Load Case 4
Lid – Local Membrane Plus Primary Bending ($P_L + P_b$)	34.04	1.75	2.60	7.76
Inner Shell – Local Membrane Plus Primary Bending ($P_L + P_b$)	4.35 (Note 2)	10.02 (Note 2)	2.19 (Note 2)	2.93 (Note 2)
Inner Shell – Primary Membrane (P_m)	4.48 (Note 2)	7.39 (Note 2)	2.45 (Note 2)	2.33 (Note 2)
Intermediate Shells - Local Membrane Plus Primary Bending ($P_L + P_b$)	6.63	7.95	2.33	1.49
Baseplate - Local Membrane Plus Primary Bending ($P_L + P_b$)	7.05	21.6	4.71	2.78
Enclosure Shell - Primary Membrane (P_m)	16.44	12.23	2.19	5.48

Notes:
1. Load cases are defined in Table 2.1.9.
2. Applicable to inner shell fabricated from SA203-E material. Safety factor must be multiplied by 0.93 if inner shell is fabricated from optional SA350-LF3 material.

Table 2.7.5 (Continued) - FINITE ELEMENT ANALYSIS RESULTS
MINIMUM SAFETY FACTORS FOR OVERPACK COMPONENTS UNDER ACCIDENT CONDITIONS (Hot Environment)

Component - Stress Result	30 Ft. C.G. Over-the-Top-Corner Drop Load Case 5	Side Puncture Load Case 6	Top End Puncture Load Case 7	Bottom End Puncture Load Case 8	30 Ft. – 30 degree Drop Load Case 20	30 Ft. – Slapdown Load Case 22
Lid – Local Membrane Plus Primary Bending ($P_L + P_b$)	3.69	5.70	2.03 (See Note 2)	6.29	1.77	2.22
Inner Shell – Local Membrane Plus Primary Bending ($P_L + P_b$)	3.16 (Note 3)	2.80 (Note 3)	29.29 (Note 3)	9.52 (Note 3)	2.78 (Note 3)	2.73 (Note 3)
Inner Shell – Primary Membrane (P_m)	2.60 (Note 3)	5.95 (Note 3)	26.5 (Note 3)	10.61 (Note 3)	2.45 (Note 3)	2.14 (Note 3)
Intermediate Shells - Local Membrane Plus Primary Bending ($P_L + P_b$)	3.52	6.19	32.52	15.12	3.28	2.88
Baseplate - Local Membrane Plus Primary Bending ($P_L + P_b$)	6.95	21.62	28.62	1.46	27.32	17.9
Enclosure Shell - Primary Membrane (P_m)	3.56	4.53	51.32	29.9	8.02	2.40

Notes:
1. Load cases are defined in Table 2.1.9.
2. Stress Intensity computed just outboard of the loaded area since surface stress is not a primary stress component.
3. Applicable to inner shell fabricated from SA203-E material. Safety factor must be multiplied by 0.93 if inner shell is fabricated from optional SA350-LF3 material.

Table 2.7.6 - FINITE ELEMENT ANALYSIS RESULTS
MINIMUM SAFETY FACTORS FOR OVERPACK COMPONENTS UNDER ACCIDENT CONDITIONS (Cold Environment)

Component – Stress Result	30 Ft. Bottom End Drop Load Case 9	30 Ft. Top End Drop Load Case 10	30 Ft. Side Drop Load Case 11	30 Ft. C.G. Over-the-Bottom-Corner Drop Load Case 12
Lid – Local Membrane Plus Primary Bending ($P_L + P_b$)	30.29	1.87	2.73	8.00
Inner Shell – Local Membrane Plus Primary Bending ($P_L + P_b$)	4.17	9.69	2.19	2.94
Inner Shell – Primary Membrane (P_m)	4.37	7.33	2.47	2.36
Intermediate Shells - Local Membrane Plus Primary Bending ($P_L + P_b$)	4.95	8.66	2.61	1.73
Baseplate - Local Membrane Plus Primary Bending ($P_L + P_b$)	7.73	17.07	4.80	2.73
Enclosure Shell - Primary Membrane (P_m)	20.08	18.4	2.45	5.71

Notes: 1. Load cases are defined in Table 2.1.9.

Table 2.7.6 (Continued) - FINITE ELEMENT ANALYSIS RESULTS
MINIMUM SAFETY FACTORS FOR OVERPACK COMPONENTS UNDER ACCIDENT CONDITIONS (Cold Environment)

Component – Stress Result	30 Ft. C.G. Over-the-Top-Corner Drop Load Case 13	Side Puncture Load Case 14	Top End Puncture Load Case 15	Bottom End Puncture Load Case 16	30 Ft.. – 30 degree Drop Load Case 21
Lid – Local Membrane Plus Primary Bending ($P_L + P_b$)	3.91	5.91	2.09 (See Note 2)	6.64	1.84
Inner Shell – Local Membrane Plus Primary Bending ($P_L + P_b$)	3.21	3.05	24.97	8.54	2.78
Inner Shell – Primary Membrane (P_m)	2.65	7.60	17.03	9.59	2.48
Intermediate Shells - Local Membrane Plus Primary Bending ($P_L + P_b$)	4.10	7.06	27.55	14.9	3.81
Baseplate - Local Membrane Plus Primary Bending ($P_L + P_b$)	7.08	29.69	47.25	1.46	21.91
Enclosure Shell - Primary Membrane (P_m)	4.13	5.17	57.21	76.5	9.64

Notes: 1. Load cases are defined in Table 2.1.9.
2. Surface pressure not included in safety factor evaluation since it is not a primary stress.

Table 2.7.7

MINIMUM SAFETY FACTORS FOR MISCELLANEOUS ITEMS - MPC FUEL BASKET/CANISTER - HYPOTHETICAL ACCIDENT CONDITIONS OF TRANSFER

Item	Loading	Safety Factor	Location in SAR Where Calculations or Results are Presented
Fuel Basket Axial Stress	End Drop	4.19	Subsection 2.7.1.1
Fuel Basket Axial Stress	Fire Transient (Regulatory Position C.7 of Regulatory Guide 7.6)	4.96	Subsection 2.7.3.4
MPC Canister Stability	30' End Drop (Load Case E3.a, Table 2.1.7)	1.92	Subsection 2.7.1.1
MPC Top Closure Lid Bending Stress	30' End Drop (Load Case E3.a in Table 2.1.7)	2.8 (single lid) 1.4 (dual lid)	Subsection 2.7.1.1
MPC Top Closure Lid – Loading in Peripheral Weld	30' End Drop (Load Case E3.a in Table 2.1.7)	2.37	Subsection 2.7.1.1
MPC Baseplate Bending Stress	30' End Drop (Load Case E3.a in Table 2.1.7)	3.04	Subsection 2.7.1.1
MPC Canister at Connection to Baseplate	30' End Drop (Load Case E3.a in Table 2.1.7)	2.14	Subsection 2.7.1.1
MPC Top Closure Lid Bending Stress	Fire accident (Load Case E5 in Table 2.1.7)	8.59	Subsection 2.7.3.3.1
MPC Baseplate Bending Stress	Fire accident (Load Case E5 in Table 2.1.7)	1.17	Subsection 2.7.3.3.1
MPC Canister Stability	Fire accident (Load Case E5 in Table 2.1.7)	1.18	Subsection 2.7.3.3.1
MPC Shell Mean Stress	Fire accident (Load Case E5 in Table 2.1.7)	4.16	Subsection 2.7.3.3.1

Table 2.7.8

MINIMUM SAFETY FACTORS FOR MISCELLANEOUS ITEMS - OVERPACK - HYPOTHETICAL ACCIDENT CONDITIONS OF TRANSPORT

Item	Loading	Safety Factor	Location in SAR Where Calculations or Results are Presented
Overpack Stability	30' End Drop (Load Cases 1 and 2 in Table 2.1.9)	2.16*	Subsection 2.7.1.1
Closure Bolts	30' End Drop (Load Case 2 in Table 2.1.9)	1.30	Subsection 2.7.1.1
Closure Bolts	Top End Puncture	1.86	Subsection 2.7.2
Overpack Inner Shell Mean Stress	Fire Transient	7.25	Subsection 2.7.3.3.2
Closure Bolts	Fire Transient	1.69	Subsection 2.7.3.3.3
Overpack Stress	Fire Transient (Regulatory Position C.7 of Regulatory Guide 7.6)	3.67	Subsection 2.7.3.4
Overpack Stability (Yield Stress Criteria)	Immersion (Load Case 18 in Table 2.1.9)	2.32*	Subsection 2.7.5
Overpack Stability (Stability Criteria)	Immersion (Load Case 18 in Table 2.1.9)	3.95	Subsection 2.7.5

* Applicable to inner shell fabricated from SA203-E material. Safety factor must be multiplied by 0.93 if inner shell is fabricated from optional SA350-LF3 material.

APPENDIX 2.A:
DESIGN, TESTING, AND COMPUTER SIMULATION OF THE AL-STAR™ IMPACT LIMITER

2.A.1 INTRODUCTION

As stated in Subsection 2.7, the central purpose of the AL-STAR™ impact limiter is to limit the package maximum deceleration, α_{max}, under a postulated drop event to a specified design value. For the regulatory 9-meter hypothetical free drop event, the AL-STAR design is engineered to limit the maximum rigid body deceleration to 60 times the acceleration due to gravity (Table 2.1.10). The HI-STAR packaging, consisting of the loaded overpack and top and bottom impact limiters (illustrated in Figure 2.A.1.1) is essentially a cylindrical body with a rigid interior (namely, the overpack) surrounded by a pair of relatively soft crushable structures. The crushable structure (impact limiter) must deform and absorb the kinetic energy of impact without detaching itself from the overpack, disintegrating, or otherwise malfunctioning. A falling cylindrical body may theoretically impact the target surface in an infinite number of orientations; the impact limiter must limit the HI-STAR 100 decelerations to below 60g's and preserve the limiter-to-overpack connection regardless of the impact orientation. Figure 2.A.1.2 presents the side drop event. In general, a drop event orientation is defined by the angle of the HI-STAR 100 longitudinal axis, θ, with the impact surface. In this notation, $\theta = 0$ means a side drop and $\theta = 90°$ implies a vertical or end drop scenario. Inasmuch as the top and bottom impact limiter are made of identical crush material, the top or bottom vertical drop events are mathematically and physically equivalent as far as the impact limiter design is concerned. In any orientation, the drop height is measured from the lowest point on the package.

An intermediate value of θ, $\theta = 67.5°$, warrants special mention. At $\theta = 67.5$ degrees, the point of impact is directly below the center of gravity (C.G.) of the HI-STAR 100 package. This drop orientation is traditionally called the C.G.-over-corner (CGOC) configuration. The CGOC orientation is the demarcation line between single and dual impact events. At $90° > \theta > 67.5°$, the leading end of the packaging (denoted as the "primary" impact limiter) is the sole participant in absorbing the incident kinetic energy. At $\theta < 67.5°$ drop orientations, the initial impact and crush of the leading (primary) impact limiter is followed by the downward rotation of the system with the initial impact surface acting as the pivot, culminating in the impact of the opposite (secondary) impact limiter on the target surface. In the dual impact scenarios, the first and second impact limiter crush events are referred to as the "primary" and "secondary" impacts, respectively. It is reasonable to speculate that for certain values of θ, the secondary impact may be the more severe of the two. As stated earlier, the design of AL-STAR must ensure that $\alpha_{max} \leq 60$, regardless of the value of θ.

The AL-STAR attachment design must ensure that both impact limiters remain attached to the cask during and after the impact event. The impact limiters are also required to prevent cask body-to-unyielding target contact.

Finally, the package design must satisfy all criteria in ambient temperature conditions ranging from -20° to 100°F, and with humidity ranging from 0 to 100%. Therefore, the impact limiter design must be functionally insensitive to temperature and environmental conditions.

An aluminum honeycomb-based impact limiter design was selected as the preferred material for development. The detailed design of the AL-STAR impact limiters is presented in Holtec Drawing C1765 located in Section 1.4. A pictorial view of AL-STAR is presented in Figure 2.A.1.3.

Figure 2.A.1.3 indicates that in addition to the crushable honeycomb, the AL-STAR contains two internal cylindrical shells (also denoted as "rings"), which are stiffened with radial gussets. These carbon steel shells are sized to behave as undeformable surfaces during impact events. They are essentially the "backbone" of the impact limiter, lending a predictability to the impact limiter crush behavior and forcing the energy absorption to occur in the honeycomb metal mass. The design of this backbone structure was a subject of in-depth computer and experimental 1/8 scale static testing, as documented in Holtec Report HI-962501 [2.A.4] and summarized in Section 2.A.4 herein.

Another noteworthy aspect of the AL-STAR impact limiter design is the arrangement of uniaxial and cross core (biaxial) honeycombs. Regions of the honeycomb space that experience impact loading in only one direction are equipped with unidirectional honeycomb sectors. The regions where the direction of the impact loads can vary have cross-core (bi-directional) honeycomb material, as detailed in Subsection 2.3.1.5.

To summarize, the design objectives of the AL-STAR impact limiter are set down as five discrete items, namely:

i. Limit peak deceleration (α_{max}) to 60g's under all potential drop orientations.

ii. Impact limiter must not detach from the cask under a 9-meter drop event, under any impact orientation.

iii. The impact limiters must bring the cask body to a complete stop, such that the overpack does not come in physical contact with the target surface.

iv. Crush material must be equally effective at -20° and 100°F, with humidity ranging from 0 to 100%.

v. All external surfaces must be corrosion-resistant.

The last two objectives are realized by utilizing aluminum honeycomb (Type 5052) as crush material and stainless steel (Type 304), for the external skin enclosure. As shown in the ASME Code (Section II, Part D, Table Y-1), the essential property of the constituent material for the honeycomb and the external skin, namely the yield strength remains constant in the -20° F to

100° F range. The surface of the carbon steel impact limiter backbone is painted to limit corrosion.

The remaining design objectives, namely, limiting of the maximum rigid body deceleration, α_{max}, to 60 g's under a 9-meter drop event, maintaining positive attachment of the AL-STAR impact limiters to the overpack, and preventing contact of the overpack with the unyielding surface, are demonstrated by a combination of numerical simulations and scale model static and dynamic testing. This was accomplished through a research and development effort that is broadly subdivided into six phases, as follows:

Phase 1: Characterize the honeycomb pressure-deflection relationship.

Phase 2: Propose a force (static) vs. crush (F vs. d) model for AL-STAR.

Phase 3: Perform 1/8 scale model static compression tests to validate the force-crush model and to establish the adequacy of the AL-STAR backbone structure.

Phase 4: Conduct 9-meter quarter-scale model dynamic drop tests in selected limiting drop configurations and obtain test data.

Phase 5: Simulate the experimental drop tests with a suitable "dynamic model" and establish that the dynamic model predictions of deceleration, crush and event time duration reasonably match the experimentally measured values. A reasonable prediction of the peak decelerations of each drop event is the minimum for the dynamic model to be acceptable.

Phase 6: Utilize the experimentally confirmed dynamic model to evaluate the effects of tolerances on crush properties and on package weight, and to confirm the adequacy of the full-scale impact limiter design.

It is of crucial importance that the dynamic model benchmarked in Phase 5 be of high reliability, since it becomes the analytical model for the accident-event response prediction of the packaging when tolerances on material behavior and package mass are considered (Phase 6).

In this appendix, a description of the overall program and results for each of the six phases is presented.

2.A.2 Phase 1: Material Pressure-Crush Relationship

The extent of deflection, Δ, sustained by a honeycomb material when subjected to a uniform pressure, p, is an essential element of information in the impact limiter design. Towards this end, coupon specimens of uniaxial and cross-core honeycomb of various nominal crush strengths and densities were compression-tested by the material manufacturer. The results showed that all honeycomb coupons shared some common load-deflection characteristics, namely:

The initial pressure-deflection curve resembled an elastic material (pressure roughly proportional to deflection).

Upon reaching a limiting pressure, the material crushed at near constant pressure until the crush reached approximately 60-70 percent of the initial thickness. The required crush force had to increase rapidly to achieve small incremental crushing for strains beyond approximately 60-70 percent.

Figure 2.A.2.1 shows a typical static pressure-deflection curve for a 1"-thick honeycomb specimen. The curve with the initial peak is that of an un-precrushed honeycomb specimen; the curve without the peak (shown as a dashed line only where a difference occurs) corresponds to a pre-crushed specimen. Dynamic testing subsequently showed that removal of the initial peak by pre-crushing the material was a desired feature whenever a large flat area of honeycomb material experienced a crush force (such as in a 90 degree end drop).

Curve fitting of data from all tested coupons indicated that a single mathematical relationship between the applied pressure and compression strain could be developed. The mathematical relationship can provide a reasonable fit for coupons of all crush strengths (crush strength defined as the pressure corresponding to the flat portion of the curve in Figure 2.A.2.1; i.e., it is the constant pressure at which the honeycomb undergoes near-perfect plastic deformation). In other words, the pressure, p, for a given strain, ε, is represented by a unique function of the crush pressure, p_c, i.e.

$$p = f(p_c, \varepsilon)$$

The relationship between p and compression strain was used in the subsequent mathematical efforts to simulate AL-STAR crush behavior. The above mathematical relation was developed to simulate material behavior for a honeycomb material under both non-pre-crushed and pre-crushed conditions.

2.A.3 Phase 2: Static Force-Crush Prediction Model

An essential step towards the development of a reliable dynamic model to simulate the impact of a dropped HI-STAR 100 package is to develop a static force-crush model that can subsequently be validated by scale model tests. The force-crush model should reliably duplicate the resistance provided by an impact limiter for a range of crush orientations for the full range of crush depths.

The required force-crush model for AL-STAR is developed using the concept of interpenetration, which is explained using the case of the side drop ($\theta = 0$) as an example (Figure 2.A.3.1(a)).

The condition existing in all impact limiter drop scenarios is that the relatively soft honeycomb material lies between two "hard" surfaces that are advancing towards each other during the impact. One of these two rigid surfaces is the essentially unyielding target (Rigid Body 1) and

the other is the structural backbone of the impact limiter (Rigid Body 2). While the target surface is flat, the backbone structure is cylindrical in profile. When squeezed between the two surfaces, the honeycomb material (at each instant in time) will crush at one or both interface locations. To determine which interface surface will undergo crushing at a given point during the impact event, the concept of interpenetration area is utilized as explained below.

In this concept, two separate crush scenarios, one assuming that the crush occurs at the external interface (target-to-impact limiter), and the other assuming that the crushing is at the internal interface (structural backbone/overpack-to-impact limiter), are compared at each instant during a simulated compression of the impact limiter. A metal honeycomb impact limiter, in general, may have multiple honeycomb material sections crushing at each interface. For simplicity in explaining the concept of interpenetration, we assume that each of the interfaces is characterized by a uniform distribution of honeycomb having crush pressures p_1 and p_2, respectively. To determine the resistive force developed to crush the impact limiter by a small amount, d, against the external target, the impact limiter is assumed to penetrate the target by the amount "d" without deformation. The resulting area A_1 for the case of side drop, illustrated in Figure 2.A.3.1(b), can be computed as an algebraic expression in the amount of approach, d. (For oblique drop events, ANSYS [2.A.1] or CADKEY [2.A.2] are used to compute interpenetration area as a function of incremental interpenetration.) The pressure-compression relationship for the honeycomb stock at the external interface provides the crush pressure p_1 that develops due to deformation "d". The total force required for crush "d", at the external interface, is therefore equal to p_1A_1.

In the second (independent) scenario, the impact limiter external surface is assumed to undergo no movement; rather, the backbone structure (along with the overpack) advances towards the target by an amount d (Figure 2.A.3.1(c)). Once again, assuming that the cylindrical rigid body moves through an amount "d", the resistance pressure developed in the honeycomb material lying in the path of penetration is available from the appropriate material pressure-compression curve. If the pressure corresponding to the deformation is p_2 and the projected area at the internal interface is A_2, then the total resistive force encountered in realizing an approach equal to "d" between the overpack-backbone assemblage and the target under this latter scenario is p_2A_2. In an actual drop event, at each instant during the event, incremental crush occurs at one of the two interfaces. If $p_1A_1 < p_2A_2$ at a given instant then crushing will occur at the external interface. Likewise, $p_1A_1 > p_2A_2$ will imply that crushing will occur internal to the impact limiter. The smaller of p_1A_1 and $p_2 A_2$ is the required crush force and the corresponding location of crush is where the honeycomb material will compress to realize the approach equal to d. This "inequality test" to determine where crushing occurs is performed at every increment of crush during the simulation of the event. The appropriate value of the crush force is used in the equilibrium equations at that instant. The concept of interpenetration at two interfaces has been confirmed during testing of the impact limiters; the total crush is observed to be a sum of compression at each of the two interfaces.

To construct a mathematical force-deformation relationship for AL-STAR in any given orientation, the above process is repeated as the crush "d" is increased in small increments starting with the beginning of compression (d = 0). It is quite clear that the development of the

force-deflection model (F-d model) for AL-STAR in any orientation is a straightforward analysis in 3-D geometry. The F-d curve for AL-STAR for any given value of θ can be developed where, other than the geometry of the impact limiter, the crush strengths p of the honeycomb materials utilized in the impact limiter are the only other required inputs.

The force (F) vs. crush (d) relationship developed using the foregoing method is referred to as the F-d model that is subject to validation by appropriate 1/8 scale model compression tests described in the following section.

2.A.4 Phase 3: One-Eighth Scale Model Static Compression Tests

The 1/8 scale model tests consist of subjecting scaled replicas of the full-size AL-STAR to static compression tests in an engineered fixture such that the force-compression curve for the scaled model can be obtained in various orientations of compression. The scale model is made by making the diameters and length of the model one-eighth of the full-size AL-STAR. The thicknesses of the backbone components (i.e., the inner and outer shells and gussets), and the external skin (see Figure 2.A.1.3) are also scaled to one-eighth times the corresponding dimensions (to the nearest sheet metal gage, where applicable) in the full-size AL-STAR. In the one-eighth model, the performance of the attachment system is not assessed nor is the cask body modeled. However, the interface between overpack and impact limiter where the compression load is resisted is properly simulated. The crush pressure is a material property of the energy absorbing material; therefore, the material (and its density) is not scaled. The 1/8 scale model, therefore, has approximately $(1/8)^3$, or 1/512 the volume and weight of the full-size unit. Holtec documents [2.A.3, 2.A.4] provide complete details on the 1/8 scale model geometry and fabrication. The static compression behavior of such a 1/8-scale model is correlated with that of a full-size unit using the geometric scaling information. For example, under an axial compression test the area under crush in the scale model will be 1/64 of the full-size AL-STAR (recall that the diameter is scaled down by a factor of 8). Therefore, the crush force (which is crush force pressure times the area under crush) will be 1/64 of the full-size unit. On the other hand, the crush stroke (extent of deformation before "lock up") will be 1/8 of the full-size AL-STAR because the axial length of the scale model (which corresponds to the height of the crush column in axial compression) is one-eighth of the full-size hardware. Thus, the total energy absorbed (force times compression) will be $(1/8)^3$ of the full-size unit. The same scaling factor can be shown to apply in all directions of crush.

In summary, the 1/8 scale model scales the geometric dimensions of AL-STAR. The previously discussed F-d model is required to translate the force-crush relationship from the 1/8 scale replica to the full-size unit. In order to use the analytical F-d model as a valid vehicle for predicting the force-crush of the full-size (or quarter-scale) AL-STAR, it is necessary to check its prediction ability against actual test data from 1/8-scale model static compression tests.

The objectives of static scale model tests are twofold:

i. Determine whether the static force-crush relationship predicted by the F-d model appropriately simulates the actual relationship determined by test;

ii. Determine whether the backbone structure of the AL-STAR impact limiter is sufficiently rigid to withstand and transmit the large loads associated with the postulated accident scenarios.

2.A.4.1 Static Compression Tests on Initial Candidate Crush Material

To assess compression performance, a QA validated AL-STAR static test procedure was prepared [2.A.3] for the one-eighth scale model static compression tests and a series of cold and hot static compression tests performed on an impact limiter configuration with the initial candidate crush material. Holtec calculation package HI-961501 [2.A.4] contains a comprehensive documentation of the 1/8 scale static test program and results for the impact limiter configuration. A summary of the complete test program and test results is presented below.

Four 1/8-scale models were fabricated with details of the impact limiter carefully scaled, including the stiffening cylinders and the stainless steel skin. No impact limiter attachment bolts were incorporated in the model.

Aluminum honeycomb segments provided for the 1/8-scale models were manufactured utilizing the same procedures and processes as for the full-scale impact limiter. As stated earlier, the crush strengths were not scaled because they are considered as material properties.

An adjustable 1/8 scale static test fixture was designed, analyzed, and fabricated. The test fixture interfaced with the impact limiter and simulated the overpack hard surface. The test fixture could be adjusted to simulate any crush orientation. Figure 2.A.4.1 shows the test fixture and the 1/8 scale impact limiter being loaded in the heavy-load testing machine.

The following static one-eighth scale test series were carried out:

Test No.	Orientation, degrees	Temperature
1	0 (side)	+120°F
2	30 (oblique)	Ambient
3	60 (oblique)	Ambient
4	90 (end)	-30°F

For all tests except the end compression (where the orientation is immaterial), the circumferential orientation of the impact limiter was selected so that the initial point of contact between the impact limiter and the test machine was at the interface of two aluminum honeycomb secttions. After each test, the impact limiters were cut open and examined.

Observations Based on 1/8 Scale Model Testing

- Effect of Ambient Temperature:

  The end compression test was performed with the impact limiter cold (-30°F), the side compression test was performed with the impact limiter hot (+120°F), and the two oblique tests performed at ambient temperature. The material behavior showed no influence of test temperature. This confirms the expected result since the aluminum honeycomb and stainless steel skin yield strengths are insensitive to temperature in the range of interest (-20° F to 100° F) as prescribed in Table Y-1 of the ASME Code.

- Side compression orientation - 0 degree:

  The inner stiffening cylinder experienced considerable permanent deformation. The gussets which buttress the inner cylinder buckled. The outer stiffening cylinder performed elastically.

- Oblique compression orientation:

  Two oblique orientation static tests were performed. The 30-degree oblique test again showed the need to thicken the inner stiffening cylinder and to rearrange the stiffening gussets.

  The 60-degree oblique test was a complete success; no plastic deformation of the backbone structure was indicated.

  As would be expected, in those cases where the hard region (backbone structure) of the impact limiter sustained deformations, the scale model exhibited greater flexibility in the physical testing than the analytical prediction (the flexibility of the backbone structure added to the crush of the honeycomb resulting in a greater total measured deflection).

- End compression orientation - 90 degree:

  The end-compression orientation is, structurally speaking, the least complicated of the four test configurations. The loading of the AL-STAR scale model in this test is purely axisymmetric. The initial peak in the pressure/deformation curve seen in the coupon tests (Figure 2.A.2.1) was clearly evident in the axial (end) compression test (Figure 2.A.4.3). The backbone structure performed without sustaining plastic deformation.

- Comparison of experimental and analytical predictions

  Out of the four static 1/8-scale model tests, two tests (side compression and 30-degree oblique) were unsatisfactory because the backbone structure of the impact limiter did not remain elastic. These tests served to identify the need to reinforce the AL-STAR backbone structure. The other tests, namely end-compression (90 degree) and 60-degree oblique, wherein the backbone structure performed as designed, showed close agreement with the numerical model. Figures 2.A.4.3 and 2.A.4.4, respectively, show the static test results for 90-degree (end-compression) and 60 degree (oblique) cases, along with the prediction of the F-d model. There is good agreement between the computer model and the test data.

In summary, the 1/8 scale model static test program identified the required design changes to the internal structure of the impact limiters. The 1/8 scale model tests showed that the load-compliance characteristics of AL-STAR are insensitive to the changes in the ambient environment. A comparison of the test results with the mathematical model predictions from the F-d model indicated that the mathematical model was in good agreement with 1/8-scale static crush tests whenever the backbone structure performed as required (i.e. remained elastic). Since the crush geometry of the scale model was *not altered* by the strengthening of the backbone, any subsequent reinforcing of the backbone did not alter the F-d relationship for the impact limiter. The two successful static tests that showed excellent agreement with the computer F-d model, therefore, continued to serve as a valid benchmark of the numerical model after the backbone is stiffened. The reinforced backbone structure is incorporated into the final design drawings for the AL-STAR, and was confirmed as acceptable during the dynamic (1/4-scale) model drop tests. Subsequent to the one-quarter scale dynamic tests and the analytical correlation (Phases 4-6), three additional $1/8^{th}$ scale confirmatory static tests were performed on impact limiters that included the internal backbone structure and the final crush material orientations used in the quarter-scale drop tests and in the analytical correlation. These additional confirmatory static tests were performed at room temperature. The tests simulated the crush orientation corresponding to the side drop, the "center-of-gravity-over corner" drop, and the end drop, respectively. Force-deflection results from the static test are compared with the predictions from the theory for the $1/8^{th}$-scale impact limiters. Subsection 2.A.10 discusses the results obtained from these three additional static tests.

2.A.5 Phase 4: 9 Meter Quarter-Scale Model Drop Tests

The one-quarter scale model dynamic tests provide physical confirmation of the HI-STAR impact limiter design and the performance of the attachment system.

In the 1/4 scale model drop test program, an instrumented scale model of the HI-STAR 100 dual-purpose cask was assembled with the top and bottom AL-STAR impact limiters, raised to a height of 9 meters (measured from the lowest point on the package), and then released to free fall onto an unyielding concrete and steel armor target (unyielding target). The impact limiter attachment system is reproduced in the model using the appropriate scale for bolt diameters, etc.

A detailed description of the quarter-scale model, instrumentation, data acquisition, and data processing is presented in a proprietary Holtec document [2.A.7]; a concise self-contained summary is provided in the following.

2.A.5.1 Test Plan:

The drop test program was performed at the drop testing facilities at the Oak Ridge National Laboratory. The target at the ORNL facility complies with guidance of IAEA Safety Series 37, Article A-618.

The quarter-scale model testing of the package required the design and fabrication of scale models of AL-STAR, the HI-STAR overpack, and the multi-purpose canister. The quarter-scale replicas of AL-STAR were prepared using the scaling procedure described previously in the context of the 1/8 scale model. In the scale model for the MPC and the overpack, the emphasis is in scaling the weight and moment of inertia, because it is these properties (translational as well as rotational) which are key to the response in the drop event. A schematic of the MPC design used in the scale model is shown in Figure 2.A.5.1. The weight of the MPC replica was set at 1,380 lbs (to simulate an 88,320 lb loaded multi-purpose canister).

The overpack scale model likewise is a cylindrical body whose length and outside diameter are 1/4, whose weight is 1/64, and whose mass moment of inertia is 1/1024 of the respective design parameters in the full-size hardware, as summarized below:

Key Quarter Scale HI-STAR Overpack Model Data			
Length (inch)	O.D. (nominal) (inch)	Overpack Plus MPC Weight (lb.)	Mass Moment of Inertia About a Transverse Centroidal Axis (Overpack Plus MPC) (lb.-in^2)
50.7813	21	3,733	1.351E+06

Figures 2.A.5.2 through 2.A.5.4 illustrate the principal geometric data of the quarter-scale overpack model. It is evident from the above description that the quarter-scale model is, from a geometrical and inertia standpoint, a quarter-scale emulation of a 84" diameter x 203.125" long, 238,900 lb. (approximate) HI-STAR system (overpack and loaded MPC). Finally, the attachment bolts which join the impact limiter to the overpack are also scaled down to 25% of their size in the full-size hardware (in both diameter and thread engagement length), as can be seen from Figures 2.A.5.3 and 2.A.5.4 or the applicable drawing in Section 1.4.

The one-quarter scale drop tests were performed with four discrete orientations of the cask longitudinal axis with respect to the impact surface, as defined below.

Test A – Vertical Drop (Top End): The cask is dropped such that the deceleration of the cask upon impact is essentially vertical.

Test B: Center of Gravity-Over-Corner (CGOC): For HI-STAR 100, C.G.-over-corner means an orientation wherein the axis of the cask is at 67.5° from the horizontal at the instant of release at the 9-meter height. This test seeks to establish the adequacy of the impact limiter under non-symmetric impact loading.

Test C – Side Drop: The cask is held horizontal with the lowest point on the package 9 meters above the target surface when released for free fall. In this test, both impact limiters participate, and the impact impulse is essentially equally divided between them.

Test D – Slapdown: In this test, the cask axis is held at 15° from the horizontal with the lowest point of the cask assembly at 9 meters from the impact surface. The orientation is such that the top end impact limiter impacts the surface first and the bottom end impact limiter experiences the secondary impact.

Each of the four tests has distinct impact characteristics. For example, in the "side drop" test both impact limiters will strike the target simultaneously; only one impact limiter sustains impact in the "end drop" test. The CGOC test involves a primary impact on one impact limiter at an angle such that the gravity vector is oriented with a line passing through the cask center of gravity and the lowest corner of the limiter. Finally, the slapdown test involves impact at both impact limiters with a very slight time separation. These four tests are deemed to adequately represent the limiting impact scenarios under the hypothetical accident conditions of 10CFR71.73.

The torque values used to secure the attachment bolts in the scale model package warrant special mention. The impact limiter attachment bolts serve two major functions during transportation:

1. During normal transport, the attachment bolts ensure that the impact limiters remain attached to the HI-STAR 100 overpack during a 10g axial deceleration as mandated by 10CFR71.45, and during exposure to normal vibratory loading that may reasonably be expected during the course of a normal transport operation. To ensure against loss of attachment due to vibratory loading during normal transport, an initial bolt pre-stress of 30,000 psi has been set, based on common engineering practice. For the bolt diameters specified for the HI-STAR 100 package, the pre-load torque is 245 ft-lb and 1,500 ft-lb for the top and bottom impact limiter attachment bolts, respectively.

2. During the hypothetical accident, the attachment bolts ensure that the impact limiters remain attached to the HI-STAR 100 overpack during and after the impact with the unyielding surface.

The bottom impact limiter is attached to the overpack by 16 bolts aligned with the longitudinal axis of the overpack and arranged in a circular pattern (Figure 2.A.5.4 shows the bottom view of the one-quarter scale replica). These bolts perform their function by developing tensile stress to resist loading during the hypothetical accident. Because of close clearances with the overpack shielding, the bottom impact limiter also has a set of eight circumferentially arranged alignment

pins that fit into mating holes in the overpack bottom plate. These mating holes are plugged when the impact limiter is not in place.

The top impact limiter is attached to the overpack using twenty radial bolts that are designed to resist relative motion and transfer loads by shear (Figure 2.A.5.3 shows the top view of the one-quarter scale replica).

Although the attachment analyses do not require pre-load (by application of an initial bolt torque) to demonstrate that the required performance during normal transport conditions is achieved, the presence of pre-load serves only to enhance the performance of bolting which resists loads by developing tensile bolt forces (bottom impact limiter attachment bolts). Pre-stress in the bottom impact limiter attachment bolts serves to develop an interfacial pressure between the two components being joined together. This interfacial pressure acts as a reserve against separation at the interface of the impact limiter and the overpack when the external force or moment act to separate them during the drop event. The actual tensile stress bolt will rise significantly over the initial pre-stress if and only if the external load acting to break apart the interface is large enough to cancel out the interfacial pressure.

The effect of pre-load on the performance of bolting that resists loads by shear (top impact limiter attachment bolts) is different. The presence of both tensile stress (due to bolt pre-load) and shear stress in the bolt (due to the impact loads in a drop event) will increase the maximum principal stress in the bolt, which will consequently reduce the shear capacity of the bolts. Applying a pre-load in excess of the required amount in the 1/4 scale HI-STAR 100 drop tests will therefore result in a conservative evaluation of the top impact limiter attachment bolts.

Based on the initial torque values set in the full-scale package, the appropriate bolt pre-load torque for the 1/4-scale impact limiter attachment bolts is (to the nearest foot-pound):

Top impact limiter (radial) bolts: 4 ft-lb. (full scale equivalent = 245 ft.-lb)
Bottom impact limiter (axial) bolts: 23 ft-lb. (full scale equivalent =1500 ft.-lb.)

Since a bolt pre-load will enhance the performance of bolts (located at the bottom impact limiter interface) that resist loading by developing tensile stress, the bolt torque was conservatively set at 20 ft-lb. or below for the bottom impact limiter bolts. Since a bolt pre-load will degrade the performance of bolts (located at the top impact limiter interface) that resist loading by developing shear stress, the bolt torque was conservatively set at 4 ft-lb. or above for the top impact limiter bolts.

The end drop onto the top impact limiter tests the resistance of the twenty radial attachment bolts against failure from shear. The use of an initial torque value (15 ft-lb.), in excess of 4 ft-lb., is conservative for evaluation of the performance of the bolts to resist shearing strains (i.e., as noted earlier, due to an interaction relation between tension and shear, the presence of any tensile strain will reduce the allowable shear strain prior to failure).

The C.G. over corner drop used an initial torque of 15 ft-lb., a value below the mandated value of 20 ft-lb. on the bottom impact limiter. This is again conservative for the evaluation of the performance of the bottom impact limiter attachment bolts, since the presence of additional prestress would enhance the ability of the bolts to retain the impact limiter in position.

The slapdown test was performed using low initial bolt torque values for both impact limiters that simulated "hand-tight" values. Thus, there is almost no contribution from pre-load on the bolts on either impact limiter. In the slapdown drop, the bottom impact limiter experienced the largest deceleration. This test demonstrated that the use of a lower pre-load on the most highly loaded attachment bolt does not affect the ability of the bolts to perform their required function.

Finally, the final side drop used the bolt pre-loads that correlate with the final bolt pre-loads specified (top impact limiter - 4 ft-lb.; bottom impact limiter - 20 ft-lb.) for the one-quarter scale tests.

A minimum of five calibrated unidirectional accelerometers was installed on the test package for each test. Schematics of the accelerometer locations and numbering system for all four tests are presented in Figures 2.A.5.5 and 2.A.5.6.

The accelerometers are placed at three axial locations along the height of the overpack model and at different circumferential locations at each axial location. The placement of the accelerometers axially reflects locations consistent with the detailed 2-D finite element analyses of the MPC that conservatively neglected the effect of stiffening provided to the MPC shell by the MPC baseplate. Figure 2.A.5..2 shows the three cutouts of the outer 5/8" thick cylinder that are machined flat to position the accelerometers. The following table provides the locations of the accelerometers.

ACCELEROMETER LOCATIONS FOR ONE-QUARTER SCALE DROP TESTS								
NUMBER	TOP END DROP		SIDE DROP		SLAPDOWN		CG-OVER-CORNER	
	Axial (inch)	Peripheral (degrees)	Axial (inch)	Peripheral (degrees)	Axial (inch)	Peripheral (degrees)	Axial (inch)	Peripheral (degrees)
1	44.781	0	5	0	44.781 25	0	5	0
2	25	0	25	0	25	0	5	+120
3	5	0	44.781	0	5	0	5	-120
4	44.781	+120	25	+90	44.781	+120	44.781	0
5	44.781	-120	25	-90	44.781	-120	44.781	+120
6	5	+120	--	--	5	+120	44.781	-120

Notes:

1. All accelerometer axial distances measured from top end surface of overpack model (without impact limiters in place).
2. Peripheral locations measured from plane containing accelerometer #1; clockwise direction, viewed from Section A-A in Figures 2.A.5.5 and 2.A.5.6, is positive.

In addition to recording the deceleration during impact, a high-speed camera and a video camera were used to record the test events. The high-speed camera was used to confirm orientation angles just prior to impact and to aid in the evaluation of extent of crush subsequent to the test. The tests were conducted by attaching the ¼ scale package to a 15-ton mobile crane through appropriate rigging and lifting the package to the required height. An electronically activated guillotine-type cable cutter device was used for releasing the package for free fall. An array of photographs labelled Figures 2.A.5.7 through 2.A.5.13 provide pre-test and post-test visuals of the package. These photographs show quite clearly that the post-crush impact limiters maintained their own physical integrity and the attachments to the overpack scale model suffered no failures.

The following acceptance criteria for the scale model dynamic drop tests were identified in the Test Plan [2.A.11]:

- Filtered decelerations limited to a maximum of 60g's (after scaling to full-scale geometry) for all drop orientations.
- No impact of the cask body on the target surface.
- No separation of impact limiters from the cask body through the entire drop event.

2.A.5.2 Results of First Series of Drop Tests

The first series of three one-quarter scale drop tests (types A, B, and C denoted above) were performed in August 1997 and produced significant information [2.A.5]. Table 2.A.1 shows the maximum filtered decelerations registered in the three one-quarter scale tests after the test results are scaled up to the full-scale AL-STAR (by dividing test results by four).

Table 2.A.1: Peak Decelerations from August 1997 Tests

Test I.D.	Orientation	Deceleration (g)
A.	End Drop	134
B.	C.G.-Over-Corner	37.84
C.	Side Drop	51.3

The peak filtered deceleration in the first end-drop test was clearly above the 60g-design limit established for the HI-STAR 100 design. The reasons for this discrepancy were determined to be the use of a low value of the dynamic multiplier assumed in designing the impact limiter, and the lack of pre-crush of the honeycomb material. Numerical analyses also indicated that the honeycomb compression modulus was dependent on the impact limiter velocity during the drops. This confirms laboratory data available in the historical literature [2.A.9]. The velocity and deceleration information obtained from the first round dynamic drop tests enabled development of a simple dynamic correlation multiplier to be applied to the honeycomb material's static F-d behavior. This multiplier is an additional "experimentally based" input term in the computer prediction model for simulation of dynamic drop events [2.A.6]. Data from the initial test series shows that this multiplier is independent of test orientation and is a function of the ratio of crush velocity during the crushing process divided by the impact velocity at the initiation of crush. Based on the numerical analysis of the August 1997 tests, the honeycomb material was appropriately revised with new crush strengths and new sets of ¼ scale model impact limiters were manufactured. The correlation of the August 1997 quarter-scale tests with the numerical results from the computer model is presented in section 2.A.6.

In summary, the chief contribution of the August tests, therefore, lay in providing the database to quantify the crushing characteristic of the honeycomb material under dynamic conditions [2.A.6]. Since none of these tests is ascribed to confirmation of the final performance of the AL-STAR impact limiters, no accelerometer raw or filtered results are included herein. The full set of acceleration data (both raw and filtered) is provided in [2.A.5].

2.A.5.3 Results of the Second Series of Drop Tests

The second round of one-quarter scale dynamic drop tests, conducted in December 1997 and February 1998, using the new (lower crush strength) impact limiter materials, occurred in three phases. The first phase consisted of the top end drop, CGOC drop, and side drop tests. While the decelerations in all cases were within the design limit, the attachment system for the bottom impact limiter did not survive the side drop test. The attachment system was redesigned prior to the remaining (slapdown) test. The slapdown test is considered to be the most definitive test of the cask/impact limiter attachment integrity. The slapdown test was successfully completed, with the bottom impact limiter remaining in place during and after the secondary impact, on December 29, 1997 in Phase 2 of the second test series. In order to confirm the adequacy of the attachment system under side drop conditions, the side drop test was repeated in February 1998 during Phase 3. This test reconfirmed the attachment system integrity.

The results from the second round test series demonstrates that the HI-STAR 100 package meets all test acceptance criteria, namely:

- Appropriately filtered decelerations of less than 60g's (after appropriate scaling to reflect the full-size mass and geometry) for all tested orientations;
- All attachment bolts remained intact, ensuring that the impact limiters do not separate from the cask body through and after the drop event;
- No impact of the cask body on the target surface.

Figures 2.A.5.14 through 2.A.5.21, drawn from reference 2.A.7, provide the raw (unfiltered) and filtered deceleration time-histories for each of the four drop scenarios for the key accelerometers used to assess package performance. The accelerometer station numbers indicated in these accelerograms are located by referring to Figures 2.A.5.5 or 2.A.5.6, as applicable. The test report [2.A.7] provides the necessary background to justify the use of this data to evaluate package performance. The following remarks are pertinent concerning the results presented in Figures 2.A.5.14 through 2.A.5.21.

End Drop Decelerations (Figures 2.A.5.14, 2.A.5.15, and 2.A.5.15a-c)

All accelerometers for this test recorded decelerations in the direction of crush. Two accelerometers were subsequently determined to be defective (documented in [2.A.7]). The figures show the raw, the filtered response at 450Hz cut-off frequency, and a combined plot of the raw and filtered data covering a reduced time period. All of these results are obtained from the records from the working accelerometers. All working accelerometers gave essentially identical response; the final evaluation of performance presented herein is the average of the response from the accelerometers deemed to be recording correctly. Figures 2.A.5.15b and 2.A.5.15c demonstrate that the sensitivity to cut-off filter frequency is small even up to 1250Hz.

Center of Gravity Over Corner Decelerations (Figures 2.A.5.16, 2.A.5.17, and 2.A5.17a)

The CGOC test was performed immediately after the end drop using the same set of accelerometers. The evaluation of the data after this test clearly determined that the same two accelerometers deemed suspect in the end drop test was also providing erroneous date here. Subsequent independent plate impact tests that definitively showed that these accelerometers were indeed faulty are documented in [2.A.7]. The acceleration data in the figures represents the vertical acceleration obtained by appropriate combination of the raw time data from the longitudinal and lateral mounted accelerometers on the inclined scale model cask. The raw vertical accelerations were then subject to filtering to remove non-rigid body behavior. Raw, filtered, and combined raw and filtered data over the strong response time period are presented.

Slap Down Decelerations (Figures 2.A.5.18, 2.A.5.19, and 2.A.5.19a)

Although the initial release of the package was at an angle of 15 degrees from the horizontal, the high-speed camera showed that impact occurred with the overpack longitudinal axis at an angle of 7.2 degrees from the horizontal. The numerical simulation of this test reflected the actual angle of impact rather than the initial setting at nine meters. The results for all accelerometers (raw data and filtered) are provided in [2.A.7]. The raw and filtered data presented in the figures here represent the deceleration at the bottom end of the package that experiences the larger magnitude secondary impact. Numerical analysis demonstrated that the peak deceleration from secondary impact is insensitive to impact angles between 5 and 12 degrees from the horizontal and decreases as the angle increases above 12 degrees. Raw, filtered, and combined raw and filtered data over the strong response time period are presented.

Side Drop Decelerations (Figures 2.A.5.20, 2.A.5.21, and 2.A.5.21a)

Both impact limiters are supposed to impact the target simultaneously in this test. An evaluation of the individual accelerometer data and an examination of the high-speed camera film clearly indicated that there was a small angle existing between the overpack longitudinal axis and the target horizontal surface at the moment of impact. This caused the expected result that accelerometer readings at one end of the package were slightly higher than readings at the other end. The results for raw and filtered data represent results obtained by averaging the data from the accelerometers at the ends of the package. Raw, filtered, and combined raw and filtered data over the strong response time period are presented.

The filter frequency used for the End Drop and CGOC Drop is 450 Hz. The filter frequency used for the Slap Down and Side Drops was 350 Hz. These filter frequencies were established by examination of the power spectral density function for each raw data trace that clearly showed that the majority of the energy occurred at frequencies well below the cut-off frequency. Independent confirmation of the appropriateness of the cut-off frequencies was made by determining the lowest frequency of elastic vibration of the package acting as either a bar or a simply supported beam. As described above, the sensitivity to cut-off frequency was examined for the end drop case by re-analyzing the data for three cut-off frequencies.

Table 2.A.2 provides the peak deceleration data culled from the above-mentioned accelograms for the four drop scenarios after filtering to remove high frequency effects. The table contains the results from the actual 1/4-scale experiments scaled up to the full-size packaging. The test report [2.A.7] provides the detailed information on this final one-quarter scale dynamic drop test series with raw and filtered outputs from all accelerometers. The test report also includes details on the filtering methodology, on the data reduction, and on the evaluation of the performance of the various accelerometers used in each of the tests.

In all of the four final one-quarter scale dynamic drop tests, the impact limiter attachments successfully performed without a single attachment bolt failure (ensuring that the impact limiters did not separate from the overpack), rigid body decelerations were below 60 g's, and the cask body did not contact the unyielding target surface. Also, additional crush margin remained in the aluminum honeycomb material.

Table 2.A.2: Peak Decelerations from AL-STAR™ Drop Tests (Second Series)

Test Case	Orientation	Peak Decelerations (g)
A	End-Drop	53.9
B	C.G.-over-Corner	38.8
C	Side Drop	45.7
D	Slap-Down	59

2.A.6 Phase 5: Numerical Prediction Model for Dynamic Analysis

The numerical prediction model for dynamic drop events utilizes the previously discussed force-crush (F-d) model and incorporates the information into the dynamic equations of equilibrium. Using the procedure discussed previously, the static F-d curves for the AL-STAR impact limiter under the four drop scenarios are readily constructed. Figures 2.A.6.1 to 2.A.6.4, respectively, provide the static force vs. crush plots for the full scale impact limiter with test orientations for drop cases A, B, C, and D (primary impact). An appropriate analytical fit for each curve is developed using the commercial graphing package Deltagraph [2.A.8]. Figures 2.A.6.1 through 2.A.6.4 also provide curves for upper and lower bound material strengths.

We now discuss the application of the F-d model to the prediction of impact limiter performance in a dynamic drop environment. In symbolic form, we can write the static resistive (crush) force, F, as a function of the crush depth, Δ, where a zero value for Δ represents an uncrushed condition.

$$F = f(\Delta)$$

The above symbolic formula represents the data on Figures 2.A.6.1 to 2.A.6.4 in analytical form. We have previously explicitly discussed the mathematical concepts underlying the above formulation by referencing the particular case of a side drop. In general, the static F-d curve can be expressed as a sum of local crush pressures multiplied by interface areas where the interface areas may be a function of the current crush. That is, the mathematical relation for static compression (which is validated by comparison to static testing) is also expressible in the form

$$f(\Delta) = \sum_i p_i A_i$$

where p_i are the crush pressures of the materials participating in the crush and A_i are the interface areas associated with the different crush strengths. The determination of the areas A_i as a function of crush depth, Δ, has previously been discussed within the context of interpenetration.

The dynamic model for simulating a packaging drop event consists of solving the classical Newtonian equations of motion. In the case of a unidirectional impact such as an end drop (θ=90°), side drop (θ=0), or CGOC drop, the equation of motion simply reduces to:

$$M\frac{d^2\Delta}{dt^2} = Force + Mg$$

where: M = mass of system undergoing deceleration

$d^2\Delta/dt^2$ = second derivative of package movement (which is equal to the impact limiter crush because the target is immovable and rigid).

The resistive "Force" opposes the downward movement and is given by the static force-crush functional relationship (appropriate for the drop orientation) multiplied by a dynamic multiplier Z. As noted earlier, there is historical evidence that metal honeycomb crush pressure is a linear function of velocity [2.A.9]. The Holtec correlation of the August 1997 test data by numerical simulation [2.A.6] also confirmed that the best correlation is achieved if the dynamic multiplier is represented by a linear function of local crush velocity ($d\Delta/dt$). Introducing the dynamic multiplier, the dynamic equation of force equilibrium for a case involving only primary impacts becomes

$$M\frac{d^2\Delta}{dt^2} = ZF + Mg = Zf(\Delta) + Mg$$

The above equation is a second order non-linear differential equation in the time coordinate t, which can be solved for the post-contact event using any standard equation solver package. The initial condition is: @ t = 0, Δ = 0, $d\Delta/dt = V_o$ (approach velocity at impact). We note that since the acceleration is an explicit function of both deformation and velocity, maximum acceleration will not, in general, occur at the instant when the velocity of the package is zero.

If the impact event involves both primary and secondary impacts, as is the case for the slapdown event (indeed any event wherein θ<67.5°), then both the mass M and rotational moment of inertia I are involved. The modeling of a dual impact event is only slightly more involved than

the single variable modeling of the single impact case discussed above. Figure 2.A.6.5 pictorially illustrates the sequence of events leading to an appropriate mathematical model. Figure 2.A.6.6 provides the appropriate free-body diagrams associated with each portion of the event.

In the first step, the inertia force of the falling package is resisted by the crush force developed at the primary impact location. While the downward momentum of the package is dissipated by the resistive force, the package also experiences the overturning couple produced by the non-co-linearity of the inertia force (which acts at the centroid) and the resistive force which acts at the primary impact zone (Figure 2.A.6.5(a)). The dynamic equation of force equilibrium is given above in terms of the downward movement of the package centroid and the resistive force static compression curve, modified by the dynamic factor Z, appropriate to the initial orientation at primary impact. The package decelerates and then begins to overturn, in effect pivoting about the initial point of contact in the primary impact region, gathering angular momentum as the second impact limiter (mounted at the far end) approaches the target surface. Referring to Figure 2.A.6.5(b), the dynamic equation insuring moment equilibrium during the overturning (before the initiation of the secondary impact) phase can be written as

$$I_p \frac{d^2\phi}{dt^2} = -MgR\cos(\phi)$$

where I_p: moment of inertia of the package about the pivot point

ϕ : angular acceleration with respect to the horizontal plane

R: radial distance of the package C.G. with respect to the pivot point.

The initial conditions for this phase are: $t = 0$, $\phi = \theta$, $d\phi/dt = 0$ where t is now redefined at the initiation of rotational motion.

Finally, the secondary impact commences wherein the angular momentum of the package plus any linear momentum not dissipated by the primary impact is dissipated by the crushing of the second impact limiter. During the secondary impact phase, the equation of dynamic moment equilibrium can be written by inspection of Figure 2.A.6.5(c):

$$I_p \frac{d^2\phi}{dt^2} = -MgR\cos(\phi) + Zf(D\phi)D$$

where $f(D\phi)$ is the static resistive force at the secondary impact location under compression $D\phi$, Z is the current dynamic multiplier appropriate to the secondary impact location, D is the moment arm, and I_p is the moment of inertia of the package about the pivot point. During this phase of the motion, the equation of dynamic force equilibrium is modified to reflect dynamic resistive forces from both impact limiters since the entire package may continue to move toward

the target surface with both impact limiters providing a dynamic resistive force. Therefore, during the final phase of the impact event, the dynamic force equilibrium equation can be written as

$$M\frac{d^2\Delta}{dt^2} = Z_1F_1 + Z_2F_2 + Mg$$

where Z_i and F_I (i=1,2) represent the dynamic multiplier and static compression force appropriate to the primary and secondary impact limiter behavior during the final phase of the event. The dynamic multipliers Z_i (i =1,2) reflect the current value of the local crush velocities at each of the limiters.

The above formulation assumes, for simplicity, that the pivot point does not slide during the overturning or secondary impact phases.

It is evident from the foregoing that the impact limiter is essentially simulated by a non-linear spring whose static force-deformation curve is known a' priori (from the F-d model) as a function of the drop orientation. The solution of this rigid body dynamics problem featuring up to two non-linear springs can be determined using any one of several standard software packages available in the public domain. Holtec International utilizes the commercial package WORKING MODEL [2.A.10], which has been validated in the company's QA system for this purpose.

The dynamic simulation model, constructed in the manner of the foregoing, was utilized to simulate all seven one-quarter scale drop events (three in the first series, four in the second series). In order to develop a high level of confidence, it was decided that the model should be validated at all <u>three</u> levels, namely, a comparison of acceleration, crush, and duration of impact. In other words, to be acceptable, the numerical prediction model must predict α_{max}, maximum crush sustained d_{max}, and the duration of impact, with reasonable accuracy. Since the actual crush d_{max} could be measured, and the duration of impact and α_{max} were available from accelerometer data, comparison between theory and experiment with respect to all three key indicators was possible. Tables 2.A.3 and 2.A.4 provide the results in a concise form for all of the one-quarter scale dynamic drop tests for the first and second series, respectively.

Note that in the tables, the comparison is made after scaling up the model results to reflect a full-scale package.

Table 2.A.3: Comparison Between Test Data and Prediction Model Results (First Test Series)

	Deceleration (g's)		Total Crush Depth (inch)		Impact Duration (milli-seconds)	
Case I.D.	Predicted	Measured	Predicted	Measured	Predicted	Measured
A. End-Drop	134.2	134.0	2.42	2.42	3.5	Not measured
B. C.G.O.C.	37.8	37.84	16	16	13.25	16.6
C. Side Drop	50.5	51.3	9.1	9.51	8.25	10.74

Table 2.A.4: Comparison Between Test Data and Prediction Model Results (Second Test Series)

	Deceleration (g's)		Total Crush Depth (inch)			Impact Duration (milli-seconds)	
Case I.D.	Predicted	Measured	Predicted	Measured	Max. Available	Predicted	Measured
A. End Drop	53.0	53.9	11.3	10.6	17.659	38.8	37.2
B. C.G.-Over-Corner	38.7	38.8	12*	9.82*	25.06	51.0	61/45.2
C. Side Drop	43.5	45.7	10.9	12.5	16	38.5	53.1 (averaged value)
D. Slap-Down							
Primary	46.4	49.0	9.50	10.7	16	48.5	44.4
Secondary	59.9	59.0	12.8	13.5	16	35.8	41.2

* For C.G.-Over-Corner, only crush at the external interface is measured.

It is evident from both Tables 2.A.3 and 2.A.4 that the numerical prediction model is robust in predicting all seven impact tests. Not only are peak values of α_{max} for each test predicted with good agreement, but also the crush depth and impact duration is also reliably simulated.

A perusal of the numerical results in Table 2.A.4 yields two additional insights into the behavior of AL-STAR which are most helpful in the "fine tuning" of the full-scale AL-STAR design:

i. The maximum deceleration, α_{max}, predicted as well as measured, under the most limiting scenario (slapdown), is close to the permissible limit of 60g's.

ii. The maximum crush, predicted as well as measured, in all drop scenarios, is well below the available limit (i.e., the value at which the crush material will "lock up").

The state-of-the-art manufacturing technology for aluminum honeycombs permits the material to be manufactured within a total tolerance range of 12 to 13% (between the maximum and minimum values). The above observations suggest that the upper and lower bound range of crush pressures for the honeycomb material in the AL-STAR impact limiter should be set at 95% and 82% of the values of honeycomb material used in the second series quarter-scale tests.

Finally, the agreement between the predictions and measured data in the above correlation effort fosters a high level of confidence in the numerical model, which can now be used to conduct sensitivity studies.

2.A.7 Phase 6: Simulation of the Effects of Material Crush Strength Variation, Package Mass Tolerances, and Oblique Drop Orientations

Having ensured the technical reliability of the numerical prediction model, it is now necessary to evaluate the system behavior under all "limiting conditions". As noted earlier, the impact limiter materials are insensitive to environmental temperature changes within the limits of -20° F and 100° F. Therefore, limiting conditions are broadly defined here as arising from two sources:

i. Variation in the impact limiter honeycomb crush strength due to material manufacturing tolerance.

ii. Variation in the package weight (due to different MPC types that may be transported in the HI-STAR 100 overpack, and manufacturing tolerances in fabrication of the overpack and impact limiters).

iii Variation in package angle of impact with the target.

To examine all limiting scenarios, additional simulations using the mathematical model were performed. The crush strength of the honeycomb material was varied within the range permitted in the Holtec Drawing 1765. The packaging weight was set at its upper bound and lower bound value (upper bound weight is 280,000 lb., and lower bound weight is 270,000 lb. based on values listed in Table 2.2.1). Three additional drop orientations (30 degree, 45 degree, and 60 degree orientation angle, measured from the horizontal) that were not the subject of tests were also analyzed numerically using input crush strength data that would maximize the decelerations with an average weight. The purpose of these additional simulations with varied drop angle is to ascertain which, if any, oblique drop orientation merits detailed finite element stress analysis to meet the requirements of the Regulatory Guide. Figures 2.A.7.1-2.A.7.3 provide the static crush force vs. crush depth information used in the dynamic simulation of these accident events. Table 2.A.5 provides key output data, peak decelerations and maximum crush, as obtained from these numerical simulations.

Table 2.A.5: Sensitivity of Package Response to Package Weight, Crush Material Strength Variations, and Package Orientation at Impact

Orientation	Case	Deceleration (g's)	Maximum Total Crush (2-interfaces) (inch)	Available Crush Stroke (inch)
End Drop	Max. Strength, Min. Weight	52.85	11.4	17.659
	Min. Strength, Max. Weight	46.3	12.8	17.659
C.G. Over Corner	Max. Strength, Min. Weight	38.25	17.0	25.06
	Min. Strength, Max. Weight	35.6	18.5	25.06
Side Drop	Max. Strength, Min. Weight	42.5	11.2	16
	Min. Strength, Max. Weight	37.5	12.7	16
Slap Down (secondary impact bounds)	Max. Strength, Min. Weight	58.5	13.2	16
	Min. Strength, Max. Weight	52.6	15.1	16
Oblique Drop – 30 degrees	Max. Strength, Min. Weight	36.44	19.57	24.1
Oblique Drop – 45 degrees	Max. Strength, Min. Weight	35.62	22.39	25.72
Oblique Drop – 60 degrees	Max. Strength, Min. Weight	38.01	19.2	25.65

The following conclusions are readily derived from Table 2.A.5 results:

i. The maximum value of α_{max} is less than 60g's in all cases.

ii. The total crush of the impact limiter is below the available "stroke", i.e., the overpack body will not contact the unyielding target surface nor will any "lock-up" of the crush material occur.

iii. The three oblique drop simulations considered all produce approximately the same vertical deceleration from the primary impact. The decelerations resulting from the subsequent secondary impact, after rotation of the HI-STAR 100, are all below the value obtained from the simulation of the "slapdown" at low angles of

impact. If the "limiting" oblique drop is considered as the simulation providing maximum deceleration perpendicular to the longitudinal axis of the cask, then the drop most likely to develop the largest bending of the overpack in the oblique orientation is at 30 degree orientation (from the horizontal axis). Therefore, this case is subjected to detailed stress analysis in Section 2.7 with the applied impact loading (along and perpendicular to the cask axis) balanced solely by the cask inertia forces and moments.

In conclusion, the above work provides full confidence that the HI-STAR 100 packaging will perform in the manner set forth in the NRC regulations (10CFR71.73) under all conceivable hypothetical accident conditions of transport.

2.A.8 One-Foot Drop

Paragraph 2.6 of Reg. Guide 7.8 requires evaluation of the package response under a one-foot drop onto a flat unyielding surface in a position that is expected to inflict maximum damage.

Using the prediction model, the maximum deceleration sustained by the package under the one-foot end and side drop scenarios, the latter expected to produce maximum stress in the fuel basket, was computed. Table 2.A.6 provides summary results for the limiting case of minimum package weight and upper bound material crush strength (so as to maximize the decelerations).

Table 2.A.6: Peak Decelerations Under One-Foot Drop Event

Scenario	Max. Deceleration in g's	Crush (inch)	Duration of Impact (milli-seconds)
90° End Drop	17.25	0.85	20.0
0° Side Drop	11.45	1.33	26.0

2.A.9 Equivalent Dynamic Factor (EDF)

It is instructive to compute an effective equivalent dynamic factor on the predicted static crush force corresponding to the instant of maximum deceleration during the drop event. Table 2.A.7 presents the pseudo-deceleration (obtained by dividing the static force by the mass of the package) and the predicted deceleration; the ratio of the two is the "equivalent dynamic factor" (EDF). The EDF is also equal to the peak dynamic crush force divided by the static resistance force at the coincident instance of crush when the dynamic crush force is maximized. Note that the differences in package weight used in the table below reflect the actual weight of the impact limiters used in each one-quarter scale drop test (after increasing to full-scale equivalent values).

Table 2.A.7: Equivalent Dynamic Factor (EDF) for Different Drop Scenarios

	Predicted Force (lbs) x 10^{-7}			Predicted Max. Deceleration		
Scenario	Static	Dynamic	Participating Package Weight (lbs)	Pseudo-Accn (static)	Dynamic (from Table 2.A.4)	EDF
End Drop	1.0785	1.454	274,336	39.313	53	1.348
CGOC Drop	0.8	1.059	273,680	29.231	38.7	1.324
Side Drop	0.4	0.597	137,270*	29.14	43.5	1.493
Slapdown	0.345	0.6607	†	†	59.9	1.915

* Only half of the total package weight participates at each impact limiter.
† Indeterminate for this drop configuration.

The last column of the above table demonstrates that the EDF, as defined above, is not a constant value independent of drop orientation.

2.A.10 Additional 1/8th Scale Static Tests

Three additional static crush tests on 1/8th scale impact limiters have been performed subsequent to the completion of all quarter-scale dynamic testing and theoretical correlation. The F-d test results for each of three impact limiter orientations are compared with the analytical F-d predictions in Figures 2.A.10.1-2.A.10.3. Figure 2.A.10.1 compares test results with theoretical prediction for the crush orientation corresponding to a side impact, Figure 2.A.10.2 presents the results for the Center-of-Gravity-Over-Corner impact orientation, and Figure 2.A.10.3 presents results for the end impact orientation. In all tests, the crush material orientation and location duplicated the final configurations subjected to quarter-scale tests. The internal backbone structure was also faithfully reproduced. The welds were also scaled to the extent practical given the thin material gages used for the one-eighth-scale model. In the three figures, the solid line without symbols represents the predictions of the theory developed for the F-d curves, while filled circles represent test results. Within the range tested for each orientation, good agreement is observed between theory and test for the side and CGOC crush orientation. For the end drop orientation, however, the tested results suggest that inclusion of some elastic behavior at the cask-impact limiter interface into the theory might improve the static correlation. The dynamic test results presented in Table 2.A.4, however, demonstrate conclusively that the prediction of peak deceleration, extent of crush, and impact duration would not be affected by these elastic effects that "smooth" the abrupt "staircase" shape of the F-d curve.

2.A.11 Conclusions

The AL-STAR impact limiter design was subjected to a series of static and dynamic tests to validate its functional performance. The 1/8 model static tests conducted under cold and hot, as well as ambient conditions, confirmed that AL-STAR's functional characteristics are independent of the environmental temperature conditions in the range specified in 10CFR71.73. The successful static tests on the 1/8 scale model (namely, end test and 60° oblique test) also correlated well with the theoretical force-crush model developed by Holtec. Subsequent static tests, performed after the final successful one-quarter scale dynamic tests, provided additional confirmation of the validity of the fundamental F-d model.

The static compression tests were followed by quarter-scale drop tests. The first series, in August 1997, consisting of three tests, provided the necessary test data to determine the dynamic multiplier applicable to the honeycomb materials. The numerical model for simulating the dynamic crushing of AL-STAR showed good agreement with the first test series data when the correct dynamic factor was incorporated in the computer model (Table 2.A.3).

While the prediction model for simulating AL-STAR crushing under 9-meter drop conditions was extremely well correlated, the peak deceleration under the end- drop condition in the August 1997 tests exceeded the acceptance criteria.

The second series of tests wherein the crush strength of the honeycomb was lowered (as selected by the prediction model), performed as expected. The agreement between the test data and the prediction model is high (Table 2.A.4).

The prediction model for AL-STAR therefore stands correlated with seven (7) quarter-scale drop events. The first three tests used different honeycomb crush strength materials than the last four, proving the ability of the prediction model to predict the AL-STAR crush performance for a wide range of crush material properties. The backbone structure of AL-STAR, enhanced after the 1/8-model static compression tests, performed as designed in all seven quarter-scale drop tests.

Finally, the AL-STAR-to-overpack attachment system remained intact and the cask did not contact the unyielding target during all four final dynamic tests.

2.A.12 References

[2.A.1] ANSYS 5.3 Ansys Inc., 1996.

[2.A.2] CADKEY, Version 7, 1996.

[2.A.3] Project Procedure No. HPP-5014-5, HI-STAR Aluminum Honeycomb 1/8 Scale Impact Limiter Static Test Procedure.

[2.A.4] HI-STAR 1/8 Scale Impact Limiter Test Report, HI-961501, Holtec International, June 1996.

[2.A.5] Holtec Report HI-971774, Revision 1, "Impact Limiter Test Results – 30' Drop Tests" – August 1997

[2.A.6] Holtec Report HI-971823, Revision 0, "Improved Correlation of ORNL 30' Drop Tests" – August 1997

[2.A.7] Holtec Report HI-981891, Revision 3, "Impact Limiter Test Report - Second Series", 2007.

[2.A.8] Deltagraph Pro 3.5, Deltapoint Software, 1995.

[2.A.9] J.M. Lewallen and E.A. Ripperger, Energy Dissipating Characteristics of Trussgrid Aluminum Honeycomb, SMRL RM-5, University of Texas Structural Mechanics Research Laboratory, 1962.

[2.A.10] Working Model 3.0, Knowledge Revolution, 1995.

[2.A.11] HI-STAR 100 Impact Limiter Test Program, Holtec Report No. HI-951278.

SUPPLEMENT 2.I: HI-STAR HB STRUCTURAL EVALUATION

2.I.0 OVERVIEW

In this supplement, the structural adequacy of the HI-STAR HB is evaluated pursuant to the guidelines of NUREG-1617 and the requirements of 10CFR71. The organization of this supplement mirrors the format and content of Chapter 2 except it only contains material directly pertinent to the HI-STAR HB.

The HI-STAR HB is a shortened version of the HI-STAR 100 that is evaluated in Chapter 2. All dimensions (radius, thickness) of the HI-STAR HB are identical to those of the HI-STAR 100 except for the overall length of the layered cylinders, the threaded diameter of the lifting trunnions, and the enclosure shell radial gussets. The impact limiters are identical in all respects except for the crush strengths of the internal aluminum honeycomb material, which are reduced to ensure that the deceleration limits are met with the lighter weight HI-STAR HB. The HI-STAR HB is configured to carry the MPC HB that has the appropriate length and fuel basket design to carry 80 spent fuel assemblies from the closed Humboldt Bay Nuclear Plant. The qualification of the MPC HB to withstand a 60g deceleration has been documented in the Part 72 license for Humboldt Bay (Humboldt Bay ISFSI, Pacific Gas and Electric Company, Final Safety Analysis Report Update, Revision 0 January 2006, NRC Docket No. 72-27). Therefore, no new analyses of the MPC HB are required in this Supplement 2.I as long as the maximum cask deceleration remains bounded by 60g.

The applicable design codes and standards, and the design criteria for the HI-STAR HB are identical to those applied to the HI-STAR 100. Therefore, since the differences between the HI-STAR HB and HI-STAR 100 are limited to:

- *Shorter overall length;*
- *Lower package weight;*
- *Reduced strength of impact limiter crush materials;*
- *Smaller diameter threads on lifting trunnions;*
- *Decreased number and length of enclosure shell radial gussets,*

the supplement is focused on documenting the results from new evaluations required because of the reported differences in length, weight, impact limiter crush strength, thread diameter, and enclosure shell geometry. The reduced length and weight of the HI-STAR HB ensures that all stress-based evaluations performed on the HI-STAR 100 produce safety factors that are lower bounds for the same evaluation on the HI-STAR HB, except for the trunnion analysis discussed below. Therefore, no stress-based calculations need to be performed, except those that involve deceleration limits, because of the change in impact limiters, those that involve the lifting trunnions, because of the smaller diameter threads, and those that involve the enclosure shell, because of the modifications to the radial gussets; this supplement focuses only on providing summaries for the new evaluations performed for the HI-STAR HB, which are documented in Holtec calculation packages HI-2084158 [2.I.7.2] and HI-2033042 [2.I.7.3].

2.I.1 STRUCTURAL DESIGN

2.I.1.1 Discussion

The general discussion presented in Subsection 2.1.1 applies to the HI-STAR HB package. Drawings for the components of the HI-STAR HB package are provided in Section 1.1.4.

2.I.1.2 Design Criteria

The HI-STAR HB package meets the design criteria espoused in Section 2.1.2 in its entirety. For the HI-STAR HB overpack, however, the option to replace the SA203-E plate used for the 2.5" thick inner shell with comparable SA350 LF3 ring forgings, stacked to form the inner shell and welded together with full penetrant welds, has been added to the drawings. The Nil Ductility Transition Temperature is still required to be less than –70 degrees F when this option is used (per Subsection 2.1.2.3). Accordingly, Table 2.1.22 lists SA350 LF3 as an optional material for the inner shell. Similarly, Table 2.1.23 lists SA350 LF3 as an option for the port cover plates.

2.I.2 WEIGHTS AND CENTERS OF GRAVITY

Table 2.I.2.1 provides the weights of HI-STAR HB components as well as the total package weight. The weight of the impact limiter is also provided. Table 2.I.2.1 also provides the location of the calculated center of gravity for the HI-STAR HB package.

2.I.3 MECHANICAL PROPERTIES OF MATERIALS

Materials for the HI-STAR HB package are identical to those used for the HI-STAR 100 package.

2.I.4 GENERAL STANDARDS FOR ALL PACKAGES

The HI-STAR HB is a shorter and lighter version of the HI-STAR 100. Therefore, the features presented in Section 2.4 apply to the HI-STAR HB.

2.I.5 LIFTING AND TIE-DOWN STANDARDS

2.I.5.1 Lifting Devices

The lifting devices for the HI-STAR HB package are identical to those for the HI-STAR 100, except that the threaded portion of the lifting trunnions has a slightly smaller diameter. Therefore, even though the HI-STAR HB is lighter than the HI-STAR 100, the safety factors for the HI-STAR HB lifting trunnions and the top flange interface are recalculated based on the smaller trunnion diameter.

The embedded trunnion is analyzed as a cantilever beam in the same manner as described in Subsection 2.5.1.1. Calculations demonstrate that the stresses in the trunnions comply with NUREG-0612 provisions.

Specifically, the following results are obtained:

Safety Factors from HI-STAR HB Lifting Trunnion Stress Analysis for a Bounding Lifted Load of 161,200 lb			
Item	*Value (ksi) or (lb) or (lb-in)*	*Allowable (ksi) or (lb) or (lb-in)*	*Safety Factor*
Bending stress (Comparison with Yield Stress/6)	*11.2*	*24.5*	*2.19*
Shear stress (Comparison with Yield Stress/6)	*4.76*	*14.7*	*3.09*
Bending Moment (Comparison with Ultimate Moment/10)	*208,600*	*574,400*	*2.75*
Shear Force (Comparison with Ultimate Force/10)	*92,690*	*282,500*	*3.05*

We note from the above that all safety factors are greater than 1.0. A factor of safety of exactly 1.0 means that the maximum stress, under apparent lift load D, is equal to the yield stress in tension or shear divided by 6, or that the section moment or shear force is equal to the ultimate section moment capacity or section force capacity divided by 10.*

It is also important to note that safety factors associated with satisfaction of 10CFR71.45(a) are double those reported in the table since 10CFR71.45 only requires a factor of safety of 3 on the yield strength.

The top flange interface with the trunnion under the lifted load is analyzed in the same manner as described in Subsection 2.5.1.2.2. The interface region is conservatively considered as subject to the provisions of NUREG-0612, and the thread shear stress and bearing stress are compared to 1/6 of the top forging yield stress in shear or compression. The following table summarizes the results:

Top Flange B Minimum Safety Factors (Interface with Trunnion) for HI-STAR HB			
Item	*Value (ksi)*	*Allowable (ksi)*	*Safety Factor*
Bearing Stress (NUREG-0612 Comparison)	*2.555*	*5.975*	*2.34*
Thread Shear Stress (NUREG-0612 Comparison)	*2.466*	*3.585*	*1.45*
Stress Intensity (NB Comparison)	*5.655*	*34.6*	*6.12*

It is noted from the above that all safety factors are greater than 1.0 and that the safety factors for bearing stress and thread shear stress represent the additional margin over the factor of safety inherent in the member by virtue of the load multiplier mandated in NUREG-0612.

2.I.5.2 Tie-Down Devices

Since the HI-STAR HB is shorter and lighter, but otherwise identical to the HI-STAR 100, the tie-down devices and the resulting tables of reaction loads in Section 2.5 bound those for the HI-STAR HB. The span between tie-down locations is less, reflecting the shorter overall length of the HI-STAR HB. The equilibrium equations presented in Subsection 2.5.2 also apply to the HI-STAR HB. No new analyses are performed.

2.I.5.3 Failure of Lifting and Tie-Down Devices

The discussion in Subsection 2.5.3 for the HI-STAR 100 also applies to the HI-STAR HB, except for the following. New calculations have been performed for the HI-STAR HB to demonstrate that the ultimate load carrying capacity of the lifting trunnions is governed by the cross section of the trunnion external to the overpack top forging rather than by any section within the top forging. It is concluded that the trunnion shank reaches ultimate load capacity limit prior to the top forging reaching its corresponding ultimate load capacity limit. Loss of the external shank of the lifting trunnion will not cause loss of any other structural or shielding function of the HI-STAR HB overpack; therefore, the requirement imposed by 10CFR71.45(a) is satisfied.

The following safety factors are established:

> *(Ultimate Bearing Capacity at Trunnion/Top Forging Interface)/(Ultimate Trunnion Load) = 1.04*
>
> *(Ultimate Moment Capacity at Trunnion/Top Forging Thread Interface)/(Ultimate Trunnion Moment Capacity) = 1.51*

2.I.6 NORMAL CONDITIONS OF TRANSPORT

The HI-STAR HB package, when subjected to the normal conditions of transport specified in 10CFR71.71, meets the design criteria in Subsection 2.1.2 (derived from the stipulations in 10CFR71.43 and 10CFR71.51). The HI-STAR HB is identical to the HI-STAR 100 in all respects except for the length of the overpack (and the MPC HB), the crush strength of the impact limiter material, the lifting trunnion thread diameter, and the configuration of the enclosure shell radial gussets; the total package weight is bounded by the package weights listed for the HI-STAR 100. Component diameters and thicknesses for the HI-STAR HB overpack and its closures are identical to those of the HI-STAR 100. Therefore, with the exception of the lifting trunnions and the enclosure shell, all stress analysis results associated with the HI-STAR HB overpack are bounded by the available results for the HI-STAR 100. No new analyses are reported in this supplement except for those associated with the performance of the impact limiter, the lifting trunnions, and the enclosure shell. Stress results for the MPC HB have been reported in detail in the Humboldt Bay ISFSI FSAR [2.I.6.1]; the MPC HB analyses were performed using the design basis deceleration.

2.I.6.1 Heat

Consistent with Regulatory Guide 7.9, the thermal evaluation of the HI-STAR HB is performed in Supplement 3.I and sets material temperatures, which are used in the structural evaluations discussed in this section and in Section 2.I.7. As the Humboldt Bay fuel is "old and cold", the operating temperatures are at or below comparable temperatures for the HI-STAR 100 analyses. This adds additional margins since the allowable strengths will generally be higher in a comparable strength analysis using the HI-STAR HB.

Design pressures and design temperatures for all conditions of transport are listed in Tables 2.1.1 and 2.1.2, respectively. Since the design pressures and temperatures for the HI-STAR 100 and the HI-STAR HB are the same, and the HI-STAR HB is shorter than the HI-STAR 100, the stress analyses for the HI-STAR 100 in Section 2.6 give bounding results for the HI-STAR HB, except for the overpack enclosure shell.

In the HI-STAR HB, the number and length of the enclosure shell radial gussets have been reduced significantly as compared to the HI-STAR 100 (see drawings in Section 1.I.4). Therefore, a new analysis has been performed for the HI-STAR HB to demonstrate the structural integrity of the overpack enclosure shell and the overpack enclosure return under a bounding internal pressure. It is shown that large safety factors exist against overstress due to an internal pressure developing from off-gassing of the neutron shield material combined with a reduced external pressure. The minimum safety factors are summarized below:

Location	*Calculated Stress (ksi)*	*Allowable Stress (ksi)*	*Safety Factor*
Enclosure Shell Return (bottom)	*1.00*	*26.3*	*26.3*
Enclosure Shell Return (top)	*3.55*	*26.3*	*7.42*
Enclosure Shell	*4.32*	*17.5*	*4.05*
Weld Shear	*0.46*	*10.5*	*22.8*

The change in the enclosure shell radial gussets also has a minor effect on the global response of the HI-STAR HB overpack to a lateral drop because of the change in the gross metal cross section. Specifically, the area moment of inertia of the HI-STAR HB, at a cross section through the enclosure shell cavity, is roughly 5% lower than the HI-STAR 100 due to the difference in the enclosure shell radial gussets. However, this small decrease in the gross section properties is completely offset by the almost 40% decrease in the cask containment cavity length. The net effect of the change in the enclosure shell radial gussets and the shorter cavity length is a HI-STAR HB overpack that is stronger in bending than the HI-STAR 100 overpack.

In summary, because of the lower weight and shorter length, all stress analyses performed for the HI-STAR 100 using the bounding deceleration inputs give stress results that are equal to or greater than results using the HI-STAR HB.

2.I.6.2 Cold

No new or modified calculations or discussions are required for this subsection.

2.I.6.3 Reduced External Pressure

No new or modified calculations or discussions are required for this subsection. The stress analysis of the overpack enclosure shell in Subsection 2.I.6.1 conservatively bounds the effect of reduced external pressure (3.5 psia) by considering a higher pressure inside the enclosure shell cavity.

2.I.6.4 Increased External Pressure

No additional analyses need be performed here to demonstrate package performance of the HI-STAR HB.

2.I.6.5 Vibration

No new or modified calculations or discussions are required for this subsection.

2.I.6.6 Water Spray

The condition is not applicable to the HI-STAR HB System per Reg. Guide 7.8 [2.1.2].

2.I.6.7 Free Drop

The structural analysis of a 1-foot side drop has been performed for the HI-STAR 100 in Subsections 2.6.1 and 2.6.2 for heat and cold conditions of normal transport. As demonstrated in Subsections 2.6.1 and 2.6.2, safety factors are well over 1.0. Since the HI-STAR HB is shorter and lighter than the HI-STAR 100, the safety factors determined in Subsections 2.6.1 and 2.6.2 are lower bounds for comparable safety factors for the HI-STAR HB. As final verification, the decelerations for the free drop for the HI-STAR HB are determined in Section 2.I.7 and shown to

be less than the design basis limits for the 1-foot free drop. Results for the 1-foot drop simulations are presented in Table 2.I.7.2.

2.I.6.8 Corner Drop

This condition is not applicable to the HI-STAR HB System per [2.1.2].

2.I.6.9 Compression

The condition is not applicable to the HI-STAR HB System per [2.1.2].

2.I.7 HYPOTHETICAL ACCIDENT CONDITIONS

The hypothetical accident conditions, as defined in 10CFR71.73 and Regulatory Guide 7.9, have been applied to the HI-STAR 100 System in the required sequence in Subsection 2.7.

It is shown in the following subsections that the HI-STAR HB System also meets the standards set forth in 10CFR71, when it is subjected to the hypothetical accident conditions specified in 10CFR71.73.

2.I.7.1 Free Drop

In this subsection the performance and structural integrity of the HI-STAR HB System is evaluated for the most severe drop events. The drop events that are potentially most damaging are the end drops (top or bottom), the side drop, the orientation for which the center of gravity is directly over the point of impact, an oblique drop where the angle of impact is somewhere between center of gravity over corner and a near side drop, and an orientation where package rotation after an impact at one end induces a larger impact deceleration when the other end impacts the target (i.e., slapdown).

As has been noted, the HI-STAR HB is shorter and lighter than the HI-STAR 100, but is identical to the HI-STAR in all other aspects of geometry. The impact limiter crush strengths are adjusted from those used in the HI-STAR 100 in order to ensure that the design basis deceleration limits for the HI-STAR family continue to be met. In Section 2.7, the analysis was performed in two parts. Initially, 1/8 and 1/4 scale testing was performed to establish the characteristics of the impact limiter and to demonstrate that the experimentally obtained decelerations for all orientations of the cask were below the design basis. Analytical models were developed and demonstrated to be capable of predicting the observed responses from the experimental results. These models were used to evaluate sensitivity to crush strength change and cask weight change. Once it was established that the impact limiter configuration and crush strengths successfully limited the rigid body decelerations of the cask to below the prescribed limits, various strength analyses were performed to assess the state of stress in the cask components and ensure that the proscribed stress limits were satisfied.

As the impact limiter for the HI-STAR HB has the same geometry as the HI-STAR 100 with the sole difference being the impact limiter crush material, no qualification testing is employed. In lieu of testing, the same analytical methodology (the differential equation method) is used to simulate the free drop tests and demonstrate the performance of the impact limiter for the HI-STAR HB. The key features of the differential equation method are presented in [2.I.7.1], which summarizes, in a single document, the general analysis method as it was first implemented for the HI-STAR 100 license under 10CFR71.

The drop analysis of the HI-STAR HB Package using the differential equation method differs from the drop analysis for the HI-STAR 100 only to the extent that:

- *the axial length of the cylindrical body is reduced;*
- *the nominal strength of the energy absorbing honeycomb material is reduced;*
- *the mass of the package is reduced.*

Sheet 1 of Holtec drawing C1765 (Rev. 4) provides the reduced nominal crush strengths used in the impact limiters for the HI-STAR HB.

The dynamic multipliers (or dynamic correlation function), which were originally determined for the HI-STAR 100, remain valid for the HI-STAR HB Package for the following reasons. The Hexcel manufacturer's catalog states that dynamic crush strengths are a function of impact velocity only; there is no information suggesting that the dynamic multipliers in the differential equation method are a function of crush material strength. Therefore, the drop analyses for the HI-STAR HB impact limiters use the same dynamic multipliers (represented as a linear function of the concomitant crush velocity) that were used for the HI-STAR 100. More information on the dynamic multipliers, including the explicit form of the dynamic correlation function, is provided in [2.I.7.1].

The results from the four free drop simulations of the HI-STAR HB are documented in Table 2.I.7.1 using the nominal strengths of the honeycomb energy absorbing material. Because of the reduced length of the HI-STAR HB Package, the CGOC and slapdown angles are 58.63 degrees

and 6 or 10 degrees from the target plane, respectively. For the slapdown, the maximum deceleration of the secondary impact (after filtering to eliminate oscillations exceeding a frequency of 350 Hz) was slightly larger at a 10 degree initial angle than it was at 6 degrees; the maximum crush, however, was larger at 6 degrees as the initial orientation angle of the cask. Therefore, simulations using nominal crush strength are reported for both orientations, although sensitivity studies were performed only for the 6 degree initial orientation. The results show that the HI-STAR HB impact limiters effectively protect the HI-STAR HB cask under the postulated 30-foot drop events by maintaining the peak cask rigid body deceleration below the design basis limit of 60 g's. Since the peak decelerations are below the values computed for the HI-STAR 100, it is assured that the pin/bolt connections between the HI-STAR HB impact limiters and the HI-STAR HB body maintain their structural integrity.

Consistent with the requirements for 1-foot free drops as part of the Normal Conditions of Transport, two free drops (end drop and side drop) are also analyzed for the HI-STAR HB Package using the nominal strengths (plus 15%) specified for the honeycomb energy absorbing material. The maximum decelerations sustained by the Package, as well as the maximum impact limiter crush and impact durations, are summarized in Table 2.I.7.2. Finally, Table 2.7.I.3 presents the results of some additional parametric simulations that set upper and lower limits on permitted variation of the strength properties for the honeycomb material The analyses leading to the reported results are documented in a supporting calculation package [2.I.7.2].

2.I.7.2 Puncture

No new or modified calculations need be performed to qualify the HI-STAR HB, as the structure at the puncture locations is unchanged from the HI-STAR 100.

2.I.7.3 Thermal

Thermal evaluation of the fire accident is presented in Supplement 3.I. No new or modified structural calculations need be performed to qualify the HI-STAR HB for the fire accident.

2.I.7.4 Immersion - Fissile Material

No new or modified calculations need be performed to qualify the HI-STAR HB.

2.I.7.5 Immersion - All Packages

No new or modified calculations need be performed to qualify the HI-STAR HB.

2.I.7.6 Summary of Damage

The results presented in Subsections 2.I.7.1 through 2.I.7.5 show that the HI-STAR HB System meets the requirements of 10CFR71.61 and 10CFR71.73. The results from simulation of the hypothetical drop conditions produce deceleration levels that are below the design basis levels for the HI-STAR 100 for crush strength variations of plus or minus 15% of the nominal values specified for the HI-STAR HB impact limiters. Therefore, safety factors for the HI-STAR HB are greater than 1.0 by virtue of comparison with the corresponding calculations for the HI-STAR 100 for the Hypothetical Accident Conditions of Transport. Therefore, the HI-STAR 100 HB package, under the Hypothetical Accident Conditions of Transport, has adequate structural integrity to satisfy the subcriticality, containment, shielding, and temperature requirements of 10CFR71.

2.I.8 SPECIAL FORM

This section is not applicable to the HI-STAR HB System. This application does not seek approval for transport of special form radioactive material as defined in 10CFR71.4.

2.I.9 FUEL RODS

The Humboldt Bay fuel is shorter than the design basis fuel carried by the HI-STAR 100; therefore, the computations and conclusions in Section 2.9 encompass the HI-STAR HB. The presence of "Undamaged Fuel Assemblies", which are defined in Table 1.0.1 will have no significant effect on the structural response of the HI-STAR HB. This is because the only fuel parameters that have an influence on the structural analyses are the fuel mass and center of gravity height. Therefore, since an undamaged fuel assembly has essentially the same mass as an intact fuel assembly, and the exterior fuel rods serve to confine the interior fuel rods (with cladding in unknown condition) preventing them from dislocating and falling to the bottom of the fuel basket, the presence of undamaged fuel assemblies has no significant effect on the total amount of stored fuel mass or the center of gravity height used as input in the drop analysis for the HI-STAR HB.

2.I.10 MISCELLANEOUS ITEMS

No new appendices are introduced in Supplement 2.I. Also, since the HI-STAR 100 Package meets applicable NUREG 1617/10CFR71 requirements, so does the HI-STAR HB.

2.I.11 REFERENCES

[2.I.6.1] *Pacific Gas and Electric Company, NRC Docket Number 72-27, Humboldt Bay ISFSI, Final Safety Analysis Report Update, Revision 0, January 2006.*

[2.I.7.1] *A Classical Dynamics Based and Experimentally Benchmarked Impact Response Computation Methodology for Al-STAR Equipped Casks, HI-2084137, Rev. 0.*

[2.I.7.2] *Calculation Package for HI-STAR HB Drop Analyses, HI-2084158, Rev. 0.*

[2.I.7.3] *Miscellaneous Calculations for the HI-STAR HB, HI-2033042, Rev. 4.*

Table 2.I.2.1 Weights and Center of Gravity of HI-STAR HB Package			
Item	*Component Weight (lb.)*	*Total Weight (lb.)*	*Location of C.G. above base of cask (inch)*
Impact Limiter	*13,000*	*26000*	-
MPC HB	*59,000**	-	-
HI-STAR HB (with loaded MPC HB)	*161,200*	-	-
Total Package Weight	-	*187,200*	-
Loaded Package Center of Gravity	-	-	*61.4*

** Includes approximately 32,000 lb of fuel*

Table 2.I.7.1 –HI-STAR HB 30' DROP RESULTS

CONFIGURATION	*MAXIMUM DECELERATION (G'S)*	*MAXIMUM CRUSH (INCH)*	*DURATION OF IMPACT (SEC.)*	*COMMENTS*
30' TOP END DROP	*56.5*	*13.1*	*0.0425*	*Avg. strength=694 psi*
30' BOTTOM END DROP	*45.6*	*13.8*	*0.047*	*Strength=390 psi*
30' SIDE DROP	*34.8*	*13.4*	*0.0485*	*-*
30' CGOC	*33.75*	*22*	*0.0665*	*Bottom down*
30' SLAPDOWN - 6 DEGREES	*45.06**	*15.08*	*0.0705*	*Secondary impact limiter*
30' SLAPDOWN - 10 DEGREES	*45.88**	*14.93*	*0.0964*	*Secondary impact limiter*
30' SLAPDOWN - 6 DEGREES	*33.52**	*11.43*	*-*	*Primary impact limiter*
30' SLAPDOWN - 10 DEGREES	*30.57**	*13.82*	*-*	*Primary impact limiter*

**Reported result is subsequent to filtering to remove high frequency effects above 350 Hz.*

Table 2.I.7.2 –HI-STAR HB 1' DROP RESULTS

COMMENTS	*MAXIMUM DECELERATION (G'S)*	*MAXIMUM CRUSH (INCH)*	*DURATION OF IMPACT (SEC.)*	*COMMENTS*
1' TOP END DROP	*14*	*1.07*	*0.0254*	*Crush strength increased by 15%*
1' SIDE DROP	*10*	*1.55*	*0.0305*	*Crush strength increased by 15%*

Table 2.I.7.3 –HI-STAR HB 30' DROP RESULTS – SENSITIVITY ANALYSES

CONFIGURATION	*MAXIMUM DECELERATION (G'S)*	*MAXIMUM CRUSH (INCH)*	*DURATION OF IMPACT (SEC.)*	*COMMENTS*
30' TOP END DROP	*59*	*12.4*	*0.040*	*15% increase in crush strength*
30' BOTTOM END DROP	*44.3*	*14.8*	*0.050*	*15% decrease in crush strength*
30' SIDE DROP	*38.5*	*12.2*	*0.0435*	*15% increase in crush strength*
30' SIDE DROP	*43**	*15.2**	*0.053*	*15% decrease in crush strength*
30' CGOC	*36.75*	*20.75*	*0.0608*	*15% increase in crush strength*
30' CGOC	*30.55*	*23.75*	*0.0728*	*15% decrease in crush strength*
30' SLAPDOWN -6 DEGREES	*49.17***	*13.6*	*0.0718*	*Secondary IL – 15% increase in crush strength*
30' SLAPDOWN -6 DEGREES	*34.9***	*10.43*	-	*Primary IL – 15% increase in crush strength*
30' SLAPDOWN -6 DEGREES	*38.82***	*17.08*	*0.0842*	*Secondary IL – 15% decrease in crush strength*
30' SLAPDOWN -6 DEGREES	*30.28***	*12.88*	-	*Primary IL – 15% decrease in crush strength*

** 1050 psi material experiences minimal lockup so peak deceleration value rises but remains below the design basis limit.*
*** No filtering performed on deceleration time histories.*

7.1 PROCEDURE FOR LOADING AND PREPARATION FOR TRANSPORT OF THE HI-STAR 100 SYSTEM

7.1.1 Overview of HI-STAR Loading Operations

The MPC loading operations described herein are for HI-STAR 100 systems prepared for "load-and-go" directly into transportation under 10CFR71. HI-STAR 100 systems that are loaded and stored on an ISFSI site must be prepared in accordance with the applicable Part 72 HI-STAR FSAR or HI-STORM FSAR license and respective Certificate of Compliance (CoC). Any HI-STAR overpack and/or MPC deployed at an ISFSI must be confirmed to meet all conditions of the 10CFR71 CoC prior to shipment. The dryness criteria under the Part 72 CoC shall be considered acceptable for use in transport under Part 71 [7.1.2], [7.1.6].

The HI-STAR 100 System (HI-STAR) is used to load and transport spent nuclear fuel (SNF). The essential elements required to prepare the HI-STAR for fuel loading, to load the fuel, to ready the system for transport, and to ship the HI-STAR are described below.

7.1.2 Preparation of HI-STAR for Loading

1. If the HI-STAR overpack has previously been used to transport SNF, the HI-STAR overpack is received and the personnel barrier, if attached, is removed. The security seals, if used, are inspected to verify there was no tampering and that they match the corresponding shipping documents.

2. The HI-STAR is visually receipt inspected to verify that there are no outward visual indications of impaired physical condition except for superficial marks and dents. Any road dirt is washed off and any foreign material is removed.

3. Radiological surveys are performed in accordance with 49CFR173.443 [7.1.3] and 10CFR20.1906 [7.1.4]. Any issues are identified to site management and the overpack is decontaminated as directed by site radiation protection and make appropriate notifications as detailed in the surveillance requirements.

4. The impact limiters, if attached, are removed and a second visual inspection to verify that there are no outward visual indications of impaired physical condition is performed.

5. The HI-STAR overpack is upended and the neutron shield relief devices are inspected to confirm that they are installed, intact, and not covered by tape or any other covering.

7.1.3 Loading of Contents into HI-STAR

7.1.3.1 Loading of SNF into HI-STAR from a Spent Fuel Pool

1. The HI-STAR is positioned in the MPC loading area.

2. An empty MPC is upended and prepared for loading. The MPC is subjected to receipt

inspection (inspected for cleanliness and outward visual indications of impaired physical condition except for superficial marks and *dents).* Road dirt/debris and any foreign material are removed from the MPC prior to placement in the spent fuel pool. Verification is made to ensure that the appropriate fuel spacers, as necessary, are used to position the active fuel zone within the neutron absorber plates of the MPC, and limit axial movement of the fuel assemblies in the MPC cavity. The empty MPC is raised and inserted into the HI-STAR overpack while being careful not to damage the HI-STAR sealing surface. The MPC is inspected to ensure that the neutron absorber panel sheathing is present and there are no signs of potential damage to the neutron absorber.

3. The annulus is filled with clean (uncontaminated) water and the annulus seal is installed in the annulus between the MPC and the HI-STAR overpack.

ALARA Note:
A bottom protective cover may be attached to the cask bottom or placed in the designated preparation area or spent fuel pool. This will help prevent embedding contaminated particles in the cask bottom surface and ease the decontamination effort. Waterproof tape placed over empty bolt holes, and bolt plugs may also reduce the time required for decontamination. Wetting the components that enter the spent fuel pool may reduce the amount of decontamination work to be performed later.

4. The MPC is filled with either spent fuel pool water or clean water and the HI-STAR is raised and lowered into the spent fuel pool for fuel loading.

5. Prior to loading the fuel into the MPC, the user identifies the fuel to be loaded. A pre-loading verification is made to assure that damaged fuel and fuel debris will be placed in damaged fuel containers and that the *DFCs* will occupy authorized locations in the MPC. The fuel is independently verified to see that it meets the conditions of the CoC. The pre-selected assemblies are loaded into the MPC using DFCs as required, and a visual verification of the assembly identification is performed.

6. While still underwater, a thickly shielded lid (the MPC lid) is positioned over the pool surface and the drain line is installed. The MPC lid drain line is guided into its receiver and the MPC lid is installed. The upper surface of the MPC lid will seat approximately flush with the top edge of the MPC shell when properly installed. The lid may be removed and the drain line replaced should it be damaged during installation of the MPC lid. The user performs a site-specific Time-to-Boil analysis. This determines a time limit that ensures water in the MPC will not boil prior to the start of the draining operations. If it appears that the Time-to-Boil limit will be exceeded prior to draining the MPC, the user shall take appropriate action to prevent water from boiling.

ALARA Note:

Activated debris may have settled on flat surfaces of the cask during fuel loading. Cask surfaces suspected of carrying activated debris should be kept under water until a preliminary dose rate scan clears the cask for removal.

7. The lift attachment engages the HI-STAR overpack lifting trunnions to lift the HI-STAR overpack and loaded MPC close to the spent fuel pool surface.

8. The HI-STAR is removed from the spent fuel pool. If a lid retention system is being used, it is installed to secure the MPC lid for the transfer to the cask preparation area. The lift attachment and HI-STAR overpack are sprayed with clean water to help remove contamination as they are removed from the spent fuel pool.

9. The HI-STAR overpack is placed in the designated preparation area and the lift attachment and lid retention system, as applicable, are removed.

10. The top surfaces of the MPC lid, upper accessible regions of the MPC external shell and the upper flange of the HI-STAR overpack are decontaminated.

ALARA Note:

The water in the HI-STAR 100 overpack-to-MPC annulus provides personnel shielding. The level should be checked periodically and refilled accordingly. Pocket trunnions, if present and not used are plugged to reduce radiation levels around the lower region of the overpack.

11. The temporary shield ring, if used, is installed. The annulus seal is removed, and an annulus shield is installed. The temporary shield ring provides additional personnel shielding around the top of the HI-STAR overpack during MPC closure operations. The annulus shield also provides additional personnel shielding at the top of the annulus and prevents small items from being dropped into the annulus.

12. Dose rates are measured at the MPC lid and around the HI-STAR overpack to establish appropriate radiological control.

ALARA Warning:

Personnel should remain clear of the drain lines any time water is being pumped or purged from the cask. Assembly crud, suspended in the water, may create a radiation hazard to workers. Dose rates will rise as water is drained from the cask. Continuous dose rate monitoring is recommended.

ALARA Warning:
The use of manual welding should be minimized and only used when deemed advantageous from an ALARA perspective. If manual welding is *elected,* it should only be performed under conditions consistent with ALARA principals (e.g., utilizing temporary shielding).

13. The MPC water level and water level in the annulus are lowered slightly; the MPC is vented or purged and checked for combustible gas concentrations. The MPC lid is seal welded using an automated welding system, by manual welding, or a combination of both.

14. Visual examinations are performed on the tack welds. Liquid penetrant (PT) examinations are performed on the root and final passes. A volumetric examination is performed on the MPC welds using the ultrasonic method to ensure that the completed weld is satisfactory. As an alternative to volumetric examination of the MPC lid-to-shell weld, a multi-layer PT may be performed including intermediate examinations after approximately every three-eighth inch of weld depth. Any unsatisfactory indications are repaired in accordance with the code requirements [7.1.1].

15. At the appropriate time in the sequence of activities, based on the type of test performed (hydrostatic or pneumatic), an ASME pressure test of the MPC enclosure vessel is performed in accordance with the requirements of Section III, Subsection NB, Article NB-6000 and applicable subarticles [7.1.1]. Any non-satisfactory conditions require the user to determine the cause of the leak and make repairs as necessary to achieve a successful result.

ALARA Note:
Dose rates will rise as water is drained from the MPC. Continuous dose rate monitoring is recommended.

16. The MPC water is displaced from the MPC and the water is drained from the annulus area.

17. The Forced Helium Dehydration (FHD) is connected to the MPC and is used to remove moisture from the MPC. To ensure that the MPC cavity is suitably dry either the temperature or the dew point of the helium exiting the FHD demoisturizer shall be less than or equal to 22.9 °F for no less than 30 minutes.

18. The MPC helium backfill is adjusted to the pressure equivalent of greater than 0 psig and less than 44.8 psig at a reference temperature of 70 degrees Fahrenheit.

19. Cover plates are installed and seal welded over the MPC vent and drain ports and PT examinations are performed on the root (for multi-pass welds) and final passes. Any unsatisfactory indications are repaired in accordance with the code requirements.

20. The MPC closure ring is placed on the MPC.

21. The closure ring is aligned, tacked in place, and seal welded. Tack welds are visually examined and PT examinations are performed on the root (for multi-pass welds) and final welds.

22. The annulus shield and the temporary shield ring (if used) are removed.

7.1.3.2 Not Used

7.1.3.3 Loading a Loaded and Sealed MPC into HI-STAR Overpack

1. After the HI-STAR overpack has been prepared in accordance with Section 7.1.2 above, it is placed in the MPC transfer location and is fitted with a mating device to interface with the transfer cask.

2. The transfer cask with loaded MPC is brought to the MPC transfer location and placed atop the HI-STAR overpack and mating device.

3. The mating device is used to open the bottom of the transfer cask and the MPC is lowered into the HI-STAR overpack.

4. The transfer cask and mating device are removed from the HI-STAR.

7.1.4 Closure of HI-STAR

1. The MPC lid and accessible areas at the top of the MPC shell are smeared for removable contamination. Decontamination of the MPC lid and accessible areas at the top of the MPC may be performed at any time prior to closure of the HI-STAR overpack.

2. The sealing surfaces for the HI-STAR overpack are inspected for signs of damage. Any damage that would prevent a seal is remedied, any old seals are discarded, new seals are inserted for the closure plate, and the closure plate is installed with the bolts torqued in accordance with requirements in Table 7.1.1 and the order prescribed in Figure 7.1.1.

3. The HI-STAR overpack annulus is dried by evacuating to a pressure of less than or equal to 3 torr. The overpack annulus shall be considered dry when it can hold a stable pressure of less than or equal to 3 torr for at least 30 minutes.

4. The HI-STAR overpack is then backfilled with helium gas to a pressure of greater than or equal to 10 psig and less than or equal to 14 psig.

5. Any old seals are removed from the HI-STAR overpack vent and drain plugs and the plugs are installed with new seals and torqued in accordance with Table 7.1.1.

6. All HI-STAR overpack containment boundary seals, e.g. closure plate, vent and drain ports, are leak tested to assure they will provide long-term retention of the annulus

helium. All HI-STAR overpack containment boundary seals shall be leak tested in accordance with ANSI N14.5 [7.1.5] and shall demonstrate compliance with the leakage rate acceptance criterion in SAR Section 4.1. Unacceptable leakage rates will require repair and re-testing of the seals. The leak test shall be performed within the 12-month period prior to each shipment *and* after de-tensioning one or more overpack lid bolts, drain port, or the vent port plug;

7. The HI-STAR 100 overpack vent and drain port cover plates are installed.

8. The HI-STAR 100 overpack is surveyed for removable contamination per 49CFR173.443 [7.1.3]. If necessary, the overpack is further decontaminated to meet the surveillance requirements.

7.1.5 Preparation of HI-STAR for Transport

1. Verify the HI-STAR has been leak tested within the past 12 months and no overpack lid bolts and vent and drain port plugs have been de-tensioned. If not, the HI-STAR is leak tested in accordance with Step *6* of Section *7.1.4* above.

2. The relief devices on the neutron shield vessel are verified that they have been replaced within the past 5 years. If not, the relief devices are replaced.

ALARA Warning:
Dose rates around the unshielded bottom end of the cask may be higher that other locations around the cask. After the cask is downended on the transport frame, the bottom impact limiter should be installed promptly. Personnel should remain clear and exercise other appropriate ALARA controls when working around the bottom end of the cask.

3. Buttress plate is installed and the HI-STAR overpack is moved to the transport location. The HI-STAR is down-ended and placed on the transport vehicle. *Pocket trunnions, if present, are plugged.*

4. HI-STAR is visually inspected for signs of impaired condition.

5. Contamination surveys are performed on the HI-STAR per 49CFR173.443 [7.1.3]. If necessary, the overpack is further decontaminated to meet the surveillance requirements.

6. The impact limiters are installed on the HI-STAR and the bolts are torqued in accordance with Table 7.1.1.

7. The tie-down system is installed and a security seal, one per impact limiter is installed and the seal numbers are recorded in the shipping documents.

8. Final radiation surveys of the package surfaces per 10CFR71.47 [7.1.4] and

49CFR173.443 [7.1.3] are performed and recorded in the shipping documents.

9. The personnel barrier is installed.

10. The assembled package is given a final inspection to verify that all conditions for transport have been met (inspection steps may be performed in any order):

    a. Verify that required radiation survey results are properly documented on the shipping documentation.

    b. Perform a HI-STAR overpack surface temperature check. The accessible surfaces of the HI-STAR Package (impact limiters and personnel barrier) shall not exceed the Exclusive Use temperature limits of 49CFR173.442 [7.1.3].

    c. Verify that all required leakage testing has been performed, the acceptance criteria have been met, and the results have been documented on the shipping documentation.

    d. Verify that the receiver has been notified of the impending shipment and that the receiver has the appropriate procedures and equipment available to safely receive and handle the HI-STAR (10CFR20.1906(e)) [7.1.4].

    e. Verify that the carrier has the written instructions and a list of appropriate contacts for notification of accidents or delays.

    f. Verify that the carrier has written instructions that the shipment is to be Exclusive Use in accordance with 49CFR173.441 [7.1.3].

    g. Verify that route approvals and notification to appropriate agencies have been completed.

    h. Verify that the appropriate labels have been applied in accordance with 49CFR172.403 [7.1.3].

    i. Verify that the appropriate placards have been applied in accordance with 49CFR172.500 [7.1.3].

    j. Verify that all required information is recorded on the shipping documentation.

11. Following the above checks, the HI-STAR 100 System is released for transport.

Table 7.1.1
HI-STAR 100 SYSTEM TORQUE REQUIREMENTS

Fastener	Torque (ft-lbs)	Pattern

Overpack Closure Plate Bolts†, ††	First Pass – Hand Tight Second Pass – Wrench Tight Third Pass – 860 +25/-25 Fourth Pass – 1725 +50/-50 Final Pass - 2000 +250/-0	See Figure 7.1.1
Overpack Vent and Drain Port Plugs	45+5/-2	None
Closure Plate Test Port Plug	45+5/-2	None
Top Impact Limiter Attachment Bolt	256+10/-0	None
Bottom Impact Limiter Attachment Bolt	1500+45/-0	None

† Detorquing shall be performed by turning the bolts counter-clockwise in 1/3 turn +/- 30 degrees increments per pass according to Figure 7.1.1 for three passes. The bolts may then be removed.

†† Bolts shall be cleaned and inspected for damage or excessive wear (replaced if necessary) and coated with a light layer of Fel-Pro Chemical Products, N-5000, Nuclear Grade Lubricant (or equivalent).

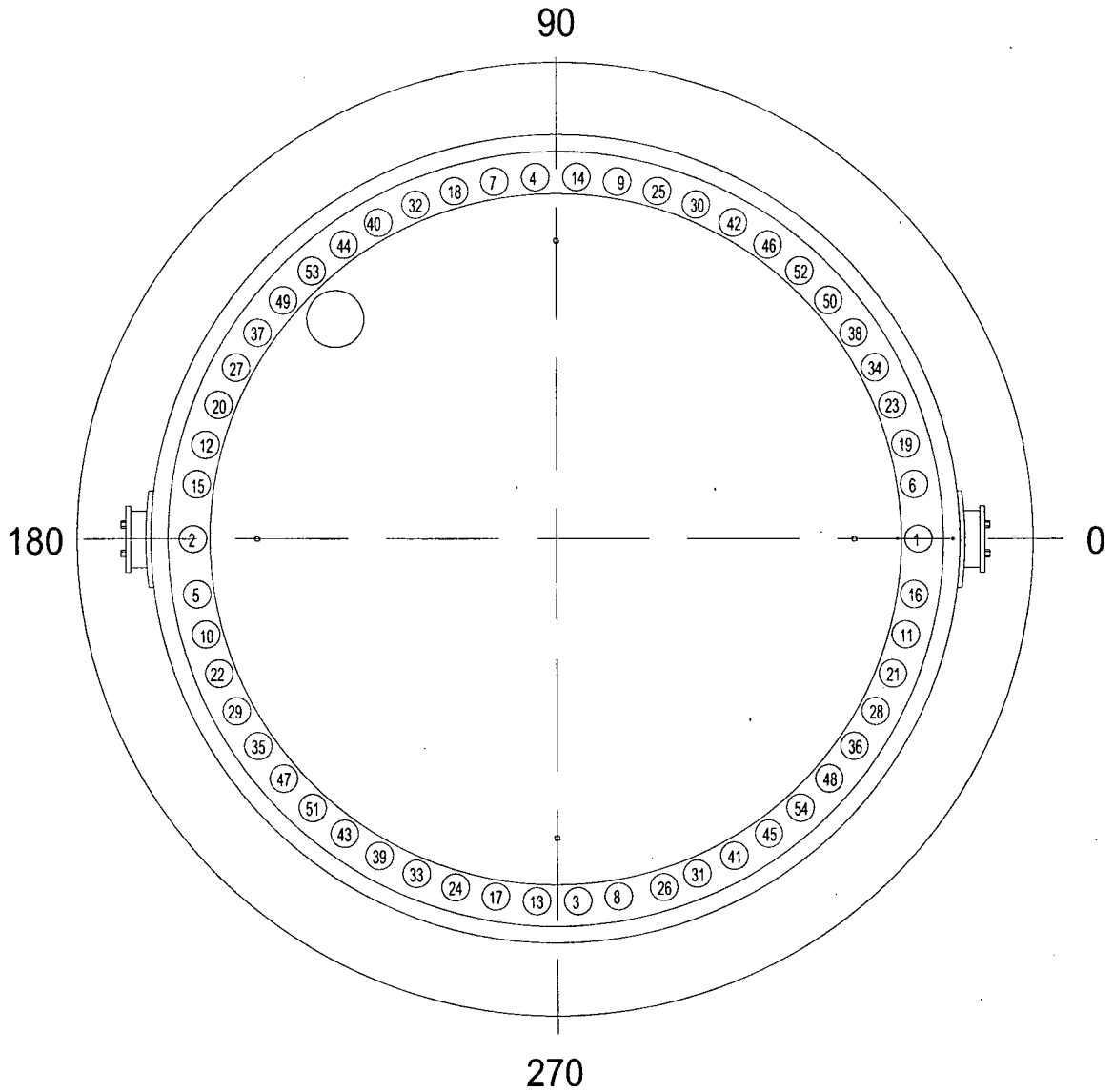

Figure 7.1.1; HI-STAR Closure Plate Bolt Torquing Pattern

CHAPTER 8: ACCEPTANCE TESTS AND MAINTENANCE PROGRAM

8.0 INTRODUCTION

This chapter identifies the acceptance tests and maintenance program to be conducted on the HI-STAR 100 Package to verify that the structures, systems, and components (SSCs) classified as important to safety have been fabricated, assembled, inspected, tested, accepted, and maintained in accordance with the requirements set forth in this Safety Analysis Report (SAR), the applicable regulatory requirements, and the Certificate of Compliance (CoC). The acceptance criteria and maintenance program described in this chapter fully comply with the requirements of 10CFR Part 71 [8.0.1].

8.1 ACCEPTANCE TESTS

This section provides the workmanship inspections and acceptance tests to be performed on the HI-STAR 100 Package prior to or during use. These inspections and tests provide assurance that the HI-STAR 100 Package has been fabricated, assembled, inspected, tested, and accepted for use and loading under the conditions specified in this SAR and the CoC issued by the NRC in accordance with the requirements of 10CFR Part 71.

8.1.1 Visual Inspections and Measurements

The following visual inspections and measurements shall be performed on the HI-STAR 100 Package, including the MPCs, in order to assure compliance with this SAR and the Certificate of Compliance. Inspections and measurements shall be performed in accordance with written and approved procedures and results shall be documented and become part of the quality documentation package. Any area found to be under the specified minimum thickness shall be repaired in accordance with the applicable ASME code requirements.

1. Visual inspections and measurements shall be made and controls shall be exercised to ensure that the packaging conforms to the dimensions and tolerances specified on the applicable drawings referenced in the CoC, specifically the following:
   a. The radial neutron shield minimum thickness
   b. The impact limiter neutron shield minimum thickness.
   c. The minimum flux trap sizes, if applicable.
   d. The minimum fuel cell pitch, if applicable.
   e. Correct thickness of top flange, closure plate, and bottom plate for gamma shielding.
   f. Correct total measured thickness of inner shell plus intermediate shells over the total surface area.
2. The packaging shall be inspected for cleanliness and proper preparation for shipping in accordance with written and approved procedures.
3. The sealing surfaces (including the lid and all penetrations) shall be inspected to ensure that there are no gouges, cracks, or scratches that could result in unacceptable leakage.

4. The locations, types, and sizes of welds shall be confirmed by measurement to be as specified on the drawings.
5. The packaging will be visually inspected to ensure it is conspicuously and durably marked with the proper markings/labels in accordance with 10CFR71.85(c) *and if applicable also in accordance with 10CFR 72.236(k).*
6. Visual inspections shall be made to verify that neutron absorber panels are present on the basket cell walls as required by the basket design.

8.1.2 Weld Examinations

All weld examinations shall be performed in accordance with the applicable ASME Code sections as specified on the drawings [8.1.1]. Examination of MPC components shall be performed per ASME Code Section III, Subsections NB, NF, and NG, per NB-5300, NF-5300, and NG-5300 and the code alternatives listed in Table 1.3.2, as applicable. Examination of the overpack shall be performed per ASME Code, Subsection NB, NB-5300 for containment boundary components, and Subsection NF, NF-5300 and the code alternatives listed in Table 1.3.2 for non-containment boundary components.

The MPC lid-to-shell weld shall be verified by either volumetric examination using ultrasonic methods or by surface examination using multi-layer liquid penetrant methods. Regardless of which method is used, the root and final layers shall be examined by liquid penetrant. If liquid penetrant alone is used, additional intermediate examinations shall be conducted after each approximately 3/8 inch of the weld is completed.

All weld examinations shall be performed in accordance with written and approved procedures, by qualified personnel, in accordance with SNT-TC-1A [8.1.2]. All results, including relevant indications, shall be made a permanent part of the quality records by video, photographic, or other means providing an equivalent retrievable record of weld integrity.

8.1.3 Structural and Pressure Tests

The HI-STAR 100 system containment boundary shall be examined and tested using pressure testing, ultrasonic testing, MT and/or PT, as applicable, to verify that it is free of cracks, pinholes, uncontrolled voids or other defects that could significantly reduce the effectiveness of the packaging.

8.1.3.1 Lifting Trunnions

Two trunnions (located near the top of the HI-STAR overpack) are provided for vertical lifting and handling of the HI-STAR 100 Package without the impact limiters installed. The trunnions are designed and shall be inspected and tested in accordance with ANSI N14.6 [8.1.3] as detailed in this Subsection. The trunnions are fabricated using a high-strength and high-ductility material (see overpack drawing in Section 1.4). The trunnions contain no welded components.

In order to ensure that the lifting trunnions do not have any hidden material flaws, the trunnions

shall be tested at 300% of the maximum design (service) lifting load. The load shall be applied for a minimum of 10 minutes to the pair of lifting trunnions. The accessible parts of the trunnions (areas outside the HI-STAR overpack), and the local HI-STAR 100 cask areas shall then be visually examined to verify no deformation, distortion, or cracking has occurred. Any evidence of deformation, distortion or cracking of the trunnion or adjacent HI-STAR 100 cask areas shall require replacement of the trunnion and/or repair of the HI-STAR 100 cask. Following any replacements and/or repair, the load testing shall be re-performed and the components re-examined in accordance with the original procedure and acceptance criteria. Testing shall be performed in accordance with written and approved procedures. Certified material test reports verifying trunnion material mechanical properties meet ASME Code Section II requirements provide further verification of the trunnion load capabilities. Test results shall be documented and shall become part of the final quality documentation package.

8.1.3.2 Pressure Testing

8.1.3.2.1 HI-STAR 100 Containment Boundary

The containment boundary of the HI-STAR Package shall be hydrostatically or pneumatically pressure tested to 150 psig +10/-0 psig, in accordance with the requirements of the ASME Code Section III, Subsection NB, Article NB-6000 and the code alternatives listed in Table 1.3.2. The test pressure of 150 psig is 150% of the Maximum Normal Operating Pressure (MNOP).

The overpack pressure test may be performed at any time during fabrication after the containment boundary is complete. The HI-STAR overpack shall be assembled for this test with the closure plate mechanical seal (only one required) or temporary test seal installed.

The test pressure shall be maintained for ten minutes. During this time period, the pressure gauge reading shall not fall below 150 psig. At the end of ten minutes, and while the pressure is being maintained at a minimum of 150 psig, the overpack shall be observed for leakage. In particular, the closure plate-to-top forging joint (the only credible leakage point) shall be examined. If a leak is discovered, the overpack shall be emptied and an evaluation shall be performed to determine the cause of the leakage. Repairs and retest shall be performed until the pressure test acceptance criterion is met.

After completion of the pressure testing, the overpack closure plate shall be removed and the internal surfaces shall be visually examined for cracking or deformation. Any evidence of cracking or deformation shall be cause for rejection or repair and retest, as applicable. The overpack shall be required to be pressure tested until the examinations are found to be acceptable.

Test results shall be documented and shall become part of the final quality documentation package.

8.1.3.2.2 MPC Pressure Boundary

Pressure testing (hydrostatic or pneumatic) of the MPC pressure boundary shall be performed in accordance with the requirements of the ASME Code Section III, Subsection NB, Article NB-6000, applicable sub-articles, and the code alternatives listed in Table 1.3.2 when field welding of the MPC lid-to-shell weld is completed. If hydrostatic testing is used, the MPC shall be pressure tested to 125% of design pressure. The minimum hydrostatic test pressure shall be 125 psig. If pneumatic testing is used, the MPC shall be pressure tested to 120% of the design pressure. The minimum pneumatic test pressure shall be 120 psig. Following completion of the required hold period at the test pressure, and after determining the leakage acceptance criterion is met, the surface of the MPC lid-to-shell weld shall be re-examined by liquid penetrant examination performed in accordance with ASME Code Section V, Article 6, with acceptance criteria per ASME Code Section III, Subsection NB, Article NB-5350.

Test results shall be documented and shall become part of the final quality documentation record package.

8.1.3.3 Pneumatic Testing of the Neutron Shield Enclosure Vessel

A pneumatic pressure test of the neutron shield enclosure vessel shall be performed following final closure welding of the enclosure shell returns and enclosure panels. The pneumatic test pressure shall be 37.5 +2.5,-0 psig, which is 125 percent of the relief device set pressure. The test shall be performed in accordance with approved written procedures.

During the test, the relief devices on the neutron shield enclosure vessel shall be removed. One of the relief device threaded connections is used for connection of the air pressure line and the other connection will be used for connection of the pressure gauge.

Following the introduction of pressurized gas into the neutron shield enclosure vessel, a 15-minute pressure hold time is required. If the neutron shield enclosure vessel fails to hold pressure, an approved soap bubble solution shall be applied to determine the location of the leak. The leak shall be repaired using weld repair procedures prepared in accordance with the ASME Code Section III, Subsection NF, Article NF-4450. The pneumatic pressure test shall be re-performed until no pressure loss is observed.

Test results shall be documented and shall become part of the final quality documentation package.

8.1.4 Leakage Tests

Leakage testing shall be performed in accordance with the requirements of ANSI N14.5-1997 [8.1.4]. Testing shall be performed in accordance with written and approved procedures. A leakage test of the HI-STAR overpack shall be performed at any time after the containment boundary fabrication is complete. The leakage test instrumentation shall have a minimum test sensitivity of 2.15×10^{-6} atm cm^3/s (helium). Containment boundary welds shall have indicated leakage rates not exceeding 4.3×10^{-6} atm cm^3/s (helium).

8.1.5 Component and Material Tests

The majority of materials used in the HI-STAR overpack are ferritic steels. ASME Code Section III and Regulatory Guides 7.11 [8.1.5] and 7.12 [8.1.6] require that certain materials be tested in order to assure that these materials are not subject to brittle fracture failures.

Each plate or forging for the HI-STAR 100 Package containment boundary (overpack inner shell, bottom plate, top flange, and closure plate) shall be required to be drop weight tested in accordance with the requirements of Regulatory Guides 7.11 and 7.12, as applicable. Additionally, per the ASME Code Section III, Subsection NB, Article NB-2300, Charpy V-notch testing shall be performed on these materials. Weld material used in welding the containment boundary shall be Charpy V-notch tested in accordance with ASME Section III, Subsection NB, Articles NB-2300 and NB-2430.

Non-containment portions of the overpack, as required, shall be Charpy V-notch tested in accordance with ASME Section III, Subsection NF, Articles NF-2300, and NF-2430. The non-containment materials to be tested include the intermediate shells, overpack port cover plates, and applicable weld materials.

Tables 2.1.22 and 2.1.23 provide the test temperatures or T_{NDT}, and test requirements to be used when performing the testing specified above.

8.1.5.1 Valves, Relief Devices, and Fluid Transport Devices

There are no fluid transport devices associated with the HI-STAR 100 Package. The only valve-like components in the HI-STAR 100 Package are the specially designed caps installed in the MPC lid for the drain and vent ports. These caps are recessed inside the MPC lid and covered by the fully welded vent and drain port cover plates. No credit is taken for the caps' ability to confine helium or radioactivity. After completion of drying and backfill operations, the drain and vent port cover plates are welded in place on the MPC lid and are leak tested to verify the MPC pressure boundary.

There are two relief devices (rupture discs) installed in the upper ledge surface of the neutron shield enclosure vessel of the HI-STAR overpack. These relief devices are provided for venting purposes under hypothetical fire accident conditions in which vapor formation from neutron shielding material degradation may occur. The relief devices are designed to relieve at 30 psig (± 5 psig).

8.1.5.2 Seals and Gaskets

Two concentric mechanical seals are provided on the HI-STAR overpack closure plate to provide containment boundary sealing. Mechanical seals are also used on the overpack vent and drain port plugs of the HI-STAR overpack containment boundary. Each primary seal is individually leak tested, in accordance with Subsection 8.1.4, prior to the HI-STAR 100 Package's first use and during each loading operation. An independent and redundant seal is provided for each penetration (e.g., closure plate, port cover plates, and closure plate test plug).

No containment credit is taken for these redundant seals and they are not leakage tested. Details on these seals are provided in Chapter 4.

8.1.5.3 Transport Impact Limiter

The removable HI-STAR transport impact limiters consist of aluminum honeycomb crush material arranged around a carbon steel structure and enclosed by a stainless steel shell. The drawings in Chapter 1 specify the crush strength of the aluminum honeycomb materials (nominal +/- 7%) for each zone of the impact limiter. For manufacturing purposes, verification of the impact limiter material is accomplished by performance of a crush test of sample blocks of aluminum honeycomb material for each large block manufactured. The verification tests are performed in accordance with approved procedures. The certified test results shall be submitted to Holtec International with each shipment of material.

All welds on the HI-STAR impact limiter shall be visually examined in accordance with the ASME Code, Section V, Article 9, with acceptance criteria per ASME Section III, Subsection NF, Article NF-5360.

8.1.5.4 Neutron Shielding Material

Neutron shield properties of Holtite-A are provided in Chapter 1. Each manufactured lot of neutron shield material shall be tested to verify that the material composition (aluminum and hydrogen), boron concentration, and neutron shield density (or specific gravity) meet the requirements specified in Chapter 1. A manufactured lot is defined as the total amount of material used to make any number of mixed batches comprised of constituent ingredients from the same lot/batch identification numbers supplied by the constituent manufacturer. Testing shall be performed in accordance with written and approved procedures and/or standards. Material composition, boron concentration, and density (or specific gravity) data for each manufactured lot of neutron shield material shall become part of the quality record documentation package.

The installation of the neutron shielding material shall be performed in accordance with written, approved, and qualified procedures. The procedures shall ensure that mix ratios and mixing methods are controlled in order to achieve proper material composition, boron concentration and distribution, and that pours are controlled in order to prevent gaps or voids from occurring in the material. Holtec International shall maintain samples of each manufactured lot of neutron shield material.

Users shall implement procedures which verify the integrity of the Holtite-A neutron shield once for each overpack. Neutron shield integrity shall be verified via measurements either at first use or with a check source using, at a maximum, a 6x6 inch test grid over the entire surface of the neutron shield, including the impact limiters. Measurements shall be compared to calculated values representative of either the check source being used or the loaded contents.

If a check source was used in the shielding integrity test, following the first fuel loading of each HI-STAR 100 Package, a shielding effectiveness test shall be performed to verify the

effectiveness of the neutron shield using written and approved procedures. Calibrated radiation detection equipment shall be used to take measurements at the surface of the HI-STAR overpack. Measurements shall be taken at three cross sectional planes through the radial shield and at four points along each plane's circumference. The average measurement results from each sectional plane shall be compared to calculated values to assess the continued effectiveness of the neutron shield. The calculated values shall be representative of the loaded contents (i.e., fuel type, enrichment, burnup, cooling time, etc...). Measurements shall be documented and become part of the quality documentation package.

8.1.5.5 Neutron Absorber Material

Each plate of neutron absorber shall be visually inspected for damage such as scratches, cracks, burrs, peeled cladding, foreign material embedded in the surfaces, voids, delamination, and surface finish.

8.1.5.5.1 Boral

After manufacturing, a statistical sample of each lot of neutron absorber shall be tested using wet chemistry and/or neutron attenuation testing to verify minimum ^{10}B content (areal density) in samples taken from the ends of the panel. The minimum ^{10}B loading of the neutron absorber panels for each MPC model must comply with the limits specified on the drawings. Any panel in which ^{10}B loading is less than the minimum allowed shall be rejected. Testing shall be performed using written and approved procedures. Results shall be documented and become part of the cask quality records documentation package.

8.1.5.5.2 METAMIC®

NUREG/CR-5661 identifies the main reason for a penalty in the neutron absorber B-10 density as the potential of neutron streaming due to non-uniformities in the neutron absorber, and recommends comprehensive acceptance tests to verify the presence and uniformity of the neutron absorber for credits more than 75%. Since a 90% credit is taken for METAMIC®, the following criteria must be satisfied:

- The boron carbide powder used in the manufacturing of METAMIC® must have small particle sizes to preclude neutron streaming.
- The ^{10}B areal density must comply with the limits specified on the drawings.
- The B_4C powder must be uniformly dispersed locally i.e. must not show any particle agglomeration. This precludes neutron streaming.
- The B_4C powder must be uniformly dispersed macroscopically i.e. must have a consistent concentration throughout the entire neutron absorber panel.
- The maximum B_4C content in METAMIC® shall be less than or equal to 33.0 weight percent.

To ensure that the above requirements are met the following tests shall be performed:

- All lots of boron carbide powder are analyzed to meet particle size distribution requirements.

- The following qualification testing shall be performed on the first production run of METAMIC® panels for the MPCs in order to validate the acceptability and consistency of the manufacturing process and verify the acceptability of the METAMIC® panels for neutron absorbing capabilities:

  1) The boron carbide powder weight percent shall be verified by testing a sample from forty different mixed batches. (A mixed batch is defined as a single mixture of aluminum powder and boron carbide powder used to make one or more billets. Each billet will produce several panels.) The samples shall be drawn from the mixing containers after mixing operations have been completed. Testing shall be performed using the wet chemistry method.

  2) The ^{10}B areal density shall be verified by testing a sample from one panel from each of forty different mixed batches. The samples shall be drawn from areas contiguous to the manufactured panels of METAMIC® and shall be tested using the wet chemistry method. Alternatively, or in addition to the wet chemistry tests, neutron attenuation tests on the samples may be performed to quantify the actual ^{10}B areal density.

  3) To verify the local uniformity of the boron particle dispersal, neutron attenuation measurements of random test coupons shall be performed. These test coupons may come from the production run or from pre-production trial runs.

  4) To verify the macroscopic uniformity of the boron particle distribution, test samples shall be taken from the sides of one panel from five different mixed batches before the panels are cut to their final sizes. The sample locations shall be chosen to be representative of the final product. Wet chemistry or neutron attenuation shall be performed on each of the samples.

- During production runs, testing of mixed batches shall be performed on a statistical basis to verify the correct boron carbide weight percent is being mixed.

- During production runs, samples from random METAMIC® panels taken from areas contiguous to the manufactured panels shall be tested via wet chemistry and/or neutron attenuation testing to verify the ^{10}B areal density. This test shall be performed to verify the continued acceptability of the manufacturing process.

The measurements of B_4C particle size, ^{10}B isotopic assay, uniformity of B_4C distribution and ^{10}B areal density shall be made using written and approved procedures. Results shall be documented and become part of the cask quality records documentation package.

8.1.5.6 Gamma Shielding

The gamma shielding (steel) in the construction of the HI-STAR 100 package is dimensionally inspected to assure compliance with the applicable drawings referenced in the CoC and as required in Subsection 8.1.1.

8.1.6 Thermal Tests

The first fabricated HI-STAR 100 overpack was tested to confirm its heat transfer capability. The test was performed and documented in Holtec Document DOC-5014-01 [8.1.7]. The tests have shown that the HI-STAR 100 system is within acceptable limits and future thermal testing is no longer required.